Entropy-Guided Sampling of Flat Modes in Discrete Spaces

Anonymous authors
Paper under double-blind review

Abstract

Sampling from flat modes in discrete spaces is a crucial yet under-explored direction. Flat modes represent robust solutions and have broad applications in combinatorial optimization and discrete generative modeling. However, existing sampling algorithms often overlook the mode volume and struggle to capture flat modes effectively. To address this limitation, we propose *Entropic Discrete Langevin Proposal* (EDLP), which incorporates local entropy into the sampling process through a continuous auxiliary variable under a joint distribution. The local entropy term guides the discrete sampler toward flat modes with a small overhead. We provide non-asymptotic convergence guarantees for EDLP in locally log-concave discrete distributions. Empirically, our method consistently outperforms traditional approaches across tasks that require sampling from flat basins, including Bernoulli distributions, restricted Boltzmann machines, combinatorial optimization, and binary neural networks.

1 Introduction

Sampling in discrete spaces is an integral component of machine learning, underpinning a diverse range of applications. Tasks such as text generation in natural language processing (NLP) (Gu et al., 2018; Devlin et al., 2019; Lewis et al., 2020), sequence alignment in bioinformatics (Shendure & Ji, 2008), the development of low-precision neural networks (Hubara et al., 2017; Peters & Welling, 2018), data generation in discrete Generative Adversarial Networks (GANs) (Goodfellow et al., 2014), and policy-based action sampling in reinforcement learning (Sutton & Barto, 2018) all rely on robust discrete sampling techniques. Recent advancements in gradient-based methods have significantly enhanced the efficiency of discrete samplers in exploring complex and multimodal landscapes, leveraging gradient-information, setting new benchmarks for probabilistic inference and combinatorial optimization (Grathwohl et al., 2021; Zhang et al., 2022; Rhodes & Gutmann, 2022; Sun et al., 2022; 2023; Li & Zhang, 2025).

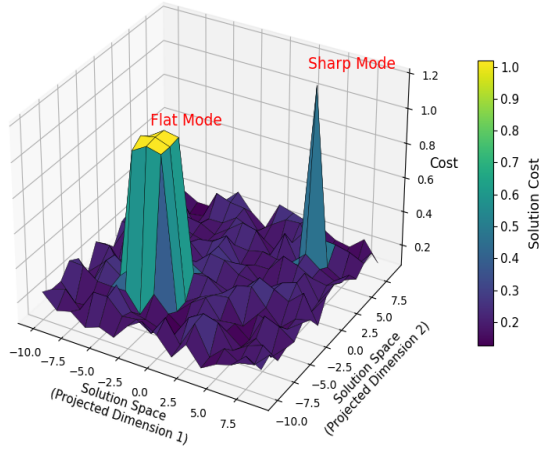

Figure 1: Cost landscape visualization on TSP: flat modes imply robust solutions under budget, whereas sharp modes are highly sensitive to small changes, leading to abrupt cost increases.

While the pursuit of flat minima (regions where neighboring states have similar energies) has revolutionized continuous neural network optimization and robustness (Hochreiter & Schmidhuber, 1997; Arbel et al., 2021; Izmailov et al., 2021; Chaudhari et al., 2019; Chang & Khanna, 2025), the geometry of discrete landscapes remains largely untouched. Through our work, we address this direction and argue that flatness is essentially desirable and beneficial for reasons that are distinct to the discrete topology. For instance, in constrained combinatorial optimization tasks, a "flat mode" represents a large cluster of valuable, distinct solutions that are structurally similar and have nearly identical costs within a given budget, which are of special interest in vehicle-routing optimization (Laporte, 2009; Toth & Vigo, 2002) . Figure 1 provides a conceptual,

low-dimensional projection of such a cost landscape for the Traveling Salesman Problem (TSP), a problem involving categorical variables.

In this paper, we aim bridge two fields by proposing *Entropic Discrete Langevin Proposal* (EDLP), that incorporates the concept of flatness-aware local entropy (Baldassi et al., 2016) into Discrete Langevin Proposal (DLP) (Zhang et al., 2022). By coupling discrete and flat-mode-guided variables, we obtain a broader, entropy-informed joint target distribution that biases sampling towards flat modes. Specifically, while updating the primary discrete variable using DLP, we simultaneously perform continuous Langevin updates on the auxiliary variable. Through the interaction between discrete and auxiliary variables, the discrete sampler will be steered toward flat regions. We summarize our core contributions as follows:

- We propose Entropic DLP (EDLP), a novel entropy-guided, gradient-based proposal for sampling from discrete flat basins. EDLP efficiently incorporates local entropy guidance by coupling discrete and continuous variables within a joint distribution (Section 4).
- We provide non-asymptotic convergence guarantees for EDLP in locally log-concave distributions, offering the **first** such bound for unadjusted gradient-based discrete sampling (Theorem 5.5 in Section 5).
- Through extensive experiments, we demonstrate that EDLP outperforms existing discrete samplers, with improvements up to 88.7%, in capturing flat-mode configurations across various tasks, including restricted Boltzmann machines, combinatorial optimization, and binary Bayesian neural networks (Section 6). We release the code at `https://anonymous.4open.science/r/EDLP-C0E8/README.md`.

Technical Overview. While our work sheds light on the overlooked role of topology in the study of discrete energy landscapes, we believe our novelty is beyond conceptual.

1. **Methodological Bridge.** While the concept of flatness in discrete spaces exists through Focused Belief Propagation(fBP) (Baldassi et al., 2019), it is purely heuristic and lacks rigorous theoretical grounding. Our work directly addresses this gap by providing non-asymptotic convergence guarantees for flatness-aware discrete sampling(Theorems 5.5, 5.6). It is also worth noting, the adaptation of EMCMC to discrete topologies is not as straightforward. Unlike EMCMC, where coupling between continuous vectors in Euclidean space is trivial, EDLP must reconcile the topological mismatch between the discrete target $\boldsymbol{\theta}$ and the continuous auxiliary $\boldsymbol{\theta}_a$ for meaningful structural guidance. This extension is challenging: it requires handling diverse discrete data types (e.g., categorical vs. ordinal). For categorical variables, "distance" to a continuous vector is undefined without a continuous embedding space. EDLP's coupling effortlessly extends in the embedding dimension, ensuring the gradient signal $\nabla\|\text{Embed}(\boldsymbol{\theta}) - \boldsymbol{\theta}_a\|^2$ is well defined. These implementation choices require careful thought, challenges absent in pure continuous sampling frameworks.
2. **Theoretical Analysis.** Further, to our knowledge, we are the first to provide non-asymptotic results for DLP-type algorithms without the MH step, as established in Theorem 5.5, addressing a critical gap in the literature. Moreover, while current proximal sampling (Chen et al., 2022) focuses on mixing rates in continuous spaces, when framed as a Proximal Sampler on a restricted discrete domain, EDLP is shown to have geometric ergodicity for the coupled chain (Theorems 5.5, 5.6). This provides necessary condition for robust inferential guarantees, such as the existence of CLT for the Markov chain. This distinguishes our contribution from standard proximal sampling analyses, offering a novel treatment of proximal dynamics in discrete landscapes. Finally, for a joint hybrid-chain (where one variable jumps and the other diffuses) providing non-asymptotic guarantees adds an addition layer of complexity beyond pure continuous diffusion as seen in Raginsky et al. (2017); Durmus et al. (2019); Durmus & Moulines (2017a). Unlike standard Langevin analyses which operate on a single homogeneous domain, our hybrid framework introduces a novel source of bias arising from the geometric interaction between the discrete target and the continuous auxiliary space. Our bounds reveal how the geometric alignment terms govern the trade-off between exploring flat regions and maintaining fidelity to the target distribution.
3. **Expanding the Utility of Flatness.** While earlier works have explored the notion of flatness, their goal has exclusively centered around better generalization or bayesian inference in deep learning (Li & Zhang, 2024; Baldassi et al., 2019; Pittorino et al., 2020). In our work, we adopt a multifaceted approach showcasing broader utility of flatness in discrete domains: 1. Flatness ensures structural robustness against perturbations, crucial for real-world constraints. 2. Flat modes represent data-centric learning prototypes, capturing the core structure of the data manifold in generative modeling. 3. We confirm the classic

generalization benefit. Thus the results presented in Section 6 are not "plug-and-play"; they require careful thinking to construct nuanced and bespoke experimental setups.

4. **Algorithmic Sophistication.** First, a naive combination of flatness and discrete sampling would rely on expensive, ad-hoc external checks (e.g., computing Hessians or Local Entropy at every step to check for flatness). Not only would this be computationally inefficient(and asymptotic at best), but also will break formal MCMC guarantees like detailed balance or convergence to any well-defined stationary distribution in high dimensions. EDLP avoids this by defining a rigorous joint probability distribution on discrete and continuous spaces to gain a richer understanding of the discrete landscape. Further, our method remains scalable in d as gradient modification is minimal(See Section 4.1) and we do provide runtime analysis to highlight this(see Fig 15). We also provide a Gibbs-like-Update(Appendix B) version of our algorithm, that reduces runtime by $\approx 50\%$. Second, since Local Entropy is the canonical metric for discrete flatness used in fBP, repurposing it as a coupling mechanism in EDLP represents the most natural and principled evolution for topology-aware discrete inference. Third, given our primary objective of designing a MCMC method that can cater to high dimensional variables while achieving fidelity to the true target distribution, we avoid the bias introduced by relaxation methods (like Gumbel-Softmax (Jang et al., 2017), Concrete distributions (Maddison et al., 2017)). Instead, our differentiable extension of the energy function maintains strict discreteness of the state space while allowing valid gradient guidance.

   Our contribution to the field of discrete sampling is the principled synthesis of two distinct ideas into a provably valid MCMC framework. The intellectual algorithmic novelty was not in merely mixing the two concepts, but in solving the theoretical challenge of how to do so correctly.

2 Related Works

State Augmentation in Sampling. While state augmentation is quite common in Markov Chain Monte Carlo(MCMC), EDLP positions itself uniquely against its predecessors. Hamiltonian Monte Carlo (HMC)(Ch 5. in Brooks et al. (2011))introduces an auxiliary continuous momentum variable to leverage inertia for efficient exploration. In EDLP, the auxiliary variable represents a continuous position, not to simulate inertia, but to smooth the energy landscape locally—effectively simulating a Moreau envelope to guide the discrete sampler toward flat basins. Also, HMC targets the marginal, whereas EDLP deliberately samples from an entropy-biased joint distribution to prioritize flatness guidance. Similarly, Slice Sampling (Neal, 2003) uses the auxiliary height variable to adapt the step size to the local flatness for better mixing, whereas EDLP uses its auxiliary variable to bias the stationary distribution itself. Compared to global flattening techniques like Parallel Tempering (Geyer, 1991), which require simulating multiple chains at different temperatures, EDLP achieves local smoothing via Gaussian convolution with a single chain. Unlike Swendsen-Wang (Swendsen & Wang, 1987), which augments the state with discrete bonds for cluster updates, EDLP utilizes gradient-based guidance from discrete-continuous coupling for efficient exploration of flat basins. EDLP also shares a fundamental mathematical structure with Proximal Sampling (Pereyra, 2016) through a quadratic auxiliary coupling that mirrors the Moreau-Yosida envelope. In this view, EDLP functions as a proximal sampler on a restricted discrete domain.

Gradient-Based Discrete Sampling. Gradient-based methods have significantly improved sampling efficiency in discrete spaces. Locally informed proposals method by Zanella (2020) leverages probability ratios to explore discrete spaces more effectively. Building on this, Grathwohl et al. (2021) introduced a gradient-based approach to approximate the probability ratio, further improving sampling efficiency. Discrete Langevin Proposal (DLP), introduced by Zhang et al. (2022), adapts the principles of the Langevin algorithm (Grenander & Miller, 1994; Roberts & Tweedie, 1996; Roberts & Rosenthal, 2002), originally designed for continuous spaces, to discrete settings. This algorithm enables parallel updates of multiple coordinates using a single gradient computation, boosting both computational efficiency and scalability.

Gaussian Auxiliary Variable in Discrete Sampling. Using a continuous Gaussian auxiliary variables to simplify sampling in discrete spaces is a well-known trick in statistical computing. This technique has a rich history, from its use in Bayesian data augmentation (Albert & Chib, 1993) to linearizing quadratic terms in energy-based models for efficient Gibbs sampling (Martens & Sutskever, 2010). More recently, this

framework has been central to developing modern, general-purpose gradient-based samplers for discrete variables (Pakman & Paninski, 2013; Rhodes & Gutmann, 2022).

Flatness-aware Optimization. In early neural network optimization, flatness in energy landscapes emerged as crucial for improving generalization. Hochreiter & Schmidhuber (1994) linked flat minima to better generalization due to their robustness to parameter perturbations. Hochreiter & Schmidhuber (1997) further emphasized the stability advantages of flat regions. Further, LeCun et al. (1990) linked learning algorithm stability to flatness, suggesting optimization methods to exploit this. Later, Gardner (1988) analyzed training algorithms using a statistical mechanics framework, highlighting energy landscape topology's role. In Bayesian deep learning, Li & Zhang (2024) introduced Entropy MCMC (EMCMC) to bias posterior sampling towards flat regions in continuous spaces, achieving better generalization of Bayesian neural networks.

3 Preliminaries

Target Distribution. We define a target distribution over a discrete space using an energy function. The target distribution is given by $\pi(\boldsymbol{\theta}) = \frac{1}{Z}\exp(U(\boldsymbol{\theta}))$, where $\boldsymbol{\theta}$ is a d-dimensional discrete variable within domain $\boldsymbol{\Theta}$, $U(\boldsymbol{\theta})$ represents the energy function, and Z is the normalizing constant ensuring $\pi(\boldsymbol{\theta})$ is a proper probability distribution. We make the following assumptions consistent with the literature on gradient-based discrete sampling (Grathwohl et al., 2021; Sun et al., 2022; Zhang et al., 2022): 1. The domain $\boldsymbol{\Theta}$ is factorized coordinatewisely i.e. $\boldsymbol{\Theta} = \Pi_{i=1}^{d}\boldsymbol{\Theta}_i$, and mainly consider it to be $\{0,1\}^d$ or $\{0,1,\cdots S\}^d$. 2. Under the Functional Extension framework, discussed in Section 3 of Grathwohl et al. (2021), discrete distributions defined by energy functions sometimes possess a 'natural differentiable extension': $U:\mathbb{R}^d \to \mathbb{R}$ to compute $\nabla_{\boldsymbol{\theta}} U(\boldsymbol{\theta})$ at discrete points. EDLP strictly adheres to this framework: we utilize the gradient of the coupled energy purely to bias the transition probabilities of the categorical proposal, ensuring that $\boldsymbol{\theta}$ remains strictly discrete throughout the process.

Langevin Algorithm. In continuous spaces, the Langevin algorithm is a powerful sampling method that follows a Langevin diffusion to update current sample $\boldsymbol{\theta}_a \in \mathbb{R}^d$: $\boldsymbol{\theta'_a} = \boldsymbol{\theta_a} + \frac{\alpha}{2}\nabla_{\boldsymbol{\theta}_a} U(\boldsymbol{\theta_a}) + \sqrt{\alpha}\boldsymbol{\epsilon}$, where $\boldsymbol{\epsilon} \sim \mathcal{N}(\mathbf{0}, \mathbf{I}_{d\times d})$. The gradient assists the sampler in efficiently exploring high-probability regions.

Discrete Langevin Proposal. The Discrete Langevin Proposal (DLP) is an extension of the Langevin algorithm tailored for discrete spaces, introduced by Zhang et al. (2022). At a given position $\boldsymbol{\theta}$, the proposal distribution $q(\cdot|\boldsymbol{\theta})$ determines the next position. The proposal distribution in DLP is formulated as:

$$q(\boldsymbol{\theta}'|\boldsymbol{\theta}) = \frac{\exp\left(-\frac{1}{2\alpha}\|\boldsymbol{\theta}' - \boldsymbol{\theta} - \frac{\alpha}{2}\nabla U(\boldsymbol{\theta})\|^2\right)}{Z_{\boldsymbol{\Theta}}(\boldsymbol{\theta})}, \tag{1}$$

where $Z_{\boldsymbol{\Theta}}(\boldsymbol{\theta})$ is the normalizing constant. DLP can be employed without or with a Metropolis-Hastings (MH) step, resulting in the discrete unadjusted Langevin algorithm (DULA) and the discrete Metropolis-adjusted Langevin algorithm (DMALA), respectively.

Local Entropy. Local entropy is a critical concept in flatness-aware optimization techniques, which is used to understand the geometric characteristics of energy landscapes. Though originally introduced by Baldassi et al. (2016) as a measure of solution density for discrete systems, local entropy was repurposed by Chaudhari et al. (2019) to characterize geometrically flat minima in continuous optimization landscapes. Here, we utilize this influential conceptual framework and explicitly choose local entropy as our metric for *flatness in discrete spaces*. Specifically, for $\boldsymbol{\Theta}$ as our discrete space equipped with an implicit Hamming metric, the local entropy at any $\boldsymbol{\theta}_a \in \mathbb{R}^d$, with a scalar parameter η controlling the sensitivity to flatness in the landscape is defined as equation 2.

$$\mathcal{F}(\boldsymbol{\theta}_a;\eta) = \log\left(\sum_{\boldsymbol{\theta}\in\boldsymbol{\Theta}} \exp\left\{U(\boldsymbol{\theta}) - \frac{1}{2\eta}\|\boldsymbol{\theta} - \boldsymbol{\theta}_a\|^2\right\}\right), \tag{2}$$

This definition is directly applicable to problems involving categorical variables, not just ordinal variables via standard embeddings (e.g., one-hot encoding; (Grathwohl et al., 2021)). In this embedding space, a well-defined distance metric between $\boldsymbol{\theta}, \boldsymbol{\theta}_a$ is established. Consequently, our local entropy formulation then operates directly on these vector representations, penalizing discrete states far from the auxiliary variable $\boldsymbol{\theta}_a$.

4 Entropic Discrete Langevin Proposal

4.1 Target Joint Distribution: Coupling Mechanism

We propose leveraging local entropy (Eq.2) to construct an auxiliary distribution that emphasizes flat regions of the target distribution. This auxiliary distribution smoothens the energy landscape, acting as an external force, driving the exploration of flat basins. Figure 3 in the Appendix A illustrates the motivation behind our approach and the impact of the parameter η on the smoothened target distribution.

We start with the original target distribution $p(\boldsymbol{\theta}) \propto \exp(U(\boldsymbol{\theta}))$. By incorporating local entropy, we derive a smoothed target distribution in terms of a new variable $\boldsymbol{\theta}_a$:

$$p(\boldsymbol{\theta}_a) \propto \exp \mathcal{F}(\boldsymbol{\theta}_a; \eta) = \sum_{\boldsymbol{\theta} \in \boldsymbol{\Theta}} \exp \left\{ U(\boldsymbol{\theta}) - \frac{1}{2\eta} \|\boldsymbol{\theta} - \boldsymbol{\theta}_a\|^2 \right\} \tag{3}$$

Inspired by the coupling method introduced by Li & Zhang (2024) in their Section 4.1, we couple $\boldsymbol{\theta}$ and $\boldsymbol{\theta}_a$ as follows:

Lemma 4.1. *Given $\widetilde{\boldsymbol{\theta}} = [\boldsymbol{\theta}^T, \boldsymbol{\theta}_a^T]^T \in \boldsymbol{\Theta} \times \mathbb{R}^d$, the joint distribution $p(\widetilde{\boldsymbol{\theta}})$ is:*

$$p(\widetilde{\boldsymbol{\theta}}) = p(\boldsymbol{\theta}, \boldsymbol{\theta}_a) \propto \exp \left\{ U(\boldsymbol{\theta}) - \frac{1}{2\eta} \|\boldsymbol{\theta} - \boldsymbol{\theta}_a\|^2 \right\} \tag{4}$$

By construction, the marginal distributions of $\boldsymbol{\theta}$ and $\boldsymbol{\theta}_a$ are the original distribution $p(\boldsymbol{\theta})$ and the smoothed distribution $p(\boldsymbol{\theta}_a)$ (Eq. 3).

This result directly follows from Lemma 1 under Section 4.1 in Li & Zhang (2024) [1]. The joint hybrid-variable, $\widetilde{\boldsymbol{\theta}}$ lies in a product space where first d coordinates are discrete-valued and the remaining d coordinates lie in $\mathbb{R}^d$. Consequently, the energy function of $\widetilde{\boldsymbol{\theta}}$ becomes,

$$U_\eta(\widetilde{\boldsymbol{\theta}}) = U(\boldsymbol{\theta}) - \frac{1}{2\eta} \|\boldsymbol{\theta} - \boldsymbol{\theta}_a\|^2$$

, and its gradient is given by:

$$\nabla_{\widetilde{\boldsymbol{\theta}}} U_\eta(\widetilde{\boldsymbol{\theta}}) = \begin{bmatrix} \nabla_{\boldsymbol{\theta}} U_\eta(\widetilde{\boldsymbol{\theta}}) \\ \nabla_{\boldsymbol{\theta}_a} U_\eta(\widetilde{\boldsymbol{\theta}}) \end{bmatrix} = \begin{bmatrix} \nabla_{\boldsymbol{\theta}} U(\boldsymbol{\theta}) - \frac{1}{\eta}(\boldsymbol{\theta} - \boldsymbol{\theta}_a) \\ \frac{1}{\eta}(\boldsymbol{\theta} - \boldsymbol{\theta}_a) \end{bmatrix}. \tag{5}$$

4.2 Sampling Algorithm: Local Entropy Guidance in Discrete Langevin Proposals

We propose EDLP, an extension of DLP designed to enhance sampling efficiency from flat modes. In our framework (Algorithm 1), the Langevin update for $\boldsymbol{\theta}_a$ follows the distribution $q_{\alpha_a}(\boldsymbol{\theta}'_a|\widetilde{\boldsymbol{\theta}})$:

$$q_{\alpha_a}(\boldsymbol{\theta}'_a|\widetilde{\boldsymbol{\theta}}) = \frac{1}{\sqrt{2\pi\alpha_a}^d} \exp\left(-\frac{1}{2\alpha_a} \|\boldsymbol{\theta}'_a - \boldsymbol{\theta}_a - \frac{\alpha_a}{2} \nabla_{\boldsymbol{\theta}_a} U_\eta(\widetilde{\boldsymbol{\theta}})\|^2 \right). \tag{6}$$

Unlike the standard DLP, where transitions are purely between discrete states, EDLP leverages the current joint variables $\widetilde{\boldsymbol{\theta}} = [\boldsymbol{\theta}^T, \boldsymbol{\theta}_a^T]^T$ to propose the next discrete state. By incorporating the coupling between the variables, we refine the DLP proposal by replacing $\nabla U(\boldsymbol{\theta})$ with $\nabla_{\boldsymbol{\theta}} U_\eta(\widetilde{\boldsymbol{\theta}})$. This adjustment results in the modified proposal:

$$q_\alpha(\boldsymbol{\theta}'|\widetilde{\boldsymbol{\theta}}) \propto \exp\left(-\frac{1}{2\alpha} \|\boldsymbol{\theta}' - \boldsymbol{\theta} - \frac{\alpha}{2} \nabla_{\boldsymbol{\theta}} U_\eta(\widetilde{\boldsymbol{\theta}})\|^2 \right). \tag{7}$$

[1] In EMCMC, $\boldsymbol{\theta}$(main) and $\boldsymbol{\theta}_a$(auxiliary) are continuous vectors operating in Euclidean space. In our framework, the main variable $\boldsymbol{\theta}$ is discrete, while the auxiliary variable $\boldsymbol{\theta}_a$ remains continuous. Thus, our notation reflects not just the functional role of the variables (main vs. auxiliary), but also the distinct topological spaces they inhabit.

To further simplify, we use coordinate-wise factorization from DLP to obtain $q_\alpha(\boldsymbol{\theta'}|\widetilde{\boldsymbol{\theta}}) = \prod_{i=1}^d q_{\alpha_i}(\theta'_i|\widetilde{\boldsymbol{\theta}})$, where $q_{\alpha_i}(\theta'_i|\widetilde{\boldsymbol{\theta}})$ is a categorical distribution:

$$\text{Cat}\left(\text{Softmax}\left(\frac{1}{2}\nabla_\theta U_\eta(\widetilde{\boldsymbol{\theta}})_i(\theta'_i - \theta_i) - \frac{(\theta'_i - \theta_i)^2}{2\alpha}\right)\right). \tag{8}$$

By synthesizing Equations equation 6 and equation 8, we derive the full proposal distribution:

$$q_\gamma(\widetilde{\boldsymbol{\theta'}}|\widetilde{\boldsymbol{\theta}}) \propto q_\alpha(\boldsymbol{\theta'}|\widetilde{\boldsymbol{\theta}}) q_{\alpha_a}(\boldsymbol{\theta'_a}|\widetilde{\boldsymbol{\theta}}) \tag{9}$$

where $\gamma = (\alpha, \alpha_a)$.

This factorized proposal in Eq. equation 9 is purely a design choice to simplify sampling. The proposal distribution is called the *Entropic Discrete Langevin Proposal* (EDLP). At the current joint position $\widetilde{\boldsymbol{\theta}}$, EDLP generates the next joint position $\widetilde{\boldsymbol{\theta'}}$. EDLP can be paired with or without a Metropolis-Hastings step (Metropolis et al., 1953; Hastings, 1970) to ensure the Markov chain's reversibility. These algorithms are referred to as EDULA (Entropic Discrete Unadjusted Langevin Algorithm) and EDMALA (Entropic Discrete Metropolis-Adjusted Langevin Algorithm), respectively. We will collect samples of $\boldsymbol{\theta}$, as the marginal distribution of $p(\widetilde{\boldsymbol{\theta}})$ over $\boldsymbol{\theta}$ yields our desired discrete target distribution.

Why does EDLP work? One notices, in flat regions the sum in Equation 2 is high due to many contributing terms, giving $\boldsymbol{\theta}_a$ *large freedom to move.* Conversely, in sharp regions, $\boldsymbol{\theta}_a$ is strongly incentivized to *stay put* as the Gaussian term rapidly decays to zero, leaving no other low-energy states nearby. This builds the intuition behind our approach: local entropy guides the sampler to regions offering the greatest configurational volume. Within a flat basin, $\boldsymbol{\theta}_a$ has more freedom to move due to many favorable neighboring states, while in a sharp, isolated peak, it is constrained. Maximizing local entropy naturally steers the sampler toward larger, more robust solution basins.

Alongside the vanilla EDLP, we introduce a computationally efficient *Gibbs-like-update* (GLU) version, in the Appendix B, which involves alternating updates instead of simultaneous updates of our variables. Sensitivity analysis of the hyperparameters and runtime analysis are presented in Appendix, in sections A and E.4 respectively.

5 Theoretical Analysis

In this section, we provide a theoretical analysis of the convergence rates for EDULA and EDMALA. We adopt the standard assumptions used in analyzing flatness-aware MCMC algorithms (Li & Zhang, 2024; Chaudhari et al., 2019), which are also consistent with the broader sampling literature (Pynadath et al., 2024; Bottou et al., 2018; Dalalyan, 2017; Durmus & Moulines, 2017b)

Assumption 5.1 (Smoothness)**.** *The function $U(\cdot) \in C^2(\mathbb{R}^d)$ has M-Lipschitz gradient.*

Assumption 5.2 (Strong Concavity)**.** *For each $\boldsymbol{\theta} \in \mathbb{R}^d$, there exists an open ball containing $\boldsymbol{\theta}$ of some radius $r_{\boldsymbol{\theta}}$, denoted by $B(\boldsymbol{\theta}, r_{\boldsymbol{\theta}})$, such that the function $U(\cdot)$ is $m_{\boldsymbol{\theta}}$-strongly concave in $B(\boldsymbol{\theta}, r_{\boldsymbol{\theta}})$ for some $m_{\boldsymbol{\theta}} > 0$.*

Assumption 5.3 (Bounded Auxiliary Space)**.** *$\boldsymbol{\theta}_a$ is restricted to a compact subset of $\mathbb{R}^d$ labeled $\boldsymbol{\Theta}_a$.*

We define $\delta(\boldsymbol{\Theta}) = \inf_{\boldsymbol{\theta},\boldsymbol{\theta}' \in \boldsymbol{\Theta}} \|\boldsymbol{\theta} - \boldsymbol{\theta}'\|$, $\text{diam}(\boldsymbol{\Theta}) = \sup_{\boldsymbol{\theta},\boldsymbol{\theta}' \in \boldsymbol{\Theta}} \|\boldsymbol{\theta} - \boldsymbol{\theta}'\|$, and $\text{diam}(\boldsymbol{\Theta_a}) = \sup_{\boldsymbol{\theta}_a,\boldsymbol{\theta}'_a \in \boldsymbol{\Theta}_a} \|\boldsymbol{\theta}_a - \boldsymbol{\theta}'_a\|$. Let $\vartheta(\boldsymbol{\Theta}, \boldsymbol{\Theta_a}) = \inf_{\boldsymbol{\theta},\boldsymbol{\theta}' \in \boldsymbol{\Theta};\boldsymbol{\theta}_a,\boldsymbol{\theta}'_a \in \boldsymbol{\Theta_a}} (\boldsymbol{\theta} - \boldsymbol{\theta}_a)^\top (\boldsymbol{\theta}' - \boldsymbol{\theta}'_a)$ and $\Delta(\boldsymbol{\Theta}, \boldsymbol{\Theta}_a) = \sup_{\boldsymbol{\theta} \in \boldsymbol{\Theta},\, \boldsymbol{\theta_a} \in \boldsymbol{\Theta_a}} \|\boldsymbol{\theta_a} - \boldsymbol{\theta}\|$. Let the joint valid bounded space be $\widetilde{\boldsymbol{\Theta}}$ and finally define $a \in \arg\min_{\boldsymbol{\theta} \in \boldsymbol{\Theta}} \|\nabla U(\boldsymbol{\theta})\|$ as the set of values which minimizes the energy function in $\boldsymbol{\Theta}$. $\delta(\boldsymbol{\Theta}) = 1$ is trivially true for most settings, even the ones discussed in Section 6.

Assumption 5.1 ensures the energy landscape does not fluctuate arbitrarily fast between any two discrete states. Under Assumption 5.2, $U(\cdot)$ is m-strongly concave on $\text{conv}(\boldsymbol{\Theta})$. This strictly bounds the curvature away from zero to guarantee geometric ergodicity (fast convergence). In our context, this still allows for "flat" modes—characterized by wide basins with small m relative to sharp modes. Assumption 5.3 prevents the continuous auxiliary variable from wandering to infinity, ensuring the entropic coupling between $\boldsymbol{\theta}$ and $\boldsymbol{\theta}_a$ remains active and meaningful. The total variation distance between two probability measures μ and ν, defined on some space $\boldsymbol{\theta} \subset \mathbb{R}^d$ is $\|\mu - \nu\|_{TV} = \sup_{A \subseteq B(\boldsymbol{\theta})} |\mu(A) - \nu(A)|$ where $B(\boldsymbol{\theta})$ is the set of all measurable sets in $\boldsymbol{\theta}$.

Algorithm 1 Entropic Discrete Langevin Proposal: EDULA and EDMALA

Inputs: Main variable $\boldsymbol{\theta} \in \boldsymbol{\Theta}$, Auxiliary variable $\boldsymbol{\theta}_a \in \mathbb{R}^d$, Main stepsize α, Auxiliary stepsize α_a, Flatness parameter η
Initialize: $\boldsymbol{\theta}_a \leftarrow \boldsymbol{\theta}, \mathcal{S} \leftarrow \emptyset$
loop
  Construct $\nabla_{\widetilde{\boldsymbol{\theta}}} U_\eta(\widetilde{\boldsymbol{\theta}})$ as in Equation equation 5
  for $i = 1$ **to** d **do**
    Construct $q_{i_\alpha}(\cdot|\widetilde{\boldsymbol{\theta}})$ as in Equation equation 8
    Sample $\boldsymbol{\theta}_i{}' \sim q_{i_\alpha}(\cdot|\widetilde{\boldsymbol{\theta}})$
  end for
  Compute $\boldsymbol{\theta}'_{\boldsymbol{a}} \leftarrow \boldsymbol{\theta}_a + \frac{\alpha_a}{2}\nabla_{\boldsymbol{\theta}_a} U_\eta(\widetilde{\boldsymbol{\theta}}) + \sqrt{\alpha_a}\boldsymbol{\epsilon}$ where $\boldsymbol{\epsilon} \sim \mathcal{N}(\mathbf{0}, \boldsymbol{I})$
  ▷ Optionally, do the MH step for EDMALA
  Compute $q_\alpha(\widetilde{\boldsymbol{\theta}'}|\widetilde{\boldsymbol{\theta}}) = \prod_i q_{i_\alpha}(\widetilde{\boldsymbol{\theta}'_{\boldsymbol{i}}}|\widetilde{\boldsymbol{\theta}})$
    and $q_\alpha(\widetilde{\boldsymbol{\theta}}|\widetilde{\boldsymbol{\theta}'}) = \prod_i q_{i_\alpha}(\widetilde{\boldsymbol{\theta}_{\boldsymbol{i}}}|\widetilde{\boldsymbol{\theta}'})$
  Set $\boldsymbol{\theta} \leftarrow \boldsymbol{\theta}'$ and $\boldsymbol{\theta}_a \leftarrow \boldsymbol{\theta}'_{\boldsymbol{a}}$ with probability

$$\min\left(1, \frac{q_\alpha(\boldsymbol{\theta}|\widetilde{\boldsymbol{\theta}'})}{q_\alpha(\boldsymbol{\theta}'|\widetilde{\boldsymbol{\theta}})} \frac{q_{\alpha_a}(\boldsymbol{\theta}_{\boldsymbol{a}}|\widetilde{\boldsymbol{\theta}'})}{q_{\alpha_a}(\boldsymbol{\theta}'_{\boldsymbol{a}}|\widetilde{\boldsymbol{\theta}})} \frac{\pi(\widetilde{\boldsymbol{\theta}'})}{\pi(\widetilde{\boldsymbol{\theta}})}\right).$$

  if *after burn-in* **then**
    Update $\mathcal{S} \leftarrow \mathcal{S} \cup \{\boldsymbol{\theta}\}$
  end if
end loop
Output: $\mathcal{S}$

5.1 Convergence Analysis for EDULA

Since EDULA does not have the target as the stationary distribution, we establish mixing bounds for it in two steps. We first prove that when both the stepsizes (α , α_a) tend to zero, the asymptotic bias of EDULA is zero for target distribution $\tilde{\pi} \propto e^{(U(\boldsymbol{\theta}) - \frac{1}{2\eta}\|\boldsymbol{\theta}-\boldsymbol{\theta}_a\|^2)}$[2]

Proposition 5.4. *Under Assumptions 5.1 and 5.3, the Markov chain as defined in equation 9 is reversible with respect to some distribution π_γ and π_γ converges weakly to π as $\alpha \to 0$ and $\alpha_a \to 0$. Further, for any $\frac{2}{M} > \alpha > 0, \alpha_a > 0$,*

$$\|\pi_\gamma - \tilde{\pi}\|_1 \leq Z \exp\left((\tfrac{M}{4} - \tfrac{1}{2\alpha})\delta(\boldsymbol{\Theta})^2 + \frac{\Delta(\boldsymbol{\Theta},\boldsymbol{\Theta_a})^2 - \vartheta(\boldsymbol{\Theta},\boldsymbol{\Theta_a})}{2\eta}\right),$$

where Z is the normalizing constant of $\pi(\boldsymbol{\theta})$.

Sketch of Proof of Proposition 5.4. Since our chain is unadjusted (no MH step), it does not leave $\tilde{\pi}$ invariant. Instead, we identify a "ghost" distribution $\pi_\gamma \propto \tilde{\pi} \cdot e^{\frac{\alpha_a}{8\eta^2}\|\boldsymbol{\theta}-\boldsymbol{\theta}_a\|^2}$ with respect to which q_γ satisfies detailed balance. We then show that the correction factor($Z'_\gamma(\tilde{\boldsymbol{\theta}})$) becomes unity as step sizes $\alpha, \alpha_a \to 0$. This implies pointwise convergence: $\pi_\gamma \to \tilde{\pi}$. Using Scheffé's Lemma, pointwise convergence implies convergence in L_1 norm. Hence, for finite step sizes we bound the distance $\|\pi_\gamma - \tilde{\pi}\|_1$ by expanding the transition kernel and applying the Lipschitz smoothness of ∇U (Assumption 5.1). □

The parameter α_a is consumed during the computation of the stationary distribution π_γ, explicitly not appearing in the bound. However, α_a indirectly influences the geometric terms $\Delta(\boldsymbol{\Theta}, \boldsymbol{\Theta}_a)$ and $\vartheta(\boldsymbol{\Theta}, \boldsymbol{\Theta}_a)$. Larger α_a increases $\Delta^2(\boldsymbol{\Theta}, \boldsymbol{\Theta}_a)$ due to a greater diameter and reduces $\vartheta(\boldsymbol{\Theta}, \boldsymbol{\Theta}_a)$ due to weaker alignment,

[2]Previously we used $p(\widetilde{\boldsymbol{\theta}})$ as generic notation to introduce the concept of auxiliary coupling. Here, we adopt $\tilde{\pi}$ to specifically denote the joint target equilibrium distributions defined by the energy function. This follows the notational convention established in EMCMC.

thereby loosening the bound. In contrast, smaller α_a tightens convergence guarantees. This parallels the observable role of α in the bound, i.e. bias vanishes to 0 as $\alpha \to 0$. Next we establish our main result for EDULA which establishes a bound on how far our Markov chain is from the target given the step-sizes. Consider $\bar{\eta}^*$ to be a constant that can be explicitly computed (see equation 20 in the Appendix).

Theorem 5.5. *Under Assumptions 5.1, and 5.3 in Algorithm 1, Markov chain P exhibits,*

$$\|P^k(x,\cdot) - \tilde{\pi}\|_{TV} \leq (1-\bar{\eta}^*)^k + Z \exp\left((\tfrac{M}{4} - \tfrac{1}{2\alpha})\delta(\boldsymbol{\Theta})^2 + \tfrac{\Delta(\boldsymbol{\Theta},\boldsymbol{\Theta}_a)^2 - \vartheta(\boldsymbol{\Theta},\boldsymbol{\Theta}_a)}{2\eta} \right)$$

Sketch of Proof of Theorem 5.5. The key idea of the proof leverages Proposition 5.4 and the ergodicity of the EDULA chain, as a consequence of Lemma D.6. Lemma D.6 states that the transition kernel for the Markov chain as defined by Algorithm 1 without the accept/reject step satisfies the Doeblin's condition Jones (2004) uniformly over the entire space $\boldsymbol{\Theta} \times \boldsymbol{\Theta}_a$. This allows us to determine that the chain is uniformly ergodic with the rate of convergence completely determined by the minorization coefficient.

The proof for Lemma D.6, follows by lower bounding the transition kernel to obtain the key inequality

$$P(\boldsymbol{\theta}, \cdot) \geq \bar{\eta}^* \mathrm{Unif}(\boldsymbol{\Theta}_a \times \boldsymbol{\Theta})(\cdot)$$

which is a result of examining the behavior of the potential function $U(\cdot)$ around the minimum point in the domain of interest. This allows us to establish the aforementioned rate as $\mathbf{1} - \eta^*$.

However, the convergence as established via lemma D.6 is not to the target but the stationary distribution of the Markov chain which differs from the target. This difference is captured and bounded in Proposition 5.4. Combining, we get the result. □

As mentioned in the Appendix, $\bar{\eta}^* = f(\alpha, \alpha_a, \mathrm{diam}(\boldsymbol{\Theta}), \mathrm{diam}(\boldsymbol{\Theta}_a), \Delta(\boldsymbol{\Theta}_a, \boldsymbol{\Theta}))$, where f is increasing exponentially in the first two arguments and decreasing exponentially in the last three arguments. Theorem 5.5 shows that sufficiently small learning rates bring the samples generated by Algorithm 1 closer to the target distribution. However, excessively small rates hinder convergence by limiting exploration, while large rates cause the sampler to overshoot the target. Thus, choosing an appropriate learning rate is critical for balancing exploration and convergence.

5.2 Convergence Analysis for EDMALA

We establish a non-asymptotic convergence guarantee for EDMALA using a uniform minorization argument.

Theorem 5.6. *Under Assumptions 5.1 ,5.2, and 5.3 , and $\alpha < \frac{2}{M}$ in Algorithm 1, Markov chain P is uniformly ergodic with,*

$$\|P^k(x,\cdot) - \tilde{\pi}\|_{TV} \leq (1-\epsilon_\gamma)^k$$

where, $\epsilon_\gamma = \exp\left\{ -\left(\frac{M}{2} + \frac{1}{\alpha} - \frac{m}{4}\right) diam(\boldsymbol{\Theta})^2 - \frac{1}{2}\|\nabla U(a)\| \, diam(\boldsymbol{\Theta}) - \left(\frac{3\alpha_a}{8\eta^2} + \frac{2}{\eta}\right)\Delta(\boldsymbol{\Theta},\boldsymbol{\Theta}_a)^2 + \frac{\vartheta(\boldsymbol{\Theta},\boldsymbol{\Theta}_a)}{\eta} \right\}$

Sketch of Proof of Theorem 5.6. We establish the convergence rate of the EDMALA chain by proving a uniform minorization condition for its transition kernel P. First, using the Lipschitz smoothness of ∇U (Assumption 5.1) and strong convexity (Assumption 5.2), we first derive a uniform lower bound on the proposal probability $q_\gamma(\widetilde{\boldsymbol{\theta}}'|\widetilde{\boldsymbol{\theta}})$ that holds for any pair of states. Next, we analyze the Metropolis-Hastings acceptance ratio $\rho(\widetilde{\boldsymbol{\theta}}'|\widetilde{\boldsymbol{\theta}})$ and show that the acceptance probability is uniformly bounded away from zero. Finally, we combine the bounds on the proposal and acceptance ratio, and show that the transition kernel satisfies $P(\widetilde{\boldsymbol{\theta}}'|\widetilde{\boldsymbol{\theta}}) \geq \epsilon\nu(\widetilde{\boldsymbol{\theta}}')$ for a probability measure ν and constant $\epsilon > 0$. This uniform Doeblin condition implies that the chain is uniformly ergodic, converging to its stationary distribution $\tilde{\pi}$ at a geometric rate $(1-\epsilon)^k$. □

One notices, ϵ_γ is exponentially decreasing in the size of the set, $\boldsymbol{\Theta}$, its distance from $\boldsymbol{\Theta}_a$. Further, as $\alpha \to 0$, $\epsilon_\gamma \to 0$, causing the convergence factor $1 - \epsilon_\gamma$ to approach 1. This slows the convergence rate, as the chain takes longer to approach the stationary distribution. Further, for $\eta \to \infty$ (weaker coupling), the bounds in

Proposition 5.4 and Theorem 5.6 align with those of DULA (Zhang et al., 2022) and DMALA (Pynadath et al., 2024), respectively. Note that the convergence of the chains for both EDULA and EDMALA imply convergence of the marginals as the projection maps are continuous. In fact, deriving a rate of convergence for them is also possible, but we omit it here as that is not the goal of this paper. We focus our analysis on the joint distribution to better capture the flatness-seeking behavior induced by the auxiliary variable(as in Theorem 1 in Li & Zhang (2024)). We shed some light on EDLP's finite-time behavior in Appendix section E.1.

6 Experiments

We conducted an empirical evaluation of the Entropic Discrete Langevin Proposal (EDLP) to demonstrate its effectiveness in sampling from flat regions compared to existing discrete samplers. Our experimental setups mainly follow Zhang et al. (2022). EDLP is benchmarked against a range of popular baselines, including Gibbs sampling, Gibbs with Gradient (GWG) (Grathwohl et al., 2021), Hamming Ball (HB) (Titsias & Yau, 2017), Discrete Unadjusted Langevin Algorithm (DULA), and Discrete Metropolis-Adjusted Langevin Algorithm (DMALA) (Zhang et al., 2022). We retain Zhang et al. (2022)'s notation for consistency: Gibbs-X for Gibbs sampling, GWG-X for Gibbs with Gradient, and HB-X-Y for Hamming Ball. To the best of our knowledge, fBP (Baldassi et al., 2016) is the only algorithm that targets flat regions in discrete spaces. However, it is not directly comparable to EDLP and the other samplers in our study due to methodological and practical reasons (see Appendix C for details).

6.1 Motivational Synthetic Example

We consider sampling from a joint quadrivariate Bernoulli distribution. Let $\boldsymbol{\theta} = (\theta_1, \theta_2, \theta_3, \theta_4)$ be a 4-dimensional binary random vector, where each $\theta_i \in \{0, 1\}$. The joint probability distribution is specified by $p_{\boldsymbol{\theta}}$, which represents the probability of the vector $(\theta_1, \theta_2, \theta_3, \theta_4)$. For a given state $\boldsymbol{\theta}$, energy function is given by :

$$U(\boldsymbol{\theta}) = \sum_{a \in \{0,1\}^4} \left(\prod_{n=1}^{4} \theta_n^{a_n} (1 - \theta_n)^{1 - a_n} \right) \ln p_a,$$

The target distribution over the 4D Joint Bernoulli space contains both sharp and flat modes, each analyzed over their 1-Hamming distance neighborhoods. Sharp modes, such as 0010 and 0111, have high probability mass but are surrounded by neighbors with significantly lower probabilities, indicating steep local gradients. In contrast, flat modes like 0100 and 1001 are characterized by relatively uniform probabilities among their immediate neighbors, reflecting smoother local geometry. For the true target distribution's visualization refer to Figure 9 in Appendix E.1. We ran 4 chains of DULA, EDULA, DMALA, and EDMALA in parallel for 1000 iterations, with an initial burn of 200. From Figure 2, EDMALA and EDULA demonstrate a strong preference to visit flat modes, without becoming stuck in the high-probability sharp modes. In contrast, DULA and DMALA show a bias toward the sharp modes, showing to be less adept at exploring the flat areas where the probability mass is more evenly distributed. Despite showing flatness bias, entropic samplers still achieve well-matching samples to the target distribution.

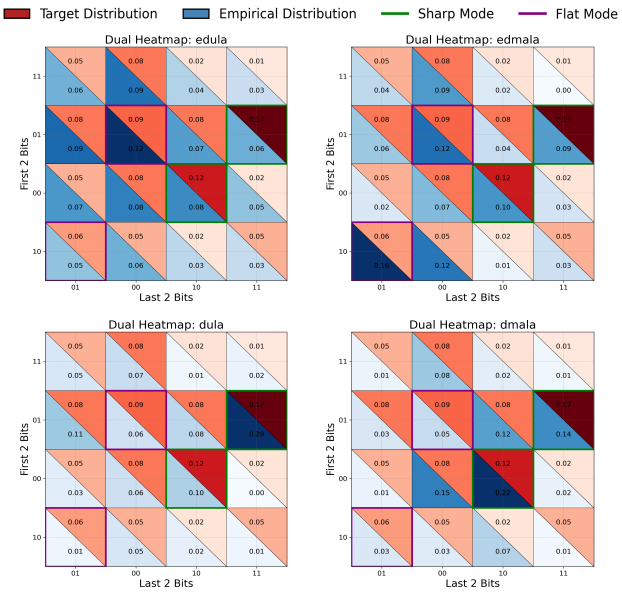

Figure 2: Overlap heatmaps demonstrating EDLP's flatness preference over DLP.

6.2 Sampling for Traveling Salesman Problems

In TSP, the objective is to find the shortest route visiting n cities exactly once and returning to the origin, choosing from $n!$ paths. However, in practical logistics and routing, structural stability and cost similarity are sometimes of greater interest than raw optimality. A sharp global minimum is brittle; if a single edge becomes infeasible (e.g., due to road closures or driving preference), re-optimization might yield a completely disjoint route , disrupting downstream logistics (Laporte, 2009; Golden et al., 2008). Therefore, in practice, the cost function is often an incomplete proxy for complex, unmodeled constraints—such as driver familiarity, road safety, or dynamic traffic patterns. Consequently, our goal here shifts from pure minimization to reliable candidate generation.

We posit that flat modes in the solution landscape naturally model robust solution basins. A flat mode corresponds to a cluster of similar-cost tours that share a high degree of structural similarity (i.e., they share many common edges). Practitioners may perform a post-hoc check to verify if the identified cluster falls within their budgetary constraints (Pugh et al., 2016; Marler & Arora, 2004). This selection eventually creates a safety buffer, allowing practitioners to choose from options based on unmodeled constraints without fear that a minor structural deviation will cause a catastrophic violation of the budget (Groër et al., 2009). Thus, sampling from flat basins allows us to implicitly impose the similarity constraint, proposing a "menu of high-quality options".

In standard TSP, $U(\boldsymbol{\theta})$ is designed to capture the total cost of a particular route configuration $\boldsymbol{\theta} = (\theta_1, \theta_2, \ldots, \theta_n)$. The expression of $U(\boldsymbol{\theta})$ is:

$$U(\boldsymbol{\theta}) = -\Big(\textstyle\sum_{i=1}^{n-1} \sqrt{(x_i - x_{i+1})^2 + (y_i - y_{i+1})^2} + \sqrt{(x_n - x_1)^2 + (y_n - y_1)^2} \Big),$$

where each city location is given by $\theta_i = (x_i, y_i) \in \mathbb{R}^2$. The final term, $\sqrt{(x_n - x_1)^2 + (y_n - y_1)^2}$, ensures that the route forms a closed loop, thereby completing the tour. We use the *eil30* dataset, a 30-city problem extracted from the 51-city Christofides/Eilon instance, available in the TSPLIB95 benchmark repository, first introduced in Reinelt (1991). The dataset consists of 2D Euclidean coordinates of cities and is publicly available.[3] Each solution is represented as a binary square matrix of size n, where each row corresponds to a position in the tour and each column corresponds to a city, with $|\boldsymbol{\Theta}| = 2.6525 \times 10^{32}$. If a proposed solution violates the uniqueness of city visits, we reject the sample and retain the current solution. We run our samplers for 100000 iterations with 50 refinements per sample, and burn 2000 initial iterations.

Table 1: EDLP finding cost-wise and structure-wise similar solutions than DLP.

Sampler	**PMC (↓)**	**Jaccard Similarity (↑)**	**Range of Cost (↓)**
DULA	413.07 ± 94.92	0.0917 ± 0.1546	336.57
DMALA	249.65 ± 104.61	0.3341 ± 0.2060	198.12
EDULA	349.92 ± 114.71	0.1704 ± 0.1993	194.75
EDMALA	$\mathbf{178.93 \pm 81.03}$	$\mathbf{0.4818 \pm 0.1790}$	**62.51**

We report the PMC(Pairwise Mismatch Count) inspired by Pairwise Order Discrepancy (Zaefferer et al., 2014; Liao et al., 2012) and Kendall's Tau (Fagin et al., 2003), and Jaccard similarity (Li et al., 2022), and the Range of Cost(difference between maximum and minimum of negative of $U(\boldsymbol{\theta})$), after collecting solutions for each sampler. From Table 1, by guiding the sampling trajectory towards flat modes, EDLP yields a set of routes that are not only cost-wise similar but also robust to local perturbations, a property that pure cost-minimization fails to capture. We offer additional insights in Appendix E.2.

6.3 Sampling From Restricted Boltzmann Machines

Restricted Boltzmann Machines (RBMs) are a class of generative stochastic neural networks that learn a probability distribution over their input data. The energy function for an RBM, which defines the joint

[3]GitHub Repository: `https://github.com/jam7/tsp/tree/master`; TSPLIB Archive: `http://comopt.ifi.uni-heidelberg.de/software/TSPLIB95/`.

configuration of visible and hidden units, is given by:

$$U(\boldsymbol{\theta}) = \sum_i \text{Softplus}(\mathbf{W}\boldsymbol{\theta} + a)_i + b^\top \boldsymbol{\theta},$$

where $\{\mathbf{W}, a, b\}$ are the weight matrix and bias parameters, respectively, and $\boldsymbol{\theta} \in \{0, 1\}^d$ represents the binary state of the visible units.

When the RBM assigns high probability to specific digit representations, a sharp mode for digit 3 (for instance) might appear as an idealized version without extraneous strokes. This configuration represents the model's interpretation of a quintessential '3' with a prominent probability peak. Any minor alteration, like flipping a single pixel, lowers the altered image's probability. The sampler has thus learned to prioritize exact, pristine versions of each digit, marking any deviation from this high-probability state as unlikely.

For MNIST, this narrow focus limits flexibility. The model assigns high probability to only a few "perfect" digit versions, treating minor variations as less probable. This rigidity makes the generated images sensitive to small changes and limits the RBM's ability to recognize natural, varied handwriting. In the context of RBMs, sampling from flat modes explores a wider range of latent handwritten styles, enhancing the model's ability to capture the underlying data distribution. This reflects a broader representation of possible input variations, crucial for tasks like image generation and data reconstruction (Murray et al., 2009). In practice, this means that images generated from flat modes in RBMs are less likely to overfit to sharp, specific patterns in the training data and are instead more reflective of the variability inherent in the dataset.

In our experiments, we generated 5000 images per sampler for the MNIST dataset, applying a thinning factor of 1000 to ensure diversity in the samples. A simple convolutional autoencoder (CAE) was used for image generation and reconstruction, allowing us to evaluate the performance and generalization capability of sampler-generated data. To assess robustness, we trained 5 CAEs on the sampler-generated images and tested them under various conditions. Initially, clean test data was used to establish baseline performance. Subsequently, we introduced Gaussian noise (with a noise factor of 0.1) to evaluate the models' resilience against perturbations, a common method for assessing adversarial robustness (Madry et al., 2018). Additionally, we examined the models with occluded images, where random sections of the images were obscured by zero-valued pixel blocks. This test simulates scenarios with missing or obstructed information, a widely used technique in robustness studies to measure model performance under partial information loss (Zhang et al., 2019). For quantitative evaluation, we rely on log-likelihood to directly measure how well our method captures the underlying data distribution and, therefore, its ability to generalize.

Table 2: EDMALA attaining the highest average log-likelihood across 3 distinct settings on MNIST.

Setting	**BG-1**	**HB-10-1**	**DULA**	**DMALA**	**EDULA**	**EDMALA**
Clean	-0.0157 ± 0.0014	-0.0134 ± 0.0009	-0.0209 ± 0.0015	-0.0156 ± 0.0011	-0.0112 ± 0.0013	**-0.0066** ± 0.0014
Noisy	0.0144 ± 0.0013	0.0165 ± 0.0011	0.0097 ± 0.0013	0.0148 ± 0.0009	0.0183 ± 0.0010	**0.0233** ± 0.0010
Occluded	-0.0179 ± 0.0013	-0.0154 ± 0.0008	-0.0233 ± 0.0014	-0.0182 ± 0.0010	-0.0138 ± 0.0013	**-0.0098** ± 0.0015

The results in Table 2 indicate that EDLP methods consistently outperform their non-entropic counterparts across all test settings; EDULA improves over DULA by 46.4%, 88.7%, and 40.8% , and EDMALA improves over DMALA by 57.7%, 57.4%, and 46.2% respectively across clean, noisy, and occluded settings. Overall, EDMALA achieves the best log-likelihood across all settings. This suggests that entropy guidance helps with superior generalization capabilities, making it especially effective for reconstructing unseen data accurately. We provide additional results in the Appendix E.3.

6.4 Binary Bayesian Neural Networks

Binary Bayesian Neural Networks (BBNNs) provide a compelling framework for deploying deep learning models in resource-constrained environments. By constraining weights to binary states ($\{-1, +1\}$), these networks can theoretically achieve a $32\times$ reduction in memory footprint compared to standard 32-bit floating-point networks, and significant acceleration via bitwise operations (Courbariaux et al., 2016; Hubara et al., 2017). Inspired by recent advances like BNN-SAM (Pu et al., 2024), which show that converging to flat

minima is crucial for generalization in binary and discrete settings, we leverage our discrete sampling technique to target these robust regions. In particular, we explore the training of BBNNs on regression tasks across four UCI datasets (Dua & Graff, 2017). The energy function for each dataset is defined as:

$$U(\boldsymbol{\theta}) = -\sum_{i=1}^{N} ||f_{\boldsymbol{\theta}}(x_i) - y_i||^2,$$

where $D = \{x_i, y_i\}_{i=1}^N$ is the training dataset, and $f_{\boldsymbol{\theta}}$ denotes a two-layer neural network with `Tanh` activation and 500 hidden neurons. After burning initial samples, we calculate and report the average test RMSE (root mean squared error) and its standard deviation. As shown in Table 3, EDMALA consistently outperform all baselines across **all** datasets. Overall, these results confirm that our method enhances generalization performance on unseen test data. We provide additional results and hyperparameter settings in the Appendix E.4.

Table 3: EDMALA achieving least average test RMSE for various datasets.

Dataset	**Gibbs**	**GWG**	**DULA**	**DMALA**	**EDULA**	**EDMALA**
COMPAS	0.4850 ±0.0077	0.4779 ± 0.0063	0.4853 ±0.0044	0.4855 ±0.0047	0.4789 ±0.0066	**0.4693** ±0.0018
News	0.1051 ±0.0007	0.1067 ±0.0010	0.0977±0.0040	0.0969 ±0.0040	0.0952 ±0.0038	**0.0948** ±0.0033
Adult	0.4940 ±0.0041	0.4861 ±0.0064	0.4041 ±0.0035	0.3949 ±0.0108	0.3952 ±0.0031	**0.3898** ±0.0024
Blog	0.4295 ±0.0092	0.4051 ±0.0205	0.3220 ±0.0091	0.3198 ±0.0097	0.3197 ±0.0032	**0.3172** ±0.0028

7 Discussion

Limitations. Since EDLP collects only discrete samples, it produces half as many samples per iteration as EMCMC. The coupling mechanism in Section 4.1 increases the computational load relative to DLP. However, as Li & Zhang (2024) state in their Section 4.2, the cost of gradient computation remains the same for d-dimensional models when $\widetilde{\boldsymbol{\theta}}$ resides in a $2d$ dimensional space. EDLP doubles memory usage compared to DLP, but the space complexity remains linear in d, ensuring scalability.

Conclusion. We propose a simple and computationally efficient gradient-based sampler designed for sampling from flat modes in discrete spaces. The algorithm leverages a guiding variable based on local entropy. We provide non-asymptotic convergence guarantees for both the unadjusted and Metropolis-adjusted versions. Empirical results on real-world datasets demonstrate the practical effectiveness of our method across a variety of applications. We hope our framework highlights the importance of flat-mode sampling in discrete systems, with broad utility across scientific and machine learning domains.

Bibliography

James H. Albert and Siddhartha Chib. Bayesian analysis of binary and polychotomous response data. *Journal of the American Statistical Association*, 88(422):669–679, 1993.

Michael Arbel, Liang Zhou, and Arthur Gretton. Generalized energy based models. In *International Conference on Learning Representations*, 2021.

Carlo Baldassi, Christian Borgs, Jennifer T Chayes, Alessandro Ingrosso, Carlo Lucibello, Luca Saglietti, and Riccardo Zecchina. Unreasonable effectiveness of learning neural networks: From accessible states and robust ensembles to basic algorithmic schemes. *Proceedings of the National Academy of Sciences*, 113(48): E7655–E7662, 2016.

Carlo Baldassi, Fabrizio Pittorino, and Riccardo Zecchina. Shaping the learning landscape in neural networks around wide flat minima. *Proceedings of the National Academy of Sciences*, 117(1):161–170, 2019.

Julian Besag. Spatial interaction and the statistical analysis of lattice systems. *Journal of the Royal Statistical Society: Series B (Methodological)*, 36(2):192–225, 1974.

Léon Bottou, Frank E Curtis, and Jorge Nocedal. Optimization methods for large-scale machine learning. *Siam Review*, 60(2):223–311, 2018.

Steve Brooks, Andrew Gelman, Galin Jones, and Xiao-Li Meng. *Handbook of Markov Chain Monte Carlo*. Chapman and Hall/CRC, May 2011. ISBN 9780429138508. doi: 10.1201/b10905. URL `http://dx.doi.org/10.1201/b10905`.

George Casella and Edward I George. Explaining the gibbs sampler. *The American Statistician*, 46(3): 167–174, 1992.

Wei-Kai Chang and Rajiv Khanna. A unified stability analysis of SAM vs SGD: Role of data coherence and emergence of simplicity bias. In *The Thirty-ninth Annual Conference on Neural Information Processing Systems*, 2025. URL `https://openreview.net/forum?id=HdY8CCHife`.

Pratik Chaudhari, Anna Choromanska, Stefano Soatto, Yann LeCun, Carlo Baldassi, Christian Borgs, Jennifer Chayes, Levent Sagun, and Riccardo Zecchina. Entropy-sgd: Biasing gradient descent into wide valleys. *Journal of Statistical Mechanics: Theory and Experiment*, 2019(12):124018, 2019.

Yongxin Chen, Sinho Chewi, Adil Salim, and Andre Wibisono. Improved analysis for a proximal algorithm for sampling. In Po-Ling Loh and Maxim Raginsky (eds.), *Proceedings of Thirty Fifth Conference on Learning Theory*, volume 178 of *Proceedings of Machine Learning Research*, pp. 2984–3014. PMLR, 02–05 Jul 2022. URL `https://proceedings.mlr.press/v178/chen22c.html`.

Matthieu Courbariaux, Itay Hubara, Daniel Soudry, Ran El-Yaniv, and Yoshua Bengio. Binarized neural networks: Training deep neural networks with weights and activations constrained to+ 1 or-1. *arXiv preprint arXiv:1602.02830*, 2016.

Arnak Dalalyan. Further and stronger analogy between sampling and optimization: Langevin monte carlo and gradient descent. In *Conference on Learning Theory*, pp. 678–689. PMLR, 2017.

Jacob Devlin, Ming-Wei Chang, Kenton Lee, and Kristina Toutanova. Bert: Pre-training of deep bidirectional transformers for language understanding. *arXiv preprint arXiv:1810.04805*, 2019.

Jean Diebolt and Christian P Robert. Estimation of finite mixture distributions through bayesian sampling. *Journal of the Royal Statistical Society: Series B (Methodological)*, 56(2):363–375, 1994.

Dheeru Dua and Casey Graff. UCI machine learning repository, 2017. URL `http://archive.ics.uci.edu/ml`.

Alain Durmus and Éric Moulines. Nonasymptotic convergence analysis for the unadjusted Langevin algorithm. *The Annals of Applied Probability*, 27(3):1551 – 1587, 2017a. doi: 10.1214/16-AAP1238. URL `https://doi.org/10.1214/16-AAP1238`.

Alain Durmus and Eric Moulines. Nonasymptotic convergence analysis for the unadjusted langevin algorithm. *The Annals of Applied Probability*, 27(3):1551–1587, 2017b.

Alain Durmus, Szymon Majewski, and Błażej Miasojedow. Analysis of langevin monte carlo via convex optimization. *J. Mach. Learn. Res.*, 20(1):2666–2711, January 2019. ISSN 1532-4435.

Cynthia Dwork, Frank McSherry, Kobbi Nissim, and Adam Smith. Calibrating noise to sensitivity in private data analysis. In *Theory of Cryptography Conference*, pp. 265–284. Springer, 2006.

Karl Oskar Ekvall and Galin L. Jones. Convergence analysis of a collapsed Gibbs sampler for Bayesian vector autoregressions. *Electronic Journal of Statistics*, 15(1):691 – 721, 2021. doi: 10.1214/21-EJS1800. URL `https://doi.org/10.1214/21-EJS1800`.

Ronald Fagin, Ravi Kumar, and Dandapani Sivakumar. Comparing top k lists. *SIAM Journal on Discrete Mathematics*, 17(1):134–160, 2003.

E Gardner. The space of interactions in neural network models. *Journal of Physics A: Mathematical and General*, 21(1):257, jan 1988. doi: 10.1088/0305-4470/21/1/030. URL `https://doi.org/10.1088/0305-4470/21/1/030`.

Charles J Geyer. Markov chain monte carlo maximum likelihood. In *Computing Science and Statistics*, 1991.

Bruce Golden, S Raghavan, and Edward Wasil. *The vehicle routing problem: Latest advances and new challenges*. Springer Science & Business Media, 2008.

Ian Goodfellow, Jean Pouget-Abadie, Mehdi Mirza, Bing Xu, David Warde-Farley, Sherjil Ozair, Aaron Courville, and Yoshua Bengio. Generative adversarial nets. In *Advances in neural information processing systems*, pp. 2672–2680, 2014.

Will Grathwohl, Kevin Swersky, Milad Hashemi, David Duvenaud, and Chris J Maddison. Oops i took a gradient: Scalable sampling for discrete distributions. *International Conference on Machine Learning*, 2021.

Ulf Grenander and Michael I Miller. Representations of knowledge in complex systems. *Journal of the Royal Statistical Society: Series B (Methodological)*, 56(4):549–581, 1994.

Chris Groër, Bruce Golden, and Edward Wasil. The consistent vehicle routing problem. *Manufacturing & Service Operations Management*, 11(4):630–643, October 2009. ISSN 1526-5498. doi: 10.1287/msom.1080.0243. URL `https://doi.org/10.1287/msom.1080.0243`.

Jiatao Gu, James Bradbury, Caiming Xiong, Victor OK Li, and Richard Socher. Non-autoregressive neural machine translation. In *International Conference on Learning Representations*, 2018.

Mangesh Gupte and Mukund Sundararajan. Universally optimal privacy mechanisms for minimax agents. In *Proceedings of the Twenty-Ninth ACM SIGMOD-SIGACT-SIGART Symposium on Principles of Database Systems*, PODS '10, pp. 135–146, New York, NY, USA, 2010. Association for Computing Machinery. ISBN 9781450300339. doi: 10.1145/1807085.1807105. URL `https://doi.org/10.1145/1807085.1807105`.

W Keith Hastings. Monte carlo sampling methods using markov chains and their applications. *Biometrika*, 1970.

Sepp Hochreiter and Jürgen Schmidhuber. Simplifying neural nets by discovering flat minima. *Advances in neural information processing systems*, 7, 1994.

Sepp Hochreiter and Jürgen Schmidhuber. Flat minima. *Neural computation*, 9(1):1–42, 1997.

Itay Hubara, Matthieu Courbariaux, Daniel Soudry, Ran El-Yaniv, and Yoshua Bengio. Quantized neural networks: Training neural networks with low precision weights and activations. *The Journal of Machine Learning Research*, 18(1):6869–6898, 2017.

Pavel Izmailov, Sharad Vikram, Matthew D Hoffman, and Andrew Gordon Gordon Wilson. What are bayesian neural network posteriors really like? In *International conference on machine learning*, pp. 4629–4640. PMLR, 2021.

Eric Jang, Shixiang Gu, and Ben Poole. Categorical reparameterization with gumbel-softmax, 2017. URL https://arxiv.org/abs/1611.01144.

Galin L. Jones. On the Markov chain central limit theorem. *Probability Surveys*, 1(none):299 – 320, 2004. doi: 10.1214/154957804100000051. URL https://doi.org/10.1214/154957804100000051.

Gilbert Laporte. Fifty years of vehicle routing. *Transportation Science*, 43(4):408–416, 2009.

Yann LeCun, John S Denker, and Sara A Solla. Optimal brain damage. In *Advances in neural information processing systems*, pp. 598–605, 1990.

Yann LeCun, Léon Bottou, Yoshua Bengio, and Patrick Haffner. Gradient-based learning applied to document recognition. *Proceedings of the IEEE*, 86(11):2278–2324, 1998.

Mike Lewis, Yinhan Liu, Naman Goyal, Marjan Ghazvininejad, Abdelrahman Mohamed, Omer Levy, Veselin Stoyanov, and Luke Zettlemoyer. Bart: Denoising sequence-to-sequence pre-training for natural language generation, translation, and comprehension. *arXiv preprint arXiv:1910.13461*, 2020.

Bolian Li and Ruqi Zhang. Entropy-MCMC: Sampling from flat basins with ease. In *Proceedings of the Twelfth International Conference on Learning Representations*, 2024.

Hui Li, Mengyao Zhang, and Chenbo Zeng. Circular jaccard distance-based multi-solution optimization for traveling salesman problems. *Mathematical Biosciences and Engineering*, 19(5):4458–4480, 2022.

Muheng Li and Ruqi Zhang. Reheated gradient-based discrete sampling for combinatorial optimization. *Transactions on Machine Learning Research*, 2025.

Jiaming Liang and Yongxin Chen. A proximal algorithm for sampling. *Transactions on Machine Learning Research*, 2023. ISSN 2835-8856. URL https://openreview.net/forum?id=CkXOwlhf27.

Yen-Far Liao, Dun-Han Yau, and Chieh-Li Chen. Evolutionary algorithm to traveling salesman problems. *Computers Mathematics with Applications*, 64(5):788–797, 2012. ISSN 0898-1221. doi: https://doi.org/10.1016/j.camwa.2011.12.018. URL https://www.sciencedirect.com/science/article/pii/S089812211101073X. Advanced Technologies in Computer, Consumer and Control.

Chris J. Maddison, Andriy Mnih, and Yee Whye Teh. The concrete distribution: A continuous relaxation of discrete random variables, 2017. URL https://arxiv.org/abs/1611.00712.

Aleksander Madry, Aleksandar Makelov, Ludwig Schmidt, Dimitris Tsipras, and Adrian Vladu. Towards deep learning models resistant to adversarial attacks. In *6th International Conference on Learning Representations, ICLR 2018*, 2018.

R. Timothy Marler and Jasbir S. Arora. Survey of multi-objective optimization methods for engineering. *Structural and Multidisciplinary Optimization*, 26(6):369–395, 2004. doi: 10.1007/s00158-003-0368-6.

James Martens and Ilya Sutskever. Parallelizable sampling of markov random fields. In Yee Whye Teh and Mike Titterington (eds.), *Proceedings of the Thirteenth International Conference on Artificial Intelligence and Statistics*, volume 9 of *Proceedings of Machine Learning Research*, pp. 517–524, Chia Laguna Resort, Sardinia, Italy, 13–15 May 2010. PMLR. URL https://proceedings.mlr.press/v9/martens10a.html.

Nicholas Metropolis, Arianna W Rosenbluth, Marshall N Rosenbluth, Augusta H Teller, and Edward Teller. Equation of state calculations by fast computing machines. *The journal of chemical physics*, 21(6):1087–1092, 1953.

Iain Murray, Ruslan Salakhutdinov, and Geoffrey Hinton. Evaluating rbm approximations: Contrastive divergence vs. alternative approaches. *Neural Computation*, 2009.

Radford M Neal. Markov chain sampling methods for dirichlet process mixture models. *Journal of Computational and Graphical Statistics*, 9(2):249–265, 2000.

Radford M Neal. Slice sampling. *Annals of statistics*, 2003.

Ari Pakman and Liam Paninski. Auxiliary-variable exact hamiltonian monte carlo samplers for binary distributions. In *Proceedings of the 27th International Conference on Neural Information Processing Systems - Volume 2*, NIPS'13, pp. 2490–2498, Red Hook, NY, USA, 2013. Curran Associates Inc.

Marcelo Pereyra. Proximal markov chain monte carlo algorithms. *Statistics and Computing*, 26:745–760, 2016.

Jorn WT Peters and Max Welling. Probabilistic binary neural networks. *arXiv preprint arXiv:1809.03368*, 2018.

Fabrizio Pittorino, Carlo Lucibello, Christoph Feinauer, Gabriele Perugini, Carlo Baldassi, Elizaveta Demyanenko, and Riccardo Zecchina. Entropic gradient descent algorithms and wide flat minima. In *International Conference on Learning Representations*, 2020.

H. Pu, D. Zhang, K. Xu, R. Mo, Z. Yan, and D. Wang. Bnn-sam: Improving generalization of binary object detector by seeking flat minima. *Applied Intelligence*, 54(8):6682–6700, 2024. doi: 10.1007/s10489-024-05512-z.

Justin K. Pugh, L. B. Soros, and Kenneth O. Stanley. Quality diversity: A new frontier for evolutionary computation. *Frontiers in Robotics and AI*, 3:40, 2016. doi: 10.3389/frobt.2016.00040.

Patrick Pynadath, Riddhiman Bhattacharya, ARUN NARAYANAN HARIHARAN, and Ruqi Zhang. Gradient-based discrete sampling with automatic cyclical scheduling. In *ICML 2024 Workshop on Structured Probabilistic Inference & Generative Modeling*, 2024. URL `https://openreview.net/forum?id=aTDId2TrtL`.

Maxim Raginsky, Alexander Rakhlin, and Matus Telgarsky. Non-convex learning via stochastic gradient langevin dynamics: a nonasymptotic analysis. In Satyen Kale and Ohad Shamir (eds.), *Proceedings of the 2017 Conference on Learning Theory*, volume 65 of *Proceedings of Machine Learning Research*, pp. 1674–1703. PMLR, 07–10 Jul 2017. URL `https://proceedings.mlr.press/v65/raginsky17a.html`.

Gerhard Reinelt. Tsplib—a traveling salesman problem library. *ORSA Journal on Computing*, 3(4):376–384, 1991. doi: 10.1287/ijoc.3.4.376.

Benjamin Rhodes and Michael U. Gutmann. Enhanced gradient-based MCMC in discrete spaces. *Transactions on Machine Learning Research*, 2022. ISSN 2835-8856. URL `https://openreview.net/forum?id=j2Mid5hFUJ`.

Gareth O. Roberts and Jeffrey S. Rosenthal. Langevin diffusions and metropolis-hastings algorithms. *Methodology and Computing in Applied Probability*, 4(4):337–357, 2002.

Gareth O Roberts and Richard L Tweedie. Exponential convergence of langevin distributions and their discrete approximations. *Bernoulli*, pp. 341–363, 1996.

Tim Salimans, Ian Goodfellow, Wojciech Zaremba, Vicki Cheung, Alec Radford, and Xi Chen. Improved techniques for training gans. In *Advances in neural information processing systems*, volume 29, pp. 2234–2242, 2016.

Jay Shendure and Hanlee Ji. Next-generation dna sequencing. *Nature biotechnology*, 26(10):1135–1145, 2008.

Haoran Sun, Hanjun Dai, Wei Xia, and Arun Ramamurthy. Path auxiliary proposal for mcmc in discrete space. In *International Conference on Learning Representations*, 2022.

Haoran Sun, Hanjun Dai, Bo Dai, Haomin Zhou, and Dale Schuurmans. Discrete langevin samplers via wasserstein gradient flow. In *International Conference on Artificial Intelligence and Statistics*, pp. 6290–6313. PMLR, 2023.

Richard S Sutton and Andrew G Barto. *Reinforcement learning: An introduction*. MIT press, 2018.

Robert H Swendsen and Jian-Sheng Wang. Nonuniversal critical dynamics in monte carlo simulations. *Physical Review Letters*, 1987.

Michalis K Titsias and Christopher Yau. The hamming ball sampler. *Journal of the American Statistical Association*, 112(520):1598–1611, 2017.

Paolo Toth and Daniele Vigo. The vehicle routing problem. *Society for Industrial and Applied Mathematics*, 2002.

Avraam Tsantekidis, Nikolaos Passalis, Anastasios Tefas, Juho Kanniainen, Moncef Gabbouj, and Alexandros Iosifidis. Forecasting stock prices from the limit order book using convolutional neural networks. pp. 7–12, 07 2017. doi: 10.1109/CBI.2017.23.

Zhou Wang, Alan C Bovik, Hamid R Sheikh, and Eero P Simoncelli. Image quality assessment: From error visibility to structural similarity. *IEEE transactions on image processing*, 13(4):600–612, 2004.

Martin Zaefferer, Jörg Stork, and Thomas Bartz-Beielstein. Distance measures for permutations in combinatorial efficient global optimization. In Thomas Bartz-Beielstein, Jürgen Branke, Bogdan Filipič, and Jim Smith (eds.), *Parallel Problem Solving from Nature – PPSN XIII*, pp. 373–383, Cham, 2014. Springer International Publishing. ISBN 978-3-319-10762-2.

Giacomo Zanella. Informed proposals for local mcmc in discrete spaces. *Journal of the American Statistical Association*, 115(530):852–865, 2020.

Hongyang Zhang, Yaodong Yu, Jiantao Jiao, Eric Xing, Laurent El Ghaoui, and Michael I Jordan. Theoretically principled trade-off between robustness and accuracy. *arXiv preprint arXiv:1901.08573*, 2019.

Ruqi Zhang, Xingchao Liu, and Qiang Liu. A langevin-like sampler for discrete distributions. In *International Conference on Machine Learning*, pp. 26375–26396. PMLR, 2022.

All experiments were run on a single RTX A6000.

A Analysis of the Effect of Flatness Parameter η

A.1 Intuition

Figure 3 illustrates the effect of varying the flatness parameter η on the probability distribution $p(\boldsymbol{\theta}_a)$ for $\boldsymbol{\theta}$ drawn from a Bernoulli(0.5) distribution. The *layered* curves represent different values of η, showing how the distribution $p(\boldsymbol{\theta}_a)$ changes as η increases.

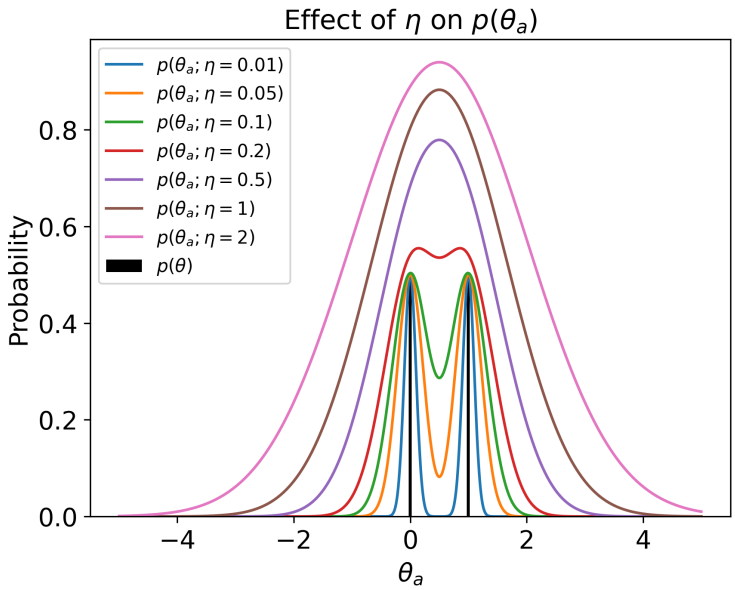

Figure 3: $p(\boldsymbol{\theta_a})$ for $\boldsymbol{\theta} \sim$ *Bernoulli*(0.5)

Effect of Small η (Strong Coupling)

For very small values of η (e.g., $\eta = 0.01$, $\eta = 0.05$, $\eta = 0.1$), the curves (blue, orange, and green) are sharply peaked and closely resemble the original $p(\boldsymbol{\theta})$. Small η values imply strong coupling between $\boldsymbol{\theta}$ and $\boldsymbol{\theta}_a$. The auxiliary distribution $p(\boldsymbol{\theta}_a)$ remains very close to $p(\boldsymbol{\theta})$, indicating that $\boldsymbol{\theta}_a$ is tightly bound to $\boldsymbol{\theta}$, and the variance is minimal.

Moderate η Values (Moderate Coupling)

As η increases (e.g., $\eta = 0.2$), the curves (red) become wider and smoother. These moderate η values adequately capture the flatness of the landscape. The distribution $p(\boldsymbol{\theta}_a)$ starts to diverge from $p(\boldsymbol{\theta})$, allowing $\boldsymbol{\theta}_a$ to explore a broader region around the peaks.

Large η (Weak Coupling)

For larger values of η (e.g., $\eta = 0.5$, $\eta = 1$, $\eta = 2$), the curves (purple, brown, and magenta) are much wider. Large η values imply weak coupling between $\boldsymbol{\theta}$ and $\boldsymbol{\theta}_a$. The auxiliary distribution $p(\boldsymbol{\theta}_a)$ is excessively smoothed out compared to $p(\boldsymbol{\theta})$, indicating that $\boldsymbol{\theta}_a$ can explore a much broader range of values with less influence from $\boldsymbol{\theta}$.

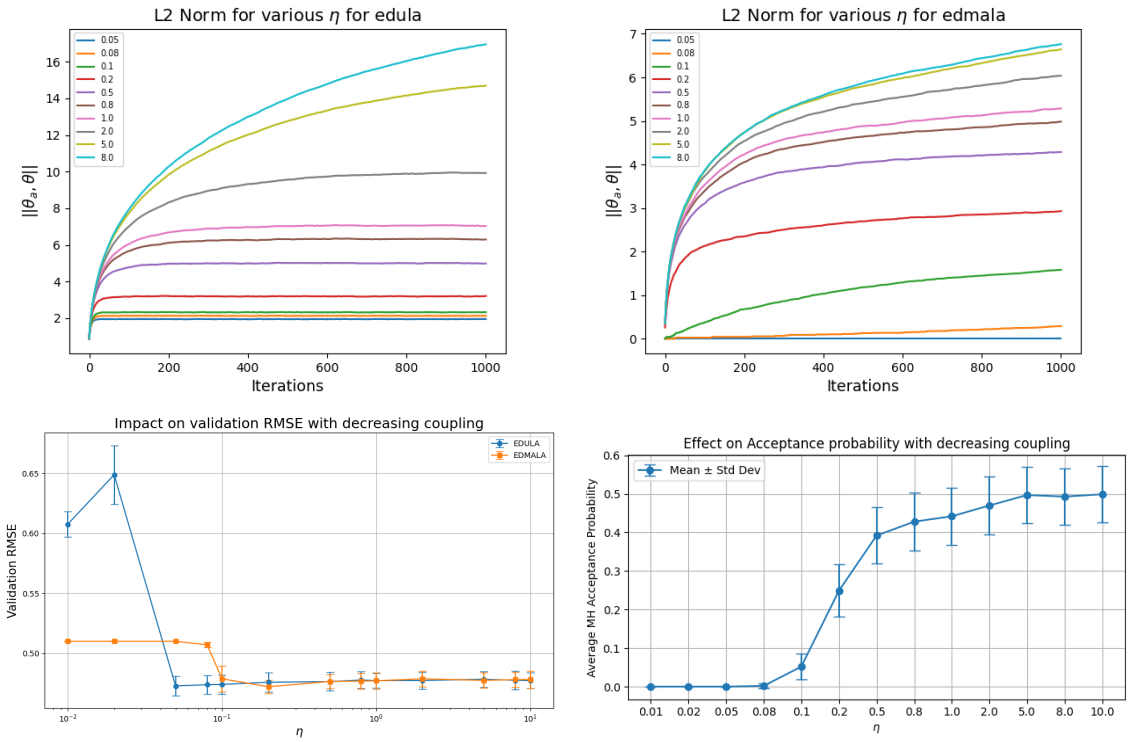

Figure 4: Diagnostics for EDLP

Considerations for η Approaching Infinity

As η approaches infinity, the auxiliary distribution $p(\boldsymbol{\theta}_a)$ flattens, and the gradient $\nabla_{\boldsymbol{\theta}_a} U_\eta(\widetilde{\boldsymbol{\theta}})$ tends toward zero. This results in an extremely weak coupling, effectively causing the EDLP framework to behave similarly to a standard DLP. The parameter η thus plays a critical role in determining the behavior of the sampler, necessitating careful tuning based on the specific requirements of the sampling task.

A.2 Sensitivity Analysis

The flatness parameter η is arguably the most crucial hyperparameter to optimize in the EDLP algorithm (Algorithm 1). Similar to the hyperparameter tuning ablation strategies employed in Li & Zhang (2024) (Appendix, Section E), we conduct hyperparameter tuning on the COMPAS dataset's validation data. Specifically, we monitor the L2 norm between sampled pairs of $\boldsymbol{\theta}$ and $\boldsymbol{\theta}_a$ for various values of η. Additionally, we plot the validation RMSE for both EDULA and EDMALA across different values of η. Finally, we plot the average MH acceptance ratio for EDMALA to assess the impact of η on the joint MH acceptance step. We maintain $\alpha = 0.1$ for both samplers and $\alpha_a = 0.01$ for EDULA and $\alpha_a = 0.001$ for EDMALA(see Figure 4).

We observe that as η increases, the coupling between the variables weakens, allowing both variables to move more freely, thus increasing the norm. This behavior is consistent across both EDULA and EDMALA. However, EDMALA exhibits a more conservative behavior at the same coupling strength compared to EDULA due to the presence of the joint Metropolis-Hastings (MH) acceptance step, which imposes stricter alignment between the variables, hence maintaining a tighter coupling.

Both samplers demonstrate robustness across a wide range of η, with relatively stable validation RMSE performance. However, EDULA shows slightly less robustness, particularly at extremely small coupling values, resulting in increased variability and higher RMSE. EDMALA maintains a stable, consistent performance, indicating better robustness to changes in the coupling parameter.

The final plot shows how the MH acceptance probability varies with coupling strength η for EDMALA. Initially, with very tight coupling , the acceptance probability is near zero, indicating overly restricted movements due to the strong alignment requirement between the discrete and continuous variables. As η increases (coupling relaxes), the acceptance probability rises significantly, reflecting greater freedom in proposing moves that the joint MH criterion accepts. After a certain coupling threshold (around 0.8 here), the acceptance rate plateaus, suggesting diminishing returns from further relaxation in coupling strength. Thus, an intermediate coupling provides a balance, allowing effective exploration without overly compromising the sampler's consistency.

B Gibbs-like Update Procedure

Gibbs-like updating procedures have been widely employed across various contexts in the sampling literature, particularly within Bayesian hierarchical models, latent variable models, and non-parametric Bayesian approaches. For instance, Gibbs sampling is a fundamental technique in hierarchical Bayesian models, where parameters are partitioned into blocks and updated conditionally on others to facilitate efficient sampling (Casella & George, 1992). In latent variable models, such as Hidden Markov Models (HMMs) and mixture models, Gibbs-like updates allow for alternating between sampling latent variables and model parameters, thereby simplifying the overall process (Diebolt & Robert, 1994). Additionally, these updates are crucial in non-parametric Bayesian approaches, such as Dirichlet Process Mixture Models (DPMMs), where they enable the efficient sampling of cluster assignments and hyperparameters (Neal, 2000). Gibbs-like updates are also prominently used in spatial statistics, particularly in Conditional Autoregressive (CAR) models, where the value at each spatial location is updated based on its neighbors (Besag, 1974).

Since our goal is to sample from a joint distribution, rather than simultaneously updating $\boldsymbol{\theta}$ and $\boldsymbol{\theta}_a$, we alternatively update these variables iteratively. The conditional distribution for the primary variable $\boldsymbol{\theta}$ is given by:

$$p(\boldsymbol{\theta}|\boldsymbol{\theta}_a) \propto \frac{1}{Z_{\boldsymbol{\theta}_a}} \exp\left\{U(\boldsymbol{\theta}) - \frac{1}{2\eta}\|\boldsymbol{\theta} - \boldsymbol{\theta}_a\|^2\right\},$$

where $Z_{\boldsymbol{\theta}_a} = \exp \mathcal{F}(\boldsymbol{\theta}_a; \eta)$ serves as the normalization constant. Correspondingly, the conditional distribution for the auxiliary variable $\boldsymbol{\theta}_a$ is:

$$p(\boldsymbol{\theta}_a|\boldsymbol{\theta}) \propto \frac{1}{Z_{\boldsymbol{\theta}}} \exp\left\{-\frac{1}{2\eta}\|\boldsymbol{\theta} - \boldsymbol{\theta}_a\|^2\right\},$$

where $Z_{\boldsymbol{\theta}} = \exp(U(\boldsymbol{\theta}))$ is the associated normalization constant. This formulation reveals that $\boldsymbol{\theta}_a$ is sampled from $\mathcal{N}(\boldsymbol{\theta}, \eta\boldsymbol{I})$, with the variance η controlling the expected distance between $\boldsymbol{\theta}$ and $\boldsymbol{\theta}_a$. During the Metropolis-Hastings (MH) step, the acceptance probability is now calculated as:

$$\min\left(1, \frac{q_\alpha(\boldsymbol{\theta}|\widetilde{\boldsymbol{\theta}'})}{q_\alpha(\boldsymbol{\theta}'|\widetilde{\boldsymbol{\theta}})} \frac{\pi(\widetilde{\boldsymbol{\theta}'})}{\pi(\widetilde{\boldsymbol{\theta}})}\right).$$

This Gibbs-like alternating update scheme offers distinct advantages: (1) exact sampling of $\boldsymbol{\theta}_a$, (2) elimination of the need for the α_a parameter, (3) a less intensive computation of the MH acceptance probability, and (4) reduced overall computational overhead, especially when the proposal step involves an MH correction. This gibbs-like updating also shares similarities with the proximal sampling methods (Pereyra, 2016; Liang & Chen, 2023). This innovation can potentially allow DLP to generalize effectively to more complex, high-dimensional, and non-differentiable discrete target distributions such as the discrete Laplace distribution, which is commonly used in privacy-preserving mechanisms(Dwork et al., 2006; Gupte & Sundararajan, 2010). We leave out the theoretical analysis of the GLU versions for future work.

C Considerations for Excluding Focussed Belief Propogation from Benchmarking

1. Fundamental Differences in Sampling Mechanism: Most of the sampling algorithms we use generate samples sequentially, with each sample x_{t+1} derived from the previous sample x_t. This sequential dependency is essential for building a Markov Chain that explores the distribution space and gradually converges to the target distribution. fBP produces samples sequentially, but instead employs a *message-passing algorithm* aimed at converging to a fixed solution or configuration. It operates to converge deterministically to a solution, rather than generating a sequence of probabilistic samples. Moreover, fBP lacks a formal proof of convergence, relying instead on heuristic principles rooted in replica theory. This absence of theoretical guarantees or established convergence rates means that even if fBP appears to perform well, we cannot interpret or quantify its reliability, efficiency, or consistency across varying datasets and tasks. In contrast, MCMC-based methods like Langevin dynamics and Gibbs sampling come with well-understood convergence properties, enabling meaningful performance evaluations and robust benchmarking. This interpretability gap makes fBP less suitable for our study, where theoretical soundness and predictable behavior are critical.

2. Technical and Practical Constraints with using fBP: While fBP is originally implemented in Julia[4], a Python wrapper[5] is also available. However, this wrapper still depends on the underlying Julia or C++ implementations, introducing potential cross-language communication overhead. This dependency complicates integration in Python workflows and creates an inherent performance disparity when compared to purely Pythonic implementations, making direct runtime comparisons less meaningful. Despite fBP's speed advantage, its execution becomes slow as sample dimensions increase and network ensembles grow larger. The volume of message-passing in high-dimensional contexts limits its scalability. As task complexity increases, fBP faces challenges in achieving stable convergence, further limiting its suitability for our high-dimensional setup. Past studies have excluded computationally expensive methods from experimental evaluations Zhang et al. (2022).

3. Computational Overhead and Efficiency Concerns Resource Demands for Multiple Runs: If we were to use fBP to generate multiple samples, we would need to reinitialize and re-run the algorithm for each sample with a new seed, effectively solving the problem from scratch each time. This is highly inefficient compared to MCMC methods, where each subsequent sample builds on the previous one without needing to restart the entire algorithm. For larger models and datasets, this repeated initialization and execution would result in a significant computational burden.

4. Nature of Tasks: In certain structured sampling tasks, such as the TSP, we enforce constraints to ensure that each proposed state is a valid TSP solution. This entails accepting only those configurations that satisfy specific requirements of the TSP. However, fBP does not adhere to such constraints, as it lacks mechanisms for directly enforcing the validity of the sampled states. Consequently, fBP is unsuitable for tasks where such structural constraints are critical, placing it outside the scope for comparison in these applications.

We conducted preliminary experiments using fBP for Restricted Boltzmann Machine (RBM) sampling on the MNIST dataset to assess its effectiveness in image generation. Figure 5 shows random image samples generated by fBP on MNIST, which resemble random unstructured noise rather than recognizable digits, compared to MNIST samples by DMALA and EDMALA in Figures 6, 7 respectively. These outputs suggest that fBP doesn't capture the underlying structure of the MNIST data.

[4]Carlo Baldassi, *BinaryCommitteeMachinefBP.jl*, GitHub repository, `https://github.com/carlobaldassi/BinaryCommitteeMachinefBP.jl`, accessed November 8, 2024.

[5]Curti, Nico and Dall'Olio, Daniele and Giampieri, Enrico, *ReplicatedFocusingBeliefPropagation*, GitHub repository, `https://github.com/Nico-Curti/rFBP`, accessed November 8, 2024.

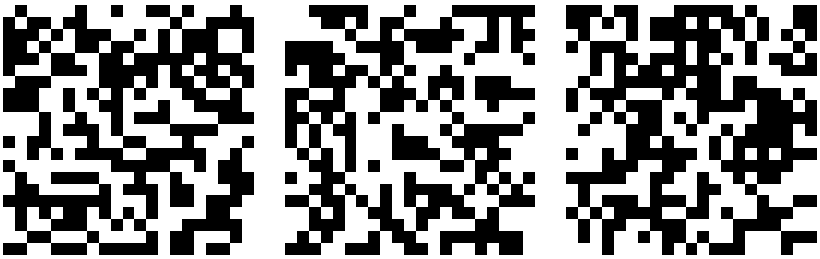

(a) (b) (c)

Figure 5: Random Image Samples for MNIST using fBP

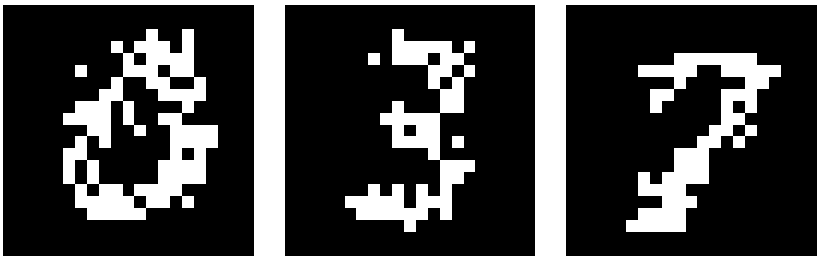

(a) (b) (c)

Figure 6: Random Image Samples for MNIST using DMALA

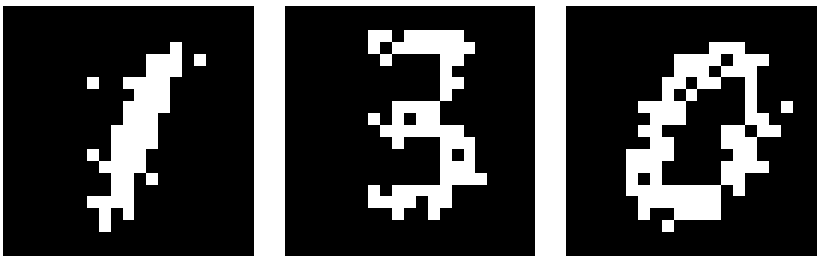

(a) (b) (c)

Figure 7: Random Image Samples for MNIST using EDMALA

fBP lacks direct use of the energy function $U(.)$ during optimization, preventing accurate data modeling. Figure 8 illustrates this through a distribution analysis of generated MNIST classes, showing significant mode collapse. Most generated samples cluster around a few classes, with an imbalance favoring certain digits and ignoring others.

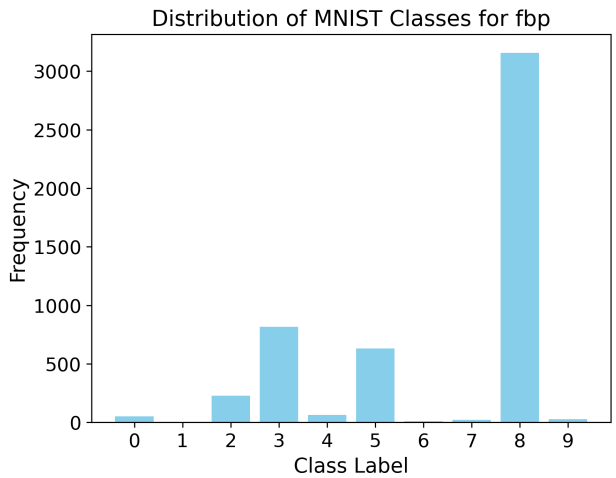

Figure 8: Mode Collapse using fBP

These findings highlight a fundamental issue with fBP in image generation tasks. Mode collapse suggests fBP struggles to explore diverse data regions, making it unsuitable for generating realistic, structured outputs that adhere to specific distribution characteristics, like image data in the MNIST dataset.

In summary, fBP diverges significantly from the MCMC-based sampling methods used in our study due to its deterministic message-passing mechanism, which converges to fixed configurations rather than generating sequential probabilistic samples. While a Python wrapper exists, its reliance on the underlying Julia or C++ implementations introduces potential cross-language communication overhead, creating performance inconsistencies when compared to native Python implementations. Moreover, fBP's lack of constraint adherence and dependence on spin-like variable encoding make it unsuitable for complex, structured sampling tasks like TSP or data-driven applications requiring diverse sampling, such as image generation on MNIST. Our preliminary experiments confirm that fBP struggles with mode collapse and fails to capture essential data distribution characteristics.

D Proofs

D.1 Proof of Lemma 4.1

Assume $\widetilde{\boldsymbol{\theta}} = [\boldsymbol{\theta}^T, \boldsymbol{\theta}_a^T]^T$ is sampled from the joint posterior distribution:

$$p(\widetilde{\boldsymbol{\theta}}) = p(\boldsymbol{\theta}, \boldsymbol{\theta}_a) \propto \exp\left\{U(\boldsymbol{\theta}) - \frac{1}{2\eta}\|\boldsymbol{\theta} - \boldsymbol{\theta}_a\|^2\right\}. \tag{10}$$

Then the marginal distribution for $\boldsymbol{\theta}$ is:

$$\begin{aligned} p(\boldsymbol{\theta}) &= \int p(\boldsymbol{\theta}, \boldsymbol{\theta}_a) d\boldsymbol{\theta}_a \\ &= (2\pi\eta)^{-\frac{d}{2}} Z^{-1} \int \exp\left\{U(\boldsymbol{\theta}) - \frac{1}{2\eta}\|\boldsymbol{\theta} - \boldsymbol{\theta}_a\|^2\right\} d\boldsymbol{\theta}_a \\ &= Z^{-1} \exp(U(\boldsymbol{\theta}))(2\pi\eta)^{-\frac{d}{2}} \int \exp\left\{-\frac{1}{2\eta}\|\boldsymbol{\theta} - \boldsymbol{\theta}_a\|^2\right\} d\boldsymbol{\theta}_a \\ &= Z^{-1} \exp(U(\boldsymbol{\theta})), \end{aligned} \tag{11}$$

where $Z = \sum_{\boldsymbol{\Theta}} \exp(U(\boldsymbol{\theta}))$ is the normalizing constant, and it is obtained by:

$$\sum_{\boldsymbol{\Theta}} \int \exp\left\{U(\boldsymbol{\theta}) - \frac{1}{2\eta}\|\boldsymbol{\theta} - \boldsymbol{\theta}_a\|^2\right\} d\boldsymbol{\theta}_a = (2\pi\eta)^{\frac{d}{2}} \sum_{\boldsymbol{\Theta}} \exp(U(\boldsymbol{\theta})) := (2\pi\eta)^{\frac{d}{2}} Z. \tag{12}$$

This verifies that the joint posterior distribution $p(\boldsymbol{\theta}, \boldsymbol{\theta}_a)$ is mathematically well-defined[6]. Similarly, the marginal distribution for $\boldsymbol{\theta}_a$ is:

$$\begin{aligned} p(\boldsymbol{\theta}_a) &= \sum_{\boldsymbol{\Theta}} p(\boldsymbol{\theta}, \boldsymbol{\theta}_a) \\ &\propto \sum_{\boldsymbol{\Theta}} \exp\left\{ U(\boldsymbol{\theta}) - \frac{1}{2\eta}\|\boldsymbol{\theta} - \boldsymbol{\theta}_a\|^2 \right\} \\ &= \exp \mathcal{F}(\boldsymbol{\theta}_a; \eta). \end{aligned} \tag{13}$$

D.2 Proof of Proposition 5.4

We follow a similar-style analysis as seen in Theorem 5.1 of Zhang et al. (2022).

Using Equation equation 9,

$$\begin{aligned} q_\gamma(\widetilde{\boldsymbol{\theta}}'|\widetilde{\boldsymbol{\theta}}) &\propto \exp\left(\frac{1}{2}\nabla_{\boldsymbol{\theta}} U_\eta(\widetilde{\boldsymbol{\theta}})^\top(\boldsymbol{\theta}' - \boldsymbol{\theta}) - \frac{1}{2\alpha}\|\boldsymbol{\theta}' - \boldsymbol{\theta}\|^2\right) \cdot \frac{1}{\sqrt{2\pi\alpha_a}^d} \exp\left(-\frac{1}{2\alpha_a}\|\boldsymbol{\theta}'_{\boldsymbol{a}} - \boldsymbol{\theta}_{\boldsymbol{a}} - \frac{\alpha_a}{2}\nabla_{\boldsymbol{\theta}_{\boldsymbol{a}}} U_\eta(\widetilde{\boldsymbol{\theta}})\|^2\right) \\ &= \frac{1}{\sqrt{2\pi\alpha_a}^d} \exp\left(\frac{1}{2}\nabla_{\boldsymbol{\theta}} U(\boldsymbol{\theta})^\top(\boldsymbol{\theta}' - \boldsymbol{\theta}) - \frac{1}{2\alpha}\|\boldsymbol{\theta}' - \boldsymbol{\theta}\|^2 - \frac{1}{2\eta}(\boldsymbol{\theta} - \boldsymbol{\theta}_a)^\top(\boldsymbol{\theta}' - \boldsymbol{\theta})\right) \cdot \\ &\quad \left(-\frac{1}{2\alpha_a}\|\boldsymbol{\theta}'_a - \boldsymbol{\theta}_a\|^2 + \frac{1}{2\eta}(\boldsymbol{\theta} - \boldsymbol{\theta}_a)^\top(\boldsymbol{\theta}'_a - \boldsymbol{\theta}_a) - \frac{\alpha_a}{8\eta^2}\|\boldsymbol{\theta} - \boldsymbol{\theta}_a\|^2\right) \\ &= \frac{1}{\sqrt{(2\pi\alpha_a)^d}} \exp\left(\frac{1}{2}(-U(\boldsymbol{\theta}) + U(\boldsymbol{\theta}')) - (\boldsymbol{\theta} - \boldsymbol{\theta}')^\top \left(\frac{1}{2\alpha}I + \frac{1}{4}\int_0^1 \nabla^2 U((1-s)\boldsymbol{\theta} + s\boldsymbol{\theta}')ds\right)(\boldsymbol{\theta} - \boldsymbol{\theta}')\right. \\ &\quad \left. -\frac{1}{2\eta}(\boldsymbol{\theta} - \boldsymbol{\theta}_a)^\top(\boldsymbol{\theta}' - \boldsymbol{\theta} + \boldsymbol{\theta}_a - \boldsymbol{\theta}'_a) - \frac{1}{2\alpha_a}\|\boldsymbol{\theta}'_a - \boldsymbol{\theta}_a\|^2 - \frac{\alpha_a}{8\eta^2}\|\boldsymbol{\theta} - \boldsymbol{\theta}_a\|^2\right) \\ &= \frac{1}{\sqrt{(2\pi\alpha_a)^d}} \exp\left(\frac{1}{2}(-U(\boldsymbol{\theta}) + U(\boldsymbol{\theta}')) - (\boldsymbol{\theta} - \boldsymbol{\theta}')^\top \left(\frac{1}{2\alpha}I + \frac{1}{4}\int_0^1 \nabla^2 U((1-s)\boldsymbol{\theta} + s\boldsymbol{\theta}')ds\right)(\boldsymbol{\theta} - \boldsymbol{\theta}')\right. \\ &\quad \left. -\frac{1}{2\eta}(\boldsymbol{\theta} - \boldsymbol{\theta}_a)^\top(\boldsymbol{\theta}' - \boldsymbol{\theta}'_a) - \frac{1}{2\alpha_a}\|\boldsymbol{\theta}'_a - \boldsymbol{\theta}_a\|^2 + \frac{4\eta - \alpha_a}{8\eta^2}\|\boldsymbol{\theta} - \boldsymbol{\theta}_a\|^2\right) \end{aligned}$$

The third line is true because we replace the linear gradient term $\nabla_{\boldsymbol{\theta}} U(\boldsymbol{\theta})^\top(\boldsymbol{\theta}' - \boldsymbol{\theta})$ with Taylor expansion with integral remainder.

The normalizing constant for Equation equation 9 $Z_{\widetilde{\boldsymbol{\Theta}}}(\widetilde{\boldsymbol{\theta}})$ is computed by integrating over $\mathbb{R}^d$ and summing over $\boldsymbol{\Theta}$:

$$Z_{\widetilde{\boldsymbol{\Theta}}}(\widetilde{\boldsymbol{\theta}}) = \frac{1}{\sqrt{2\pi\alpha_a}^d} \int_{\boldsymbol{\theta}'_a} \sum_{\boldsymbol{\theta}' \in \Theta} \exp\left(\frac{1}{2}\nabla_{\boldsymbol{\theta}} U_\eta(\widetilde{\boldsymbol{\theta}})^\top(\boldsymbol{\theta}' - \boldsymbol{\theta}) - \frac{1}{2\alpha}\|\boldsymbol{\theta}' - \boldsymbol{\theta}\|^2 - \frac{1}{2\alpha_a}\|\boldsymbol{\theta}'_a - \boldsymbol{\theta}_a - \frac{\alpha_a}{2}\nabla_{\boldsymbol{\theta}_a} U_\eta(\widetilde{\boldsymbol{\theta}})\|^2\right) d\boldsymbol{\theta}'_a \tag{14}$$

We note that since $\nabla^2 U(\cdot)$ is continuous(from Assumption 5.2), we know that

$$\min_{x,y \in \boldsymbol{\Theta}} (x - y)^T \left(\int_0^1 \nabla^2 U((1-s)x + sy)ds\right)(x - y)$$

is well-defined.

Consequently, the modified normalizing constant(Equation equation 14), $Z_\gamma(\widetilde{\boldsymbol{\theta}})$, becomes

$$\begin{aligned} Z_\gamma(\widetilde{\boldsymbol{\theta}}) = \frac{1}{\sqrt{(2\pi\alpha_a)^d}} \int_{\boldsymbol{\theta}'_a} \sum_{\boldsymbol{\theta}' \in \boldsymbol{\Theta}} \exp\Bigg(&\frac{1}{2}\big(-U(\boldsymbol{\theta}) + U(\boldsymbol{\theta}')\big) - (\boldsymbol{\theta} - \boldsymbol{\theta}')^\top \left(\frac{1}{2\alpha}I + \frac{1}{4}\int_0^1 \nabla^2 U\big((1-s)\boldsymbol{\theta} + s\boldsymbol{\theta}'\big)\, ds\right)(\boldsymbol{\theta} - \boldsymbol{\theta}') \\ &- \frac{1}{2\eta}(\boldsymbol{\theta} - \boldsymbol{\theta}_a)^\top(\boldsymbol{\theta}' - \boldsymbol{\theta}'_a) - \frac{1}{2\alpha_a}\|\boldsymbol{\theta}'_a - \boldsymbol{\theta}_a\|^2 + \frac{4\eta - \alpha_a}{8\eta^2}\|\boldsymbol{\theta} - \boldsymbol{\theta}_a\|^2\Bigg). \end{aligned} \tag{15}$$

[6]The exact form of the joint posterior is $p(\boldsymbol{\theta}, \boldsymbol{\theta}_a) = (2\pi\eta)^{-\frac{d}{2}} Z^{-1} \exp(U(\boldsymbol{\theta}) - \frac{1}{2\eta}\|\boldsymbol{\theta} - \boldsymbol{\theta}_a\|^2)$.

Now, we establish that $q(\widetilde{\boldsymbol{\theta}}|\widetilde{\boldsymbol{\theta}}')$ is reversible with respect to π_γ, where

$$\pi_\gamma = \frac{Z_\gamma(\widetilde{\boldsymbol{\theta}}) \exp\{\frac{\alpha_a}{8\eta^2}\|\boldsymbol{\theta}-\boldsymbol{\theta}_a\|^2\}\pi(\widetilde{\boldsymbol{\theta}})}{\int_y \sum_{x\in\boldsymbol{\Theta}} Z_\gamma([x^\top, y^\top]^\top) \exp\frac{\alpha_a}{8\eta^2}\|x-y\|^2 \pi([x^\top, y^\top]^\top) dy}$$

.

Note that,

$$\begin{aligned}
\pi_\gamma(\widetilde{\boldsymbol{\theta}}) q_\gamma(\widetilde{\boldsymbol{\theta}}'|\widetilde{\boldsymbol{\theta}}) &= \frac{Z_\gamma(\widetilde{\boldsymbol{\theta}}) \exp\left(\frac{\alpha_a}{8\eta^2}\|\boldsymbol{\theta}-\boldsymbol{\theta}_a\|^2\right)\pi(\widetilde{\boldsymbol{\theta}})}{\int_y \sum_{x\in\boldsymbol{\Theta}} Z_\gamma([x^\top, y^\top]^\top) \exp\left(\frac{\alpha_a}{8\eta^2}\|x-y\|^2\right)\pi([x^\top, y^\top]^\top)\, dy} \frac{1}{Z_\gamma(\widetilde{\boldsymbol{\theta}})} \frac{1}{(\sqrt{2\pi\alpha_a})^d} \\
&\quad \exp\left(\frac{1}{2}\big(-U(\boldsymbol{\theta})+U(\boldsymbol{\theta}')\big) - (\boldsymbol{\theta}-\boldsymbol{\theta}')^\top \left(\frac{1}{2\alpha}I + \frac{1}{4}\int_0^1 \nabla^2 U((1-s)\boldsymbol{\theta}+s\boldsymbol{\theta}')\, ds\right)(\boldsymbol{\theta}-\boldsymbol{\theta}')\right. \\
&\quad \left. - \frac{1}{2\eta}(\boldsymbol{\theta}-\boldsymbol{\theta}_a)^\top(\boldsymbol{\theta}'-\boldsymbol{\theta}'_{\boldsymbol{a}}) - \frac{1}{2\alpha_a}\|\boldsymbol{\theta}'_a-\boldsymbol{\theta}_a\|^2 + \frac{4\eta-\alpha_a}{8\eta^2}\|\boldsymbol{\theta}-\boldsymbol{\theta}_a\|^2\right) \\
&= \frac{1}{\int_y \sum_{x\in\boldsymbol{\Theta}} Z_\gamma([x^\top, y^\top]^\top) \exp\left(\frac{\alpha_a}{8\eta^2}\|x-y\|^2\right)\pi([x^\top, y^\top]^\top)\, dy} \frac{1}{(\sqrt{2\pi\alpha_a})^d} \\
&\quad \exp\left(\frac{1}{2}\big(U(\boldsymbol{\theta})+U(\boldsymbol{\theta}')\big) - \frac{1}{2}(\boldsymbol{\theta}-\boldsymbol{\theta}')^\top \left(\frac{1}{\alpha}I + \frac{1}{2}\int_0^1 \nabla^2 U((1-s)\boldsymbol{\theta}+s\boldsymbol{\theta}')\, ds\right)(\boldsymbol{\theta}-\boldsymbol{\theta}')\right. \\
&\quad \left. - \frac{1}{2\eta}(\boldsymbol{\theta}-\boldsymbol{\theta}_a)^\top(\boldsymbol{\theta}'-\boldsymbol{\theta}'_a) - \frac{1}{2\alpha_a}\|\boldsymbol{\theta}'_a-\boldsymbol{\theta}_a\|^2\right) \\
&= \pi_\gamma(\boldsymbol{\theta}') q_\gamma(\boldsymbol{\theta}|\boldsymbol{\theta}').
\end{aligned}$$

Chain looks symmetric and reversible with respect to π_γ.

Now, given this, note that $Z'_\gamma(\widetilde{\boldsymbol{\theta}})$ converges to 1 as $\alpha \to 0$ and $\alpha_a \to 0$.

$$\begin{aligned}
Z'_\gamma(\widetilde{\boldsymbol{\theta}}) &= Z_\gamma(\widetilde{\boldsymbol{\theta}}) \exp\left(\frac{\alpha_a}{8\eta^2}\|\boldsymbol{\theta}-\boldsymbol{\theta}_a\|^2\right) \\
&= \frac{1}{\sqrt{(2\pi\alpha_a)^d}} \int_y \sum_x \exp\left(-\frac{1}{2}\left(U(\boldsymbol{\theta})-U(x)\right) - (\boldsymbol{\theta}-x)^\top \left(\frac{1}{2\alpha}I + \frac{1}{4}\int_0^1 \nabla^2 U((1-s)\boldsymbol{\theta}+s\boldsymbol{\theta}')\, ds\right)(\boldsymbol{\theta}-x)\right. \\
&\quad \left. - \frac{1}{2\alpha_a}\|y-\boldsymbol{\theta}_a\|^2 + \frac{4\eta}{8\eta^2}\|\boldsymbol{\theta}-\boldsymbol{\theta}_a\|^2\right) dy \\
&\underset{\alpha\to 0}{=} \frac{1}{\sqrt{(2\pi\alpha_a)^d}} \int_y \sum_x \exp\left(\frac{1}{2}\left(U(x)-U(\boldsymbol{\theta})\right) - \frac{1}{2\alpha_a}\|y-\boldsymbol{\theta}_a\|^2 + \frac{1}{2\eta}\|\boldsymbol{\theta}-\boldsymbol{\theta}_a\|^2 - \frac{1}{2\eta}(\boldsymbol{\theta}-\boldsymbol{\theta}_a)^\top(x-y)\right)\delta_{\boldsymbol{\theta}}(x)\, dy \\
&= \int_y \exp\left(\frac{1}{2\eta}\|\boldsymbol{\theta}-\boldsymbol{\theta}_a\|^2 - \frac{1}{2\eta}(\boldsymbol{\theta}-\boldsymbol{\theta}_a)^\top(\boldsymbol{\theta}-y)\right) dy \\
&\underset{\alpha_a\to 0}{=} \int_y \exp\left(\frac{1}{2\eta}\|\boldsymbol{\theta}-\boldsymbol{\theta}_a\|^2 - \frac{1}{2\eta}(\boldsymbol{\theta}-\boldsymbol{\theta}_a)^\top(\boldsymbol{\theta}-\boldsymbol{\theta}_a)\right) dy \\
&= 1.
\end{aligned}$$

where $\delta_\theta(.)$ is a Dirac delta. It follows that π_γ converges pointwisely to $\pi(\widetilde{\boldsymbol{\theta}})$ as $\alpha \to 0$ and $\alpha_a \to 0$.

By Scheffé's Lemma, this implies global convergence in total variation distance. Let us consider the convergence rate in terms of the L_1-norm

$$\|\pi_\gamma - \tilde{\pi}\|_1 = \int_{\theta_a} \sum_{\theta \in \mathbf{\Theta}} \left| \frac{Z'_\gamma(\widetilde{\boldsymbol{\theta}})\pi(\widetilde{\boldsymbol{\theta}})}{\int_y \sum_{x\in\mathbf{\Theta}} Z'_\gamma([x^\top, y^\top]^\top)\pi([x^\top, y^\top]^\top)dy} - \pi(\widetilde{\boldsymbol{\theta}}) \right| d\boldsymbol{\theta}_a$$

We write out each absolute value term

$$\left| \frac{Z'_\gamma(\widetilde{\boldsymbol{\theta}})\pi(\widetilde{\boldsymbol{\theta}})}{\int_y \sum_{x\in\mathbf{\Theta}} Z'_\gamma([x^\top, y^\top]^\top)\pi([x^\top, y^\top]^\top)dy} - \pi(\widetilde{\boldsymbol{\theta}}) \right| = \pi(\widetilde{\boldsymbol{\theta}}) \left| \frac{Z'_\gamma(\widetilde{\boldsymbol{\theta}})}{\int_y \sum_{x\in\mathbf{\Theta}} Z'_\gamma([x^\top, y^\top]^\top)\pi([x^\top, y^\top]^\top)dy} - 1 \right|$$

First, recall under Assumption 5.1, we note that since U is M-gradient Lipschitz and $\frac{\alpha}{2} < \frac{1}{M}$, this makes matrix

$$\frac{1}{2\alpha} I - \frac{1}{4}\int_0^1 \nabla^2 U((1-s)\boldsymbol{\theta} + s\boldsymbol{\theta}')ds > \frac{1}{4}\left(\frac{2}{\alpha} - M\right) I$$

positive definite.

We notice for the sub-expression in Eq. 15,

$$\begin{aligned}
-\frac{1}{2}(\boldsymbol{\theta} - x)^\top \left(\frac{1}{\alpha} I + \frac{1}{2}\int_0^1 \nabla^2 U((1-s)\boldsymbol{\theta} + sx)\, ds\right)(\boldsymbol{\theta} - x) &= -\frac{1}{2\alpha}\|\boldsymbol{\theta} - x\|^2 - \frac{1}{4}(\boldsymbol{\theta} - x)^\top \left(\int_0^1 \nabla^2 U((1-s)\boldsymbol{\theta} + sx)\, ds\right)(\boldsymbol{\theta} - x) \\
&\leq -\frac{1}{2\alpha}\|\boldsymbol{\theta} - x\|^2 + \frac{M}{4}\|\boldsymbol{\theta} - x\|^2 \\
&= (-\frac{1}{2\alpha} + \frac{M}{4})\|\boldsymbol{\theta} - x\|^2
\end{aligned}$$

The second line is true because, $(\boldsymbol{\theta} - x)^\top \nabla^2 U(\boldsymbol{\theta} - x) \geq -M\|\boldsymbol{\theta} - x\|^2$ from Assumption 5.1.

We know from above, $\frac{\alpha}{2} < \frac{1}{M}$ for stability. Since the coefficient is negative, the expression is maximized when the distance $\|\boldsymbol{\theta} - x\|^2$ is minimized. Therefore,

$$-\frac{1}{2}(\boldsymbol{\theta} - x)^\top \left(\frac{1}{\alpha} I + \frac{1}{2}\int_0^1 \nabla^2 U((1-s)\boldsymbol{\theta} + sx)\, ds\right)(\boldsymbol{\theta} - x) \leq (\frac{M}{4} - \frac{1}{2\alpha})\delta(\mathbf{\Theta})^2 \tag{16}$$

Second, for $x' \in \mathbf{\Theta}$ and $y' \in \mathbf{\Theta}_a$ (under Assumptions 5.1 and 5.3), we know that the following minimum exists and is well-defined: $\min_{\substack{x\in\mathbf{\Theta}\setminus\{x'\} \\ y\in\mathbf{\Theta}_a\setminus\{y'\}}} (x - y)^\top (x' - y')$

Thus when, $\dfrac{Z'_\gamma(\widetilde{\boldsymbol{\theta}})}{\int_y \sum_{x\in\mathbf{\Theta}} Z'_\gamma\left(\begin{bmatrix} x^\top \\ y^\top \end{bmatrix}\right)\pi\left(\begin{bmatrix} x^\top \\ y^\top \end{bmatrix}\right)dy} - 1 \geq 0$, we get,

$$\begin{aligned}
\left| \frac{Z'_\gamma(\widetilde{\boldsymbol{\theta}})\pi(\widetilde{\boldsymbol{\theta}})}{\int_y \sum_{x\in\mathbf{\Theta}} Z'_\gamma\left(\begin{bmatrix} x^\top \\ y^\top \end{bmatrix}\right)\pi\left(\begin{bmatrix} x^\top \\ y^\top \end{bmatrix}\right)dy} - \pi(\widetilde{\boldsymbol{\theta}}) \right| &= \pi(\widetilde{\boldsymbol{\theta}}) \left| \frac{Z'_\gamma(\widetilde{\boldsymbol{\theta}})}{\int_y \sum_{x\in\mathbf{\Theta}} Z'_\gamma\left(\begin{bmatrix} x^\top \\ y^\top \end{bmatrix}\right)\pi\left(\begin{bmatrix} x^\top \\ y^\top \end{bmatrix}\right)dy} - 1 \right| \\
&\leq \pi(\widetilde{\boldsymbol{\theta}}) \Bigg(1 + \frac{1}{\sqrt{(2\pi\alpha_a)^d}} \int_{y\neq\theta_a} \sum_{x\neq\theta} \exp\Bigg(\frac{1}{2}(U(x) - U(\boldsymbol{\theta})) - \frac{1}{2}(\boldsymbol{\theta} - x)^\top \left(\frac{1}{\alpha} I + \frac{1}{2}\int_0^1 \nabla^2 U((1-s)\boldsymbol{\theta} + sx)\, ds\right)(\boldsymbol{\theta} - x) \\
&\quad - \frac{1}{2\alpha_a}\|y - \boldsymbol{\theta}_a\|^2 + \frac{4\eta}{8\eta^2}\|\boldsymbol{\theta} - \boldsymbol{\theta}_a\|^2 - \frac{1}{2\eta}(\boldsymbol{\theta} - \boldsymbol{\theta}_a)^\top (x - y)\Bigg) dy - 1\Bigg) \\
&\leq \frac{\pi(\widetilde{\boldsymbol{\theta}})}{\sqrt{(2\pi\alpha_a)^d}} \exp\left((\frac{M}{4} - \frac{1}{2\alpha})\delta(\mathbf{\Theta})^2 + \frac{1}{2\eta}\|\boldsymbol{\theta} - \boldsymbol{\theta}_a\|^2 - \frac{\vartheta(\mathbf{\Theta}, \mathbf{\Theta}_a)}{2\eta}\right) \cdot \left(\int_{y\neq\theta_a} \sum_{x\neq\theta} \exp\left(\frac{1}{2}U(x) - \frac{1}{2}U(\boldsymbol{\theta}) - \frac{1}{2\alpha_a}\|y - \theta_a\|^2\right) dy\right) \\
&\leq \pi(\widetilde{\boldsymbol{\theta}}) \exp\left((\frac{M}{4} - \frac{1}{2\alpha})\delta(\mathbf{\Theta})^2 + \frac{1}{2\eta}\|\boldsymbol{\theta} - \boldsymbol{\theta}_a\|^2 - \frac{\vartheta(\mathbf{\Theta}, \mathbf{\Theta}_a)}{2\eta}\right) \left(\sum_x \exp(U(x))\right) \\
&= \pi(\widetilde{\boldsymbol{\theta}}) Z \exp\left((\frac{M}{4} - \frac{1}{2\alpha})\delta(\mathbf{\Theta})^2 + \frac{1}{2\eta}\|\boldsymbol{\theta} - \boldsymbol{\theta}_a\|^2 - \frac{\vartheta(\mathbf{\Theta}, \mathbf{\Theta}_a)}{2\eta}\right) \\
&\leq \pi(\widetilde{\boldsymbol{\theta}}) Z \exp\left((\frac{M}{4} - \frac{1}{2\alpha})\delta(\mathbf{\Theta})^2 + \frac{\Delta(\mathbf{\Theta}, \mathbf{\Theta}_a)^2 - \vartheta(\mathbf{\Theta}, \mathbf{\Theta}_a)}{2\eta}\right).
\end{aligned}$$

Third line is true because of Eq. 16.

Similarly, when $\dfrac{Z'_\gamma(\widetilde{\boldsymbol{\theta}})}{\int_y \sum_{x\in\boldsymbol{\Theta}} Z'_\gamma\left(\begin{bmatrix} x^\top \\ y^\top \end{bmatrix}\right)\pi\left(\begin{bmatrix} x^\top \\ y^\top \end{bmatrix}\right)dy} - 1 < 0$, we get

$$
\begin{aligned}
&\left|\frac{Z'_\gamma(\widetilde{\boldsymbol{\theta}})\pi(\widetilde{\boldsymbol{\theta}})}{\int_y \sum_{x\in\boldsymbol{\Theta}} Z'_\gamma\left(\begin{bmatrix} x^\top \\ y^\top \end{bmatrix}\right)\pi\left(\begin{bmatrix} x^\top \\ y^\top \end{bmatrix}\right)dy} - \pi(\widetilde{\boldsymbol{\theta}})\right| \\
&= \pi(\widetilde{\boldsymbol{\theta}})\left(1 - \frac{1 + \frac{1}{\sqrt{(2\pi\alpha_a)^d}}\int_{y\neq\theta_a}\sum_{x\neq\theta}\exp\left(\frac{1}{2}(U(x)-U(\boldsymbol{\theta})) - \frac{1}{2}(\boldsymbol{\theta}-x)^\top\left(\frac{1}{\alpha}I + \frac{1}{2}\int_0^1\nabla^2 U((1-s)\theta + sx)ds\right)(\boldsymbol{\theta}-x) - \frac{1}{2\alpha_a}\|y-\boldsymbol{\theta_a}\|^2 + \frac{4\eta}{8\eta^2}\|\boldsymbol{\theta}-\boldsymbol{\theta}_a\|^2 - \frac{1}{2\eta}(\boldsymbol{\theta}-\boldsymbol{\theta}_a)^\top(x-y)\right)dy}{1 + \frac{1}{\sqrt{2\pi\alpha_a}^d}\int_p\frac{1}{\sqrt{\pi}^d}\exp(-p^2)\int_{q\neq p}\sum_r\frac{1}{Z}\exp(U(r))\sum_{s\neq r}\exp\left(\frac{1}{2}\left(U(s)-\frac{1}{2}U(r)\right) - \frac{1}{2}(r-s)^\top\left(\frac{1}{\alpha}I + \frac{1}{2}\int_0^1\nabla^2 U((1-l)r+ls)dl\right)(r-s) - \frac{1}{2\alpha_a}\|q-p\|^2 + \frac{4\eta}{8\eta^2}\|r-p\|^2 - \frac{1}{2\eta}(r-p)^\top(s-q)\right)dq\,dp}\right) \\
&\leq \pi(\widetilde{\boldsymbol{\theta}})\left(1 - \frac{1}{1 + \frac{1}{\sqrt{2\pi\alpha_a}^d}\int_p\frac{1}{\sqrt{\pi}^d}\exp(-p^2)\int_{q\neq p}\exp\left(-\frac{1}{2\alpha_a}\|q-p\|^2\right)\sum_r\exp\left(\frac{4\eta}{8\eta^2}\|r-p\|^2\right)\frac{1}{Z}\exp(U(r))\sum_{s\neq r}\exp\left(\frac{1}{2}(U(s)-U(r)) - \frac{1}{2}(r-s)^\top\left(\frac{1}{\alpha}I + \frac{1}{2}\int_0^1\nabla^2 U((1-l)r+ls)dl\right)(r-s) - \frac{1}{2\eta}(r-p)^\top(s-q)\right)dq\,dp}\right) \\
&= \pi(\widetilde{\boldsymbol{\theta}})\left(\frac{\frac{1}{\sqrt{2\pi\alpha_a}^d}\int_p\frac{1}{\sqrt{\pi}^d}\exp(-p^2)\int_{q\neq p}\exp\left(-\frac{1}{2\alpha_a}\|q-p\|^2\right)\sum_r\exp\left(\frac{4\eta}{8\eta^2}\|r-p\|^2\right)\frac{1}{Z}\exp(U(r))\sum_{s\neq r}\exp\left(\frac{1}{2}(U(s)-U(r)) - \frac{1}{2}(r-s)^\top\left(\frac{1}{\alpha}I + \frac{1}{2}\int_0^1\nabla^2 U((1-l)r+ls)dl\right)(r-s) - \frac{1}{2\eta}(r-p)^\top(s-q)\right)dq\,dp}{1 + \frac{1}{\sqrt{2\pi\alpha_a}^d}\int_p\frac{1}{\sqrt{\pi}^d}\exp(-p^2)\int_{q\neq p}\exp\left(-\frac{1}{2\alpha_a}\|q-p\|^2\right)\sum_r\exp\left(\frac{4\eta}{8\eta^2}\|r-p\|^2\right)\frac{1}{Z}\exp(U(r))\sum_{s\neq r}\exp\left(\frac{1}{2}(U(s)-U(r)) - \frac{1}{2}(r-s)^\top\left(\frac{1}{\alpha}I + \frac{1}{2}\int_0^1\nabla^2 U((1-l)r+ls)dl\right)(r-s) - \frac{1}{2\eta}(r-p)^\top(s-q)\right)dq\,dp}\right) \\
&\leq \frac{\pi(\widetilde{\boldsymbol{\theta}})}{\sqrt{2\pi\alpha_a}^d}\left(\int_p\frac{1}{\sqrt{\pi}^d}\exp(-p^2)\int_{q\neq p}\exp\left(-\frac{1}{2\alpha_a}\|q-p\|^2\right)\sum_r\exp\left(\frac{4\eta}{8\eta^2}\|r-p\|^2\right)\frac{1}{Z}\exp(U(r))\sum_{s\neq r}\exp\left(\frac{1}{2}(U(s)-U(r)) - \frac{1}{2}(r-s)^\top\left(\frac{1}{\alpha}I + \frac{1}{2}\int_0^1\nabla^2 U((1-l)r+ls)dl\right)(r-s) - \frac{1}{2\eta}(r-p)^\top(s-q)\right)\right)dqdp \\
&\leq \frac{\pi(\widetilde{\boldsymbol{\theta}})}{\sqrt{(2\pi\alpha_a)^d}}\exp\left((\frac{M}{4} - \frac{1}{2\alpha})\delta(\boldsymbol{\Theta})^2\right)\left(\int_p\frac{1}{\sqrt{\pi}^d}\exp(-p^2)\right)\int_{q\neq p}\exp\left(-\frac{1}{2\alpha_a}\|q-p\|^2\right)\sum_r\exp\left(\frac{1}{2\eta}\|r-p\|^2\right)\frac{1}{Z}\exp(U(r))\sum_{s\neq r}\exp\left(\frac{1}{2}(U(s)-U(r)) - \frac{1}{2\eta}(r-p)^\top(s-q)\right)\Bigg)dqdp \\
&\leq \frac{\pi(\widetilde{\boldsymbol{\theta}})}{\sqrt{2\pi\alpha_a}^d}\exp\left((\frac{M}{4} - \frac{1}{2\alpha})\delta(\boldsymbol{\Theta})^2 + \frac{\Delta(\boldsymbol{\Theta},\boldsymbol{\Theta}_a)^2 - \vartheta(\boldsymbol{\Theta},\boldsymbol{\Theta}_a)}{2\eta}\right)\left(\int_p\frac{1}{\sqrt{\pi}^d}\exp(-p^2)\int_{q\neq p}\exp\left(-\frac{1}{2\alpha_a}\|q-p\|^2\right)\sum_r\frac{1}{Z}(U(r))\sum_{s\neq r}\exp\left(\frac{1}{2}(U(s)-U(r))\right)dq\,dp\right) \\
&\leq \frac{\pi(\widetilde{\boldsymbol{\theta}})}{\sqrt{2\pi\alpha_a}^d}Z\exp\left((\frac{M}{4} - \frac{1}{2\alpha})\delta(\boldsymbol{\Theta})^2 + \frac{\Delta(\boldsymbol{\Theta},\boldsymbol{\Theta}_a)^2 - \vartheta(\boldsymbol{\Theta},\boldsymbol{\Theta}_a)}{2\eta}\right)\left(\int_p\frac{1}{\sqrt{\pi}^d}\exp(-p^2)\int_{q\neq p}\exp\left(-\frac{1}{2\alpha_a}\|q-p\|^2\right)dq\,dp\right) \\
&= \pi(\widetilde{\boldsymbol{\theta}})Z\exp\left((\frac{M}{4} - \frac{1}{2\alpha})\delta(\boldsymbol{\Theta})^2 + \frac{\Delta(\boldsymbol{\Theta},\boldsymbol{\Theta}_a)^2 - \vartheta(\boldsymbol{\Theta},\boldsymbol{\Theta}_a)}{2\eta}\right)\int_p\left(\frac{1}{\sqrt{\pi}^d}\exp(-p^2)\right)dp \\
&= \pi(\widetilde{\boldsymbol{\theta}})Z\exp\left((\frac{M}{4} - \frac{1}{2\alpha})\delta(\boldsymbol{\Theta})^2 + \frac{\Delta(\boldsymbol{\Theta},\boldsymbol{\Theta}_a)^2 - \vartheta(\boldsymbol{\Theta},\boldsymbol{\Theta}_a)}{2\eta}\right)
\end{aligned}
$$

Therefore, the difference between π_γ and $\tilde{\pi}$ can be bounded as follows

$$
\begin{aligned}
\|\pi_\gamma - \tilde{\pi}\|_1 &\leq \int_{\theta_a}\sum_{\theta\in\boldsymbol{\Theta}}\pi(\widetilde{\boldsymbol{\theta}})Z\exp\left((\frac{M}{4} - \frac{1}{2\alpha})\delta(\boldsymbol{\Theta})^2 + \frac{\Delta(\boldsymbol{\Theta},\boldsymbol{\Theta}_a)^2 - \vartheta(\boldsymbol{\Theta},\boldsymbol{\Theta}_a)}{2\eta}\right)d\theta_a \\
&\leq Z\exp\left((\frac{M}{4} - \frac{1}{2\alpha})\delta(\boldsymbol{\Theta})^2 + \frac{\Delta(\boldsymbol{\Theta},\boldsymbol{\Theta}_a)^2 - \vartheta(\boldsymbol{\Theta},\boldsymbol{\Theta}_a)}{2\eta}\right)
\end{aligned}
$$

D.3 Proofs for EDULA

We start by establishing results for a more general case in which Assumption 5.3 is dropped. We establish that in this setting geometric rates of convergence exist. However, in this case proving that the stationary distribution is close to the target remains an open problem.

Remark (Implementation of Compactness via Truncated Normals): Assumption 5.3 from Section 5, restricts the auxiliary variable $\boldsymbol{\theta}_a$ to a compact subset $\boldsymbol{\Theta}_a \subset \mathbb{R}^d$. In the context of our theoretical analysis, this implies that the transition kernel for the auxiliary update, denoted as $q_{\alpha_a}(\boldsymbol{\theta}'_a|\tilde{\boldsymbol{\theta}})$ in Eq. 6, is formally treated as a Truncated Normal distribution supported on $\boldsymbol{\Theta}_a$:

$$
q^{\text{trunc}}_{\alpha_a}(\boldsymbol{\theta}'_a|\tilde{\boldsymbol{\theta}}) \propto \mathcal{N}\left(\boldsymbol{\theta}_a + \frac{\alpha_a}{2}\nabla_{\boldsymbol{\theta}_a}U_\eta(\tilde{\boldsymbol{\theta}}), \alpha_a I\right)\cdot\mathbb{I}(\boldsymbol{\theta}'_a \in \boldsymbol{\Theta}_a)
$$

The normalization constant of this truncated distribution is strictly lower-bounded away from zero because $\boldsymbol{\Theta}_a$ is compact and the mean of the un-truncated normal is a continuous function of $\tilde{\boldsymbol{\theta}}$. Crucially, this ensures that the transition probabilities are bounded away from zero within the compact set, a necessary condition to establish the minorization condition required for geometric ergodicity. Note that while the mean of the

proposal distribution may theoretically lie outside $\boldsymbol{\Theta}_a$ (e.g., if $\tilde{\boldsymbol{\theta}}$ is near the boundary), the truncation ensures the sample remains within the valid domain, preserving the well-definedness of the chain without affecting the validity of the subsequent drift analysis.

Theorem D.1. *Let Assumption 5.1 hold. Then for the Markov chain with transition operator P as in Algorithm 1, the drift condition is satisfied as follows:*

$$PV(\tilde{\boldsymbol{\theta}}) \leq \alpha_a\, d + 2\left(1 - \frac{\alpha_a}{\eta}\right)^2 V(\tilde{\boldsymbol{\theta}}) + 2\,\frac{\alpha_a^2}{\eta^2} \sup_{\boldsymbol{\theta}\in\boldsymbol{\Theta}} \|\boldsymbol{\theta}\|^2.$$

Proof. We establish an explicit drift and minorization condition for the joint chain, which confirms the convergence rate. Note that

$$p((\boldsymbol{\theta}'_a, \boldsymbol{\theta}') \mid (\boldsymbol{\theta}'_a, \boldsymbol{\theta}')) = p(\boldsymbol{\theta}'_a \mid \boldsymbol{\theta}, \boldsymbol{\theta}_a) \cdot p(\boldsymbol{\theta}' \mid \boldsymbol{\theta}_a, \boldsymbol{\theta}).$$

Now,

$$p(\boldsymbol{\theta}'_a \mid \boldsymbol{\theta}, \boldsymbol{\theta}_a) = \frac{1}{(2\pi\alpha_a)^{d/2}} \exp\left\{-\frac{1}{2\alpha_a}\left\|\boldsymbol{\theta}'_a - \boldsymbol{\theta}_a\left(1 - \frac{\alpha_a}{\eta}\right) - \frac{\alpha_a}{\eta}\boldsymbol{\theta}\right\|^2\right\}$$

and

$$p(\boldsymbol{\theta}' \mid \boldsymbol{\theta}_a, \boldsymbol{\theta}) = \frac{\exp\left\{-\frac{1}{2\alpha}\left\|\boldsymbol{\theta}' - \boldsymbol{\theta} + \alpha\nabla U(\boldsymbol{\theta}) - \frac{\alpha}{\eta}(\boldsymbol{\theta} - \boldsymbol{\theta}_a)\right\|^2\right\}}{\sum_{\boldsymbol{x}\in\boldsymbol{\Theta}} \exp\left\{-\frac{1}{2\alpha}\left\|\boldsymbol{x} - \boldsymbol{\theta} + \alpha\nabla U(\boldsymbol{\theta}) - \frac{\alpha}{\eta}(\boldsymbol{\theta} - \boldsymbol{\theta}_a)\right\|^2\right\}}.$$

Therefore, our Markov transition operator P is given as

$$P((\boldsymbol{\theta}_a, \boldsymbol{\theta}), A) = \int_A p((\boldsymbol{\theta}'_a, \boldsymbol{\theta}') \mid (\boldsymbol{\theta}, \boldsymbol{\theta}_a))\, d\mu,$$

where $A \in \boldsymbol{\Theta} \times \mathbb{R}^d$ and μ is the product of the counting measure and Lebesgue measure.

We shall first establish a drift condition:

$$PV \leq \lambda V + b,$$

where we choose the Lyapunov function $V(\boldsymbol{x}_1, \boldsymbol{x}_2) = \|\boldsymbol{x}_1\|^2$ and some constant $b > 0$.

We note that

$$\begin{aligned} PV(\boldsymbol{\theta}_a, \boldsymbol{\theta}) = \frac{1}{(2\pi\alpha_a)^{d/2}} \sum_{\boldsymbol{\theta}'\in\boldsymbol{\Theta}} \int \|\boldsymbol{\theta}'_a\|^2 \exp\left\{-\frac{1}{2\alpha_a}\left\|\boldsymbol{\theta}'_a - \boldsymbol{\theta}_a\left(1 - \frac{\alpha_a}{\eta}\right) - \frac{\alpha_a}{\eta}\boldsymbol{\theta}\right\|^2\right\} \\ \cdot \frac{\exp\left\{-\frac{1}{2\alpha}\left\|\boldsymbol{\theta}' - \boldsymbol{\theta} + \alpha\nabla U(\boldsymbol{\theta}) - \frac{\alpha}{\eta}(\boldsymbol{\theta} - \boldsymbol{\theta}_a)\right\|^2\right\}}{\sum_{\boldsymbol{x}\in\boldsymbol{\Theta}} \exp\left\{-\frac{1}{2\alpha}\left\|\boldsymbol{x} - \boldsymbol{\theta} + \alpha\nabla U(\boldsymbol{\theta}) - \frac{\alpha}{\eta}(\boldsymbol{\theta} - \boldsymbol{\theta}_a)\right\|^2\right\}}\, d\boldsymbol{\theta}_a. \end{aligned}$$

Using a change of variables, we have

$$\begin{aligned} PV(\boldsymbol{\theta}_a, \boldsymbol{\theta}) &= \frac{1}{(2\pi\alpha_a)^{d/2}} \sum_{\boldsymbol{\theta}'\in\boldsymbol{\Theta}} \int \left\|u + \boldsymbol{\theta}_a\left(1 - \frac{\alpha_a}{\eta}\right) + \frac{\alpha_a}{\eta}\boldsymbol{\theta}\right\|^2 \exp\left\{-\frac{1}{2\alpha_a}\|u\|^2\right\} \\ &\quad \cdot \frac{\exp\left\{-\frac{1}{2\alpha}\left\|\boldsymbol{\theta}' - \boldsymbol{\theta} + \alpha\nabla U(\boldsymbol{\theta}) - \frac{\alpha}{\eta}(\boldsymbol{\theta} - \boldsymbol{\theta}_a)\right\|^2\right\}}{\sum_{\boldsymbol{x}\in\boldsymbol{\Theta}} \exp\left\{-\frac{1}{2\alpha}\left\|\boldsymbol{x} - \boldsymbol{\theta} + \alpha\nabla U(\boldsymbol{\theta}) - \frac{\alpha}{\eta}(\boldsymbol{\theta} - \boldsymbol{\theta}_a)\right\|^2\right\}}\, du \\ &\leq \alpha_a\, d + 2\left(1 - \frac{\alpha_a}{\eta}\right)^2 \|\boldsymbol{\theta}_a\|^2 + 2\,\frac{\alpha_a^2}{\eta^2} \sup_{\boldsymbol{\theta}\in\boldsymbol{\Theta}} \|\boldsymbol{\theta}\|^2. \end{aligned}$$

Note that when $\lambda = 2\left(1 - \frac{\alpha_a}{\eta}\right)^2 < 1$, then this is a proper drift condition with $b = \alpha_a\, d + 2\,\frac{\alpha_a^2}{\eta^2} \sup_{\boldsymbol{\theta}\in\boldsymbol{\Theta}} \|\boldsymbol{\theta}\|^2$.

Theorem D.2. *Under Assumption 5.1, the Markov chain with transition operator P as in Algorithm 1 satisfies,*

$$P(\tilde{\boldsymbol{\theta}}, A) \geq \bar{\eta}\mu(A)$$

where $\bar{\eta} > 0$ is defined in equation 18 and $\mu(\cdot)$ is the product of Lebesgue measure and counting measure and $\tilde{\boldsymbol{\theta}} \in C_\alpha$ as in equation 17 .

Proof. We establish a minorization on the set,

$$C_{\alpha_a} = \left\{ x : V(x) \leq \frac{2\left(\alpha_a\, d + 2\,\frac{\alpha_a^2}{\eta^2}\sup_{\boldsymbol{\theta}\in\boldsymbol{\Theta}} \|\boldsymbol{\theta}\|^2\right)}{\left(1 - \frac{\alpha_a}{\eta}\right)^2} \right\} \tag{17}$$

We define

$$\begin{aligned}\bar{\eta} = {} & \frac{1}{(2\pi\alpha_a)^{d/2}} \exp\left\{ -\frac{4}{\alpha_a} \frac{\left(\alpha_a\, d + 2\,\frac{\alpha_a^2}{\eta^2}\sup_{\boldsymbol{\theta}\in\boldsymbol{\Theta}} \|\boldsymbol{\theta}\|^2\right)}{\left(1 - \frac{\alpha_a}{\eta}\right)^2} \right\} \cdot \frac{1}{|\boldsymbol{\Theta}|} \\ & \cdot \exp\left\{ -\frac{1}{2\alpha} \left[\left((\alpha\, M + 1)^2 + \alpha\, M^2\right) \mathrm{diam}(\boldsymbol{\Theta})^2 + (2\,(M + \alpha) + 2\alpha M)\, \|\nabla U(a)\| \mathrm{diam}(\boldsymbol{\Theta}) + \left(\alpha^2 + \alpha\right) \|\nabla U(a)\|^2 \right.\right. \\ & \left.\left. + 2\frac{\alpha}{\eta} \left[(\alpha\, M + 1)^2\, \mathrm{diam}(\boldsymbol{\Theta})^2 + 2\,(M + \alpha) \|\nabla U(a)\| \mathrm{diam}(\boldsymbol{\Theta}) + \alpha^2 \|\nabla U(a)\|^2 \right]^{1/2} \mathrm{diam}(\boldsymbol{\Theta}) \right] \right\}\end{aligned} \tag{18}$$

We start with considering any $(\boldsymbol{\theta_1}, \boldsymbol{\theta_2}) \in C_\alpha$. Further, we also have $(\boldsymbol{\theta_a}, \boldsymbol{\theta}) \in C_{\alpha_a}$. Therefore

$$\begin{aligned} p((\boldsymbol{\theta_1}, \boldsymbol{\theta_2}) \mid (\boldsymbol{\theta_a}, \boldsymbol{\theta})) = {} & \frac{1}{(2\pi\alpha_a)^{d/2}} \exp\left\{ -\frac{1}{2\alpha_a} \left\| \boldsymbol{\theta_1} - \boldsymbol{\theta_a}\left(1 - \frac{\alpha_a}{\eta}\right) - \frac{\alpha_a}{\eta}\boldsymbol{\theta} \right\|^2 \right\} \\ & \cdot \frac{\exp\left\{ -\frac{1}{2\,\alpha} \left\| \boldsymbol{\theta_2} - \boldsymbol{\theta} + \alpha\nabla U(\boldsymbol{\theta}) - \frac{\alpha}{\eta}\left(\boldsymbol{\theta} - \boldsymbol{\theta_a}\right) \right\|^2 \right\}}{\sum_{x\in\boldsymbol{\Theta}} \exp\left\{ -\frac{1}{2\,\alpha} \left\| x - \boldsymbol{\theta} + \alpha\nabla U(\boldsymbol{\theta}) - \frac{\alpha}{\eta}\left(\boldsymbol{\theta} - \boldsymbol{\theta_a}\right) \right\|^2 \right\}}. \end{aligned}$$

For the first term, we note that

$$\begin{aligned} \left\| \boldsymbol{\theta_1} - \boldsymbol{\theta_a}\left(1 - \frac{\alpha_a}{\eta}\right) - \frac{\alpha_a}{\eta}\boldsymbol{\theta} \right\|^2 & \leq 2\, \|\boldsymbol{\theta_1}\|^2 + 2 \left\| \left(1 - \frac{\alpha_a}{\eta}\right)\boldsymbol{\theta_a} + \frac{\alpha_a}{\eta}\boldsymbol{\theta} \right\|^2 \\ & \leq 2\, \|\boldsymbol{\theta_1}\|^2 + 2\left(1 - \frac{\alpha_a}{\eta}\right) \|\boldsymbol{\theta_a}\|^2 + 2\,\frac{\alpha_a}{\eta}\, \|\boldsymbol{\theta}\|^2 \\ & \leq 8\, \frac{\left(\alpha_a\, d + 2\,\frac{\alpha_a^2}{\eta^2}\sup_{\boldsymbol{\theta}\in\boldsymbol{\Theta}} \|\boldsymbol{\theta}\|^2\right)}{\left(1 - \frac{\alpha_a}{\eta}\right)^2}. \end{aligned}$$

Therefore, the first term is greater than

$$\begin{aligned} & \frac{1}{(2\pi\alpha_a)^{d/2}} \exp\left\{ -\frac{1}{2\alpha_a} \left\| \boldsymbol{\theta_1} - \boldsymbol{\theta_a}\left(1 - \frac{\alpha_a}{\eta}\right) - \frac{\alpha_a}{\eta}\boldsymbol{\theta_2} \right\|^2 \right\} \\ & \geq \frac{1}{(2\pi\alpha_a)^{d/2}} \exp\left\{ -\frac{4}{\alpha_a} \frac{\left(\alpha_a\, d + 2\,\frac{\alpha_a^2}{\eta^2}\sup_{\boldsymbol{\theta}\in\boldsymbol{\Theta}} \|\boldsymbol{\theta}\|^2\right)}{\left(1 - \frac{\alpha_a}{\eta}\right)^2} \right\}. \end{aligned}$$

For the second term, note that

$$\frac{\exp\left\{ -\frac{1}{2\,\alpha} \left\| \boldsymbol{\theta_2} - \boldsymbol{\theta} + \alpha\nabla U(\boldsymbol{\theta}) - \frac{\alpha}{\eta}\left(\boldsymbol{\theta} - \boldsymbol{\theta_a}\right) \right\|^2 \right\}}{\sum_{x\in\boldsymbol{\Theta}} \exp\left\{ -\frac{1}{2\,\alpha} \left\| x - \boldsymbol{\theta} + \alpha\nabla U(\boldsymbol{\theta}) - \frac{\alpha}{\eta}\left(\boldsymbol{\theta} - \boldsymbol{\theta_a}\right) \right\|^2 \right\}} \geq \frac{1}{|\boldsymbol{\Theta}|} \exp\left\{ -\frac{1}{2\,\alpha} \left\| \boldsymbol{\theta_2} - \boldsymbol{\theta} + \alpha\nabla U(\boldsymbol{\theta}) - \frac{\alpha}{\eta}\left(\boldsymbol{\theta} - \boldsymbol{\theta_a}\right) \right\|^2 \right\}.$$

For the numerator, one sees,

$$\left\|\boldsymbol{\theta_2} - \boldsymbol{\theta} + \alpha\nabla U(\boldsymbol{\theta}) - \frac{\alpha}{\eta}\left(\boldsymbol{\theta} - \boldsymbol{\theta_a}\right)\right\|^2 \leq \|\boldsymbol{\theta_2} - \boldsymbol{\theta} + \alpha\nabla U(\boldsymbol{\theta})\|^2 + \frac{\alpha^2}{\eta^2}\|\boldsymbol{\theta} - \boldsymbol{\theta_a}\|^2 + 2\frac{\alpha}{\eta}\|\boldsymbol{\theta_2} - \boldsymbol{\theta} + \alpha\nabla U(\boldsymbol{\theta})\|\,\|\boldsymbol{\theta} - \boldsymbol{\theta_a}\|\,.$$

For the first term, we have

$$\|\boldsymbol{\theta_2} - \boldsymbol{\theta} + \alpha\nabla U(\boldsymbol{\theta})\|^2 \leq \|\boldsymbol{\theta_2} - \boldsymbol{\theta}\|^2 + \alpha^2\|\nabla U(\boldsymbol{\theta})\|^2 + 2\,\alpha\,\|\boldsymbol{\theta_2} - \boldsymbol{\theta}\|\,\|\nabla U(\boldsymbol{\theta})\|.$$

Define $a = \text{argmin}_{\boldsymbol{\theta}\in\boldsymbol{\Theta}}\|\nabla U(\boldsymbol{\theta})\|$. Therefore, the above expression is less than

$$\begin{aligned}\|\boldsymbol{\theta_2} - \boldsymbol{\theta} + \alpha\nabla U(\boldsymbol{\theta})\|^2 &\leq \text{diam}(\boldsymbol{\Theta})^2 + \alpha^2\left(M^2\text{diam}(\boldsymbol{\Theta})^2 + \|\nabla U(a)\|^2 + 2\,M\,\text{diam}(\boldsymbol{\Theta})\|\nabla U(a)\|\right)\\ &\quad + 2\alpha\,\text{diam}(\boldsymbol{\Theta})\left(M\,\text{diam}(\boldsymbol{\Theta}) + \|\nabla U(a)\|\right)\\ &\leq (\alpha\,M+1)^2\,\text{diam}(\boldsymbol{\Theta})^2 + 2\,(M+\alpha)\|\nabla U(a)\|\text{diam}(\boldsymbol{\Theta}) + \alpha^2\|\nabla U(a)\|^2.\end{aligned}$$

For the second term, we have

$$\alpha\|\nabla U(\boldsymbol{\theta})\|^2 \leq \alpha M^2\text{diam}(\boldsymbol{\Theta})^2 + \alpha\|\nabla U(a)\|^2 + 2\alpha\,M\,\text{diam}(\boldsymbol{\Theta})\|\nabla U(a)\|$$

and for the final term we have

$$\begin{aligned}2\frac{\alpha}{\eta}\|\boldsymbol{\theta_2} - \boldsymbol{\theta} + \alpha\nabla U(\boldsymbol{\theta})\|\,\|\boldsymbol{\theta} - \boldsymbol{\theta_a}\| \leq 2\frac{\alpha}{\eta}&\Big[(\alpha M+1)^2\,\text{diam}(\boldsymbol{\Theta})^2 + 2(M+\alpha)\|\nabla U(a)\|\text{diam}(\boldsymbol{\Theta})\\ &+\alpha^2\|\nabla U(a)\|^2\Big]^{1/2}\text{diam}(\boldsymbol{\Theta}).\end{aligned} \tag{19}$$

Therefore we have

$$\begin{aligned}&\frac{\exp\left\{-\frac{1}{2\,\alpha}\left\|\boldsymbol{\theta_2} - \boldsymbol{\theta} + \alpha\nabla U(\boldsymbol{\theta}) - \frac{\alpha}{\eta}\left(\boldsymbol{\theta} - \boldsymbol{\theta_a}\right)\right\|^2\right\}}{\sum_{x\in\boldsymbol{\Theta}}\exp\left\{-\frac{1}{2\,\alpha}\left\|x - \boldsymbol{\theta} + \alpha\nabla U(\boldsymbol{\theta}) - \frac{\alpha}{\eta}\left(\boldsymbol{\theta} - \boldsymbol{\theta_a}\right)\right\|^2\right\}}\\ &\geq \frac{1}{|\boldsymbol{\Theta}|}\exp\Big\{-\frac{1}{2\alpha}\Big[\left((\alpha\,M+1)^2 + \alpha\,M^2\right)\text{diam}(\boldsymbol{\Theta})^2 + (2\,(M+\alpha) + 2\alpha M)\,\|\nabla U(a)\|\text{diam}(\boldsymbol{\Theta}) + \left(\alpha^2+\alpha\right)\|\nabla U(a)\|^2\\ &\qquad +2\frac{\alpha}{\eta}\left[(\alpha\,M+1)^2\,\text{diam}(\boldsymbol{\Theta})^2 + 2\,(M+\alpha)\|\nabla U(a)\|\text{diam}(\boldsymbol{\Theta}) + \alpha^2\|\nabla U(a)\|^2\right]^{1/2}\text{diam}(\boldsymbol{\Theta})\Big]\Big\}.\end{aligned}$$

This finally gives $\tilde{\eta}$ as

$$\begin{aligned}\bar{\eta} = &\frac{1}{(2\pi\alpha_a)^{d/2}}\exp\left\{-\frac{4}{\alpha_a}\frac{\left(\alpha_a\,d + 2\,\frac{\alpha_a^2}{\eta^2}\sup_{\boldsymbol{\theta}\in\boldsymbol{\Theta}}\|\boldsymbol{\theta}\|^2\right)}{\left(1-\frac{\alpha_a}{\eta}\right)^2}\right\}\\ &\cdot\frac{1}{|\boldsymbol{\Theta}|}\exp\Big\{-\frac{1}{2\alpha}\Big[\left((\alpha\,M+1)^2 + \alpha\,M^2\right)\text{diam}(\boldsymbol{\Theta})^2 + (2\,(M+\alpha) + 2\alpha M)\,\|\nabla U(a)\|\text{diam}(\boldsymbol{\Theta}) + \left(\alpha^2+\alpha\right)\|\nabla U(a)\|^2\\ &\qquad +2\frac{\alpha}{\eta}\left[(\alpha\,M+1)^2\,\text{diam}(\boldsymbol{\Theta})^2 + 2\,(M+\alpha)\|\nabla U(a)\|\text{diam}(\boldsymbol{\Theta}) + \alpha^2\|\nabla U(a)\|^2\right]^{1/2}\text{diam}(\boldsymbol{\Theta})\Big]\Big\}\end{aligned}$$

with the reference measure $\mu(\cdot)$ is the product measure of the Lebesgue measure and the counting measure.

Lemma D.3. *The Markov chain defined by Algorithm 1 is irreducible, aperiodic and Harris recurrent.*

Proof. For any Borel measurable A with $\lambda(A) > 0$ and any $\boldsymbol{\theta} \in \boldsymbol{\Theta}$, we have

$$\mathbb{P}\left(\boldsymbol{\theta}'_a \in A,\, \boldsymbol{\theta}' = \boldsymbol{\theta}^* \mid \boldsymbol{\theta}_a,\, \boldsymbol{\theta}\right) = \mathbb{P}\left(\boldsymbol{\theta}'_a \in A \mid \boldsymbol{\theta}_a,\, \theta\right)\mathbb{P}\left(\boldsymbol{\theta}' = \boldsymbol{\theta}^* \mid \boldsymbol{\theta}_a,\, \boldsymbol{\theta}\right).$$

Note that both the above terms are positive since the first distribution is Gaussian and the second term is positive by definition. We can similarly establish aperiodicity by noting that there is no partition of $\boldsymbol{\Theta}\times\mathbb{R}^d$ such that the previous probability is 1. Finally, due to the fact that the algorithm satisfies a drift condition, the Markov chain is Harris.

We may leverage the above results to obtain a rate of convergence of the sampler using Ekvall & Jones (2021).

Theorem D.4. *The Markov chain has a stationary distribution dependent on $\gamma = (\alpha, \alpha_a)$, π_γ, and is (M, ρ) geometrically ergodic with*

$$\|P^k(x, \cdot) - \pi_\gamma(\cdot)\|_{TV} \leq M(x)\rho^k$$

where

$$M(x) = 2 + \frac{\tilde{b}}{1 - \tilde{\lambda}} + \tilde{V}(x)$$

and

$$\rho \leq \max\left\{(1 - \bar{\eta})^r, \left(\frac{1 + 2\tilde{b} + \tilde{\lambda} + \tilde{\lambda}d}{1 + d}\right)^{1-r} \left(1 + 2\tilde{b} + 2\tilde{\lambda}d\right)^r\right\}$$

for some free parameter $0 < r < 1$ and where $\bar{\eta}$, b, λ are previously defined.

Proof. The proof follows directly from Theorem D.1, Theorem D.2 and Lemma D.3 Ekvall & Jones (2021).

Theorem D.5. *For any function $f : \mathbb{R}^p \to \mathbb{R}$ with $f^2(x) \leq V(x)$ for all $x \in \mathbb{R}^p$ one has*

$$\sqrt{n}\left(\bar{f} - \mathbb{E}_{\pi_\gamma} f\right) \xrightarrow{d} N(0, \sigma_f^2)$$

as $n \to \infty$, where $\sigma_f^2 \in [0, \infty)$. , where

$$\bar{f} = \frac{1}{n}\sum_{i=1}^{n} f(X_i).$$

Proof. The proof follows from Theorem D.1 by noting that $PV \leq \lambda V + b$ implies

$$P\left(V + 1\right) \leq \lambda\left(V + 1\right) + \left(b + 1 - \lambda\right).$$

This implies a drift condition holds with $V : \mathbb{R}^d \to [1, \infty)$. Hence the result follows via Jones (2004). Note that $\sigma_f^2 = 0$ implies convergence to a Gaussian degenerate at 0.

Define

$$\begin{aligned}
\bar{\eta}^* = \exp&\left\{-\frac{1}{\alpha_a}\operatorname{diam}(\boldsymbol{\Theta}_a)^2 - \frac{\alpha_a}{\eta^2}\Delta(\boldsymbol{\Theta}, \boldsymbol{\Theta}_a)^2\right\} \\
&\times \exp\left\{-\frac{1}{2\alpha}\left[\left((\alpha M + 1)^2 + \alpha M^2\right)\operatorname{diam}(\boldsymbol{\Theta})^2\right.\right. \\
&\quad + \left(2(M + \alpha) + 2\alpha M\right)\|\nabla U(a)\|\operatorname{diam}(\boldsymbol{\Theta}) \\
&\quad + \left(\alpha^2 + \alpha\right)\|\nabla U(a)\|^2 \\
&\quad \left.\left. + 2\frac{\alpha}{\eta}\left[(\alpha M + 1)^2\operatorname{diam}(\boldsymbol{\Theta})^2 + 2(M + \alpha)\|\nabla U(a)\|\operatorname{diam}(\boldsymbol{\Theta}) + \alpha^2\|\nabla U(a)\|^2\right]^{1/2}\operatorname{diam}(\boldsymbol{\Theta})\right]\right\}
\end{aligned} \tag{20}$$

where $\mathrm{Leb}(\cdot)$ is the Lebesgue measure of a particular set.

Lemma D.6. *Under Assumptions 5.1 and 5.3, the Markov chain with transition operator P as in Algorithm 1 satisfies,*

$$P((\boldsymbol{\theta}_a, \boldsymbol{\theta}), A) \geq \bar{\eta}^*\mu(A)$$

where $\bar{\eta}^* > 0$ is as defined in equation 20 and $\mu(\cdot)$ is the uniform probability measure on $\Theta_a \times \Theta$.

Proof. We consider the case where $\boldsymbol{\theta}_a$ is restricted to some compact subset of $\mathbb{R}^d$, which we refer to as $\boldsymbol{\Theta}_a$. In this case, note that the transition kernel changes to

$$\begin{aligned}
p((\boldsymbol{\theta}_1, \boldsymbol{\theta}_2) \mid (\boldsymbol{\theta}_a, \boldsymbol{\theta})) = &\frac{1}{\mathrm{Leb}(\boldsymbol{\Theta}_a)}\exp\left\{-\frac{1}{2\alpha_a}\left\|\boldsymbol{\theta}_1 - \boldsymbol{\theta}_a\left(1 - \frac{\alpha_a}{\eta}\right) - \frac{\alpha_a}{\eta}\boldsymbol{\theta}\right\|^2\right\} \\
&\times \frac{\exp\left\{-\frac{1}{2\alpha}\left\|\boldsymbol{\theta}_2 - \boldsymbol{\theta} + \alpha\nabla U(\boldsymbol{\theta}) - \frac{\alpha}{\eta}\left(\boldsymbol{\theta} - \boldsymbol{\theta}_a\right)\right\|^2\right\}}{\sum_{\boldsymbol{x}\in\boldsymbol{\Theta}}\exp\left\{-\frac{1}{2\alpha}\left\|\boldsymbol{x} - \boldsymbol{\theta} + \alpha\nabla U(\boldsymbol{\theta}) - \frac{\alpha}{\eta}\left(\boldsymbol{\theta} - \boldsymbol{\theta}_a\right)\right\|^2\right\}}.
\end{aligned}$$

The proof is similar to Theorem D.2. The key difference is that we can minorize on the entire set. Noting that

$$\left\|\boldsymbol{\theta}_1 - \boldsymbol{\theta}_a\left(1-\frac{\alpha_a}{\eta}\right) - \frac{\alpha_a}{\eta}\boldsymbol{\theta}\right\|^2 \leq 2\,\|\boldsymbol{\theta}_1 - \boldsymbol{\theta}_a\|^2 + 2\frac{\alpha_a^2}{\eta^2}\,\|\boldsymbol{\theta}_a - \boldsymbol{\theta}\|^2$$
$$\leq 2\,\mathrm{diam}(\boldsymbol{\Theta}_a)^2 + 2\frac{\alpha_a^2}{\eta^2}\,\Delta(\boldsymbol{\Theta},\boldsymbol{\Theta}_a)^2.$$

Using the same argument as Theorem D.2, we get a uniform minorization with

$$\begin{aligned}\bar{\eta}^* = &\frac{1}{\mathrm{Leb}(\boldsymbol{\Theta}_a)}\exp\left\{-\frac{1}{\alpha_a}\,\mathrm{diam}(\boldsymbol{\Theta}_a)^2 - \frac{\alpha_a}{\eta^2}\,\Delta(\boldsymbol{\Theta},\boldsymbol{\Theta}_a)^2\right\}\\ &\times\frac{1}{|\boldsymbol{\Theta}|}\exp\Big\{-\frac{1}{2\alpha}\Big[\left((\alpha\,M+1)^2+\alpha\,M^2\right)\mathrm{diam}(\boldsymbol{\Theta})^2\\ &\quad+(2(M+\alpha)+2\alpha M)\,\|\nabla U(a)\|\,\mathrm{diam}(\boldsymbol{\Theta})\\ &\quad+\left(\alpha^2+\alpha\right)\|\nabla U(a)\|^2\\ &\quad+2\frac{\alpha}{\eta}\left[(\alpha\,M+1)^2\,\mathrm{diam}(\boldsymbol{\Theta})^2+2(M+\alpha)\|\nabla U(a)\|\,\mathrm{diam}(\boldsymbol{\Theta})+\alpha^2\|\nabla U(a)\|^2\right]^{1/2}\mathrm{diam}(\boldsymbol{\Theta})\Big]\Big\}.\end{aligned}$$

with the reference measure

$$\mu(\cdot) = \frac{1}{\mathrm{Leb}(\Theta_a)|\Theta|}$$

is the uniform measure.

Proof of Theorem 5.5. Using Lemma D.6 and Proposition 5.4, we further have

$$\|P^k(x,\cdot) - \tilde{\pi}\|_{TV} \leq (1-\bar{\eta}^*)^k + Z\exp\left(\frac{M}{4} - \frac{1}{2\alpha} + \frac{\Delta(\boldsymbol{\Theta},\boldsymbol{\Theta}_a)^2 - \vartheta(\boldsymbol{\Theta},\boldsymbol{\Theta}_a)}{2\eta}\right)$$

for all $x \in \mathbb{R}^d$ and $M(x), \rho$ is as defined in Theorem D.1 itself. Hence we are done.

Theorem D.7. *Let assumptions 5.1, 5.3 hold. Then, for any function $f : \mathbb{R}^p \to \mathbb{R}$ with $\|f\|_{\mathbb{L}^2_\pi} < \infty$, one has*

$$\sqrt{n}\left(\bar{f} - \mathbb{E}_{\pi_\gamma} f\right) \xrightarrow{d} N(0,\sigma_f^2)$$

as $n \to \infty$, where $\sigma_f^2 \in [0,\infty)$.

Proof. Using Theorem 5.5, the proof follows directly from Jones (2004).

D.4 Proofs for EDMALA

Proposition D.8. *For EDMALA(EDLP with MH step, refer Algorithm 1) the drift condition is satisfied with drift function $V(x_1,x_2) = \|x_1\|^2$.*

Proof. The proof follows from Theorem D.1 by observing that

$$PV(\boldsymbol{\theta}_a,\boldsymbol{\theta}) \leq \int \|\boldsymbol{\theta}_{a_1}\|^2 q((\boldsymbol{\theta}_a,\boldsymbol{\theta}),(\boldsymbol{\theta}_{a_1},\boldsymbol{\theta}_1))d\boldsymbol{\theta}_{a_1} + 1$$
$$\leq \lambda V(\boldsymbol{\theta}_a,\boldsymbol{\theta}) + (b+1).$$

Lemma D.9. *Under Assumptions 5.1, 5.2, 5.3, and $\alpha < \frac{2}{M}$, for Markov chain P in Algorithm 1, we have for any $\widetilde{\boldsymbol{\theta}},\widetilde{\boldsymbol{\theta}}' \in \widetilde{\boldsymbol{\Theta}}$,*

$$p(\widetilde{\boldsymbol{\theta}}|\widetilde{\boldsymbol{\theta}}') \geq \epsilon_\gamma \frac{\exp\left\{\frac{1}{2}U(\boldsymbol{\theta}')\right\}}{\sum_{x\in\boldsymbol{\Theta}}\exp\left(\frac{U(x)}{2}\right)}.\frac{\exp\left\{-\frac{1}{2\alpha_a}\,diam(\boldsymbol{\Theta}_a)^2\right\}}{\Phi_{\alpha_a}(\boldsymbol{\Theta}_a)}$$

, where

$$\epsilon_\gamma = \exp\left\{\begin{array}{l} -\left(\frac{M}{2}+\frac{1}{\alpha}-\frac{m}{4}\right) diam(\boldsymbol{\Theta})^2 - \frac{1}{2}\|\nabla U(a)\|\, diam(\boldsymbol{\Theta}) \\ -\left(\frac{3\alpha_a}{8\eta^2}+\frac{2}{\eta}\right)\Delta(\boldsymbol{\Theta},\boldsymbol{\Theta}_a)^2 + \frac{\vartheta(\boldsymbol{\Theta},\boldsymbol{\Theta}_a)}{\eta} \end{array}\right\},$$

with $a \in \arg\min_{\boldsymbol{\theta}\in\boldsymbol{\Theta}} \|\nabla U(\boldsymbol{\theta})\|$

Proof. We follow a similar minorization proof style as of Lemma 5.3 from Pynadath et al. (2024). We know from Equation 15,

$$Z_\gamma(\widetilde{\boldsymbol{\theta}}) = \frac{1}{\sqrt{(2\pi\alpha_a)^d}} \int_{\boldsymbol{\theta}'_a} \sum_{\boldsymbol{\theta}'\in\boldsymbol{\Theta}} \exp\left(\frac{1}{2}\big(-U(\boldsymbol{\theta})+U(\boldsymbol{\theta}')\big) - (\boldsymbol{\theta}-\boldsymbol{\theta}')^\top\left(\frac{1}{2\alpha}I + \frac{1}{4}\int_0^1 \nabla^2 U\big((1-s)\boldsymbol{\theta}+s\boldsymbol{\theta}'\big)\,ds\right)(\boldsymbol{\theta}-\boldsymbol{\theta}')\right.$$
$$\left. -\frac{1}{2\eta}(\boldsymbol{\theta}-\boldsymbol{\theta}_a)^\top(\boldsymbol{\theta}'-\boldsymbol{\theta}'_a) - \frac{1}{2\alpha_a}\|\boldsymbol{\theta}'_a-\boldsymbol{\theta}_a\|^2 + \frac{4\eta-\alpha_a}{8\eta^2}\|\boldsymbol{\theta}-\boldsymbol{\theta}_a\|^2\right).$$

Recall, from Assumption 5.1,U is M-gradient Lipschitz, we have

$$\frac{1}{\alpha}I + \frac{1}{2}\int_0^1 \nabla^2 U((1-s)\boldsymbol{\theta}+s\boldsymbol{\theta}')\,ds) \geq \left(\frac{1}{\alpha}-\frac{M}{2}\right) I$$

Since $\alpha < \frac{2}{M}$, the matrix $\left(\frac{1}{\alpha}-\frac{M}{2}\right) I$is positive definite.

This implies,

$$\begin{aligned} Z_\gamma(\widetilde{\boldsymbol{\theta}}) &\leq \frac{1}{\sqrt{2\pi\alpha_a}^d} \exp\left(-\frac{U(\boldsymbol{\theta})}{2} - \frac{\alpha_a}{8\eta^2}\|\boldsymbol{\theta}-\boldsymbol{\theta}_a\|^2 + \frac{1}{2\eta}\|\boldsymbol{\theta}-\boldsymbol{\theta}_a\|^2\right) \sum_{x\in\boldsymbol{\Theta}} \exp\left(\frac{U(x)}{2}\right) \\ &\int_y \sum_x \exp\left(-\frac{1}{2\alpha_a}\|y-\boldsymbol{\theta}_a\|^2 - \frac{1}{2\eta}(\boldsymbol{\theta}-\boldsymbol{\theta}_a)^\top(x-y)\right) dy \\ &\leq \sum_{x\in\boldsymbol{\Theta}} \exp\left(\frac{U(x)}{2}\right) \exp\left(-\frac{U(\boldsymbol{\theta})}{2} + \frac{1}{2\eta}(\|\boldsymbol{\theta}-\boldsymbol{\theta}_a\|^2 - \vartheta(\boldsymbol{\Theta},\boldsymbol{\Theta}_a))\right) \\ &\leq \sum_{x\in\boldsymbol{\Theta}} \exp\left(\frac{U(x)}{2}\right) \exp\left(-\frac{U(\boldsymbol{\theta})}{2} + \frac{\Delta(\boldsymbol{\Theta},\boldsymbol{\Theta}_a)^2 - \vartheta(\boldsymbol{\Theta},\boldsymbol{\Theta}_a)}{2\eta}\right) \end{aligned}$$

Since Assumption 5.2 holds true in this setting, we have an $m > 0$ such that for any $\boldsymbol{\theta} \in conv(\boldsymbol{\Theta})$

$$-\nabla^2 U(\boldsymbol{\theta}) \geq m\, I.$$

From this, one notes that

$$\begin{aligned} Z_\gamma(\widetilde{\boldsymbol{\theta}}) &\geq \frac{1}{\sqrt{2\pi\alpha_a}^d} \exp\left\{-\frac{U(\boldsymbol{\theta})}{2} - \frac{\alpha_a}{8\eta^2}\|\boldsymbol{\theta}-\boldsymbol{\theta}_a\|^2 + \frac{1}{2\eta}\|\boldsymbol{\theta}-\boldsymbol{\theta}_a\|^2\right\} \exp\left\{-\frac{1}{2}\left(\frac{1}{\alpha}-\frac{m}{2}\right) \operatorname{diam}(\boldsymbol{\Theta})^2\right\} \\ &\sum_{x\in\boldsymbol{\Theta}} \exp\left(\frac{U(x)}{2}\right) \int_y \sum_x \exp\left(-\frac{1}{2\alpha_a}\|y-\boldsymbol{\theta}_a\|^2 - \frac{1}{2\eta}(\boldsymbol{\theta}-\boldsymbol{\theta}_a)^\top(x-y)\right) dy \\ &\geq \sum_{x\in\boldsymbol{\Theta}} \exp\left(\frac{U(x)}{2}\right) \exp\left\{-\frac{U(\boldsymbol{\theta})}{2} - \frac{\alpha_a}{8\eta^2}\|\boldsymbol{\theta}-\boldsymbol{\theta}_a\|^2 - \frac{1}{2}\left(\frac{1}{\alpha}-\frac{m}{2}\right) \operatorname{diam}(\boldsymbol{\Theta})^2 - \frac{1}{2\eta}\Delta(\boldsymbol{\Theta},\boldsymbol{\Theta}_a)^2\right\} \\ &\geq \sum_{x\in\boldsymbol{\Theta}} \exp\left(\frac{U(x)}{2}\right) \exp\left\{-\frac{U(\boldsymbol{\theta})}{2} - \frac{\alpha_a}{8\eta^2}\Delta(\boldsymbol{\Theta},\boldsymbol{\Theta}_a)^2 - \frac{1}{2}\left(\frac{1}{\alpha}-\frac{m}{2}\right) \operatorname{diam}(\boldsymbol{\Theta})^2 - \frac{1}{2\eta}\Delta(\boldsymbol{\Theta},\boldsymbol{\Theta}_a)^2\right\} \end{aligned}$$

In other words,

$$\exp\left((-\frac{\alpha_a}{8\eta^2}-\frac{1}{2\eta})\Delta(\boldsymbol{\Theta},\boldsymbol{\Theta}_a)^2-\frac{1}{2}\left(\frac{1}{\alpha}-\frac{m}{2}\right)\text{diam}(\boldsymbol{\Theta})^2\right)\leq\frac{Z_\gamma(\widetilde{\boldsymbol{\theta}})}{\sum_{x\in\boldsymbol{\Theta}}\exp\left(\frac{U(x)}{2}\right)\exp\left(-\frac{U(\boldsymbol{\theta})}{2}\right)}\leq\exp\left(\frac{\Delta(\boldsymbol{\Theta},\boldsymbol{\Theta}_a)^2-\vartheta(\boldsymbol{\Theta},\boldsymbol{\Theta}_a)}{2\eta}\right)$$

Consequently,

$$\frac{\frac{Z_\gamma(\widetilde{\boldsymbol{\theta}})}{\sum_{x\in\boldsymbol{\Theta}}\exp\left(\frac{U(x)}{2}\right)\exp\left(-\frac{U(\boldsymbol{\theta})}{2}\right)}}{\frac{Z_\gamma(\widetilde{\boldsymbol{\theta}}')}{\sum_{x\in\boldsymbol{\Theta}}\exp\left(\frac{U(x)}{2}\right)\exp\left(-\frac{U(\boldsymbol{\theta}')}{2}\right)}}\geq\frac{\exp\left((-\frac{\alpha_a}{8\eta^2}-\frac{1}{2\eta})\Delta(\boldsymbol{\Theta},\boldsymbol{\Theta}_a)^2-\frac{(2-m\alpha)\text{diam}(\boldsymbol{\Theta})^2}{4\alpha}\right)}{\exp\left(\frac{\Delta(\boldsymbol{\Theta},\boldsymbol{\Theta}_a)^2-\vartheta(\boldsymbol{\Theta},\boldsymbol{\Theta}_a)}{2\eta}\right)}$$

This implies

$$\frac{Z_\gamma(\widetilde{\boldsymbol{\theta}})}{Z_\gamma(\widetilde{\boldsymbol{\theta}}')}\geq\exp\left(\frac{1}{2}(-U(\boldsymbol{\theta})+U(\boldsymbol{\theta}'))\right)\frac{\exp\left((-\frac{\alpha_a}{8\eta^2}-\frac{1}{2\eta})\Delta(\boldsymbol{\Theta},\boldsymbol{\Theta}_a)^2-\frac{(2-m\alpha)\text{diam}(\boldsymbol{\Theta})^2}{4\alpha}\right)}{\exp\left(\frac{\Delta(\boldsymbol{\Theta},\boldsymbol{\Theta}_a)^2-\vartheta(\boldsymbol{\Theta},\boldsymbol{\Theta}_a)}{2\eta}\right)}$$

One notices from equation 9,

$$\begin{aligned}
q_\gamma(\widetilde{\boldsymbol{\theta}}'|\widetilde{\boldsymbol{\theta}}) &= \frac{Z_\gamma(\widetilde{\boldsymbol{\theta}})^{-1}}{\sqrt{(2\pi\alpha_a)^d}}\exp\left(\frac{1}{2}(-U(\boldsymbol{\theta})+U(\boldsymbol{\theta}'))-(\boldsymbol{\theta}-\boldsymbol{\theta}')^\top\left(\frac{1}{2\alpha}I+\frac{1}{4}\int_0^1\nabla^2U((1-s)\boldsymbol{\theta}+s\boldsymbol{\theta}')ds\right)(\boldsymbol{\theta}-\boldsymbol{\theta}')\right.\\
&\quad\left.-\frac{1}{2\eta}(\boldsymbol{\theta}-\boldsymbol{\theta}_a)^\top(\boldsymbol{\theta}'-\boldsymbol{\theta}'_a)-\frac{1}{2\alpha_a}\|\boldsymbol{\theta}'_a-\boldsymbol{\theta}_a\|^2+\frac{4\eta-\alpha_a}{8\eta^2}\|\boldsymbol{\theta}-\boldsymbol{\theta}_a\|^2\right)\\
&\geq\frac{Z_\gamma(\widetilde{\boldsymbol{\theta}})^{-1}}{\sqrt{(2\pi\alpha_a)^d}}\exp\left(\frac{1}{2}\left\langle\nabla U(\boldsymbol{\theta}),\boldsymbol{\theta}'-\boldsymbol{\theta}\right\rangle-\frac{1}{2\alpha}\|\boldsymbol{\theta}-\boldsymbol{\theta}'\|^2-\frac{1}{2\eta}(\boldsymbol{\theta}-\boldsymbol{\theta}_a)^\top(\boldsymbol{\theta}'-\boldsymbol{\theta}'_a)\right.\\
&\quad\left.-\frac{1}{2\alpha_a}\|\boldsymbol{\theta}'_a-\boldsymbol{\theta}_a\|^2-\frac{\alpha_a}{8\eta^2}\|\boldsymbol{\theta}-\boldsymbol{\theta}_a\|^2\right)
\end{aligned}$$

We also note that

$$\begin{aligned}
-\frac{1}{2}\left\langle\nabla U(\boldsymbol{\theta}),\boldsymbol{\theta}'-\boldsymbol{\theta}\right\rangle+\frac{1}{2\alpha}\|\boldsymbol{\theta}-\boldsymbol{\theta}'\|^2 &= \frac{1}{2}\left\langle-\nabla U(\boldsymbol{\theta})+\nabla U(a),\boldsymbol{\theta}'-\boldsymbol{\theta}\right\rangle+\frac{1}{2}\left\langle-\nabla U(a),\boldsymbol{\theta}'-\boldsymbol{\theta}\right\rangle+\frac{1}{2\alpha}\|\boldsymbol{\theta}-\boldsymbol{\theta}'\|^2\\
&\leq\frac{1}{2}\left\langle-\nabla U(\boldsymbol{\theta})+\nabla U(a),\boldsymbol{\theta}'-\boldsymbol{\theta}\right\rangle+\frac{1}{2}\left\langle-\nabla U(a),\boldsymbol{\theta}'-\boldsymbol{\theta}\right\rangle+\frac{1}{2\alpha}diam(\boldsymbol{\Theta})^2\\
&\leq\frac{1}{2}\left\|-\nabla U(\boldsymbol{\theta})+\nabla U(a)\right\|\left\|\boldsymbol{\theta}'-\boldsymbol{\theta}\right\|+\frac{1}{2}\left\|\nabla U(a)\right\|\left\|\boldsymbol{\theta}'-\boldsymbol{\theta}\right\|+\frac{1}{2\alpha}diam(\boldsymbol{\Theta})^2\\
&\leq\frac{1}{2}\|-\nabla U(\boldsymbol{\theta})+\nabla U(a)\|diam(\boldsymbol{\Theta})+\frac{1}{2}\|\nabla U(a)\|diam(\boldsymbol{\Theta})+\frac{1}{2\alpha}diam(\boldsymbol{\Theta})^2\\
&\leq\frac{1}{2}(M\|a-\boldsymbol{\theta}\|)diam(\boldsymbol{\Theta})+\frac{1}{2}\|\nabla U(a)\|diam(\boldsymbol{\Theta})+\frac{1}{2\alpha}diam(\boldsymbol{\Theta})^2\\
&\leq\left(\frac{1}{2}M+\frac{1}{2\alpha}\right)diam(\boldsymbol{\Theta})^2+\frac{1}{2}\|\nabla U(a)\|\,diam(\boldsymbol{\Theta}).
\end{aligned}$$

Combining, we get

$$\begin{aligned}
q_\gamma(\widetilde{\boldsymbol{\theta}}'|\widetilde{\boldsymbol{\theta}}) &\geq\frac{Z_\gamma(\widetilde{\boldsymbol{\theta}})^{-1}}{\sqrt{(2\pi\alpha_a)^d}}\exp\left\{(-\frac{M}{2}-\frac{1}{2\alpha})\text{diam}(\boldsymbol{\Theta})^2-\frac{1}{2}\|\nabla U(a)\|\text{diam}(\boldsymbol{\Theta})-\frac{1}{2\eta}(\boldsymbol{\theta}-\boldsymbol{\theta}_a)^\top(\boldsymbol{\theta}'-\boldsymbol{\theta}'_a)-\frac{1}{2\alpha_a}\|\boldsymbol{\theta}'_a-\boldsymbol{\theta}_a\|^2-\frac{\alpha_a}{8\eta^2}\|\boldsymbol{\theta}-\boldsymbol{\theta}_a\|^2\right\}\\
&\geq\frac{\frac{1}{\sqrt{(2\pi\alpha_a)^d}}\exp\left\{(-\frac{M}{2}-\frac{1}{2\alpha})\text{diam}(\boldsymbol{\Theta})^2-\frac{1}{2}\|\nabla U(a)\|\text{diam}(\boldsymbol{\Theta})-\frac{1}{2\eta}(\boldsymbol{\theta}-\boldsymbol{\theta}_a)^\top(\boldsymbol{\theta}'-\boldsymbol{\theta}'_a)-\frac{1}{2\alpha_a}\|\boldsymbol{\theta}'_a-\boldsymbol{\theta}_a\|^2-\frac{\alpha_a}{8\eta^2}\|\boldsymbol{\theta}-\boldsymbol{\theta}_a\|^2\right\}}{\sum_{x\in\boldsymbol{\Theta}}\exp\left(\frac{U(x)}{2}\right)\exp\left(-\frac{U(\boldsymbol{\theta})}{2}+\frac{\Delta(\boldsymbol{\Theta},\boldsymbol{\Theta}_a)^2-\vartheta(\boldsymbol{\Theta},\boldsymbol{\Theta}_a)}{2\eta}\right)}\\
&\geq\frac{\exp\left\{-\frac{1}{2\alpha_a}\text{diam}(\boldsymbol{\Theta}_a)^2\right\}}{\Phi_{\alpha_a}(\boldsymbol{\Theta}_a)}\frac{\exp\left\{(-\frac{M}{2}-\frac{1}{2\alpha})\text{diam}(\boldsymbol{\Theta})^2-\frac{1}{2}\|\nabla U(a)\|\text{diam}(\boldsymbol{\Theta})+(-\frac{1}{2\eta}-\frac{\alpha_a}{8\eta^2})\Delta(\boldsymbol{\Theta},\boldsymbol{\Theta}_a)^2\right\}}{\sum_{x\in\boldsymbol{\Theta}}\exp\left(\frac{U(x)}{2}\right)\exp\left(-\frac{U(\boldsymbol{\theta})}{2}+\frac{\Delta(\boldsymbol{\Theta},\boldsymbol{\Theta}_a)^2-\vartheta(\boldsymbol{\Theta},\boldsymbol{\Theta}_a)}{2\eta}\right)}
\end{aligned}$$

Acceptance Ratio,

$$
\begin{aligned}
\rho(\widetilde{\boldsymbol{\theta}'} \mid \widetilde{\boldsymbol{\theta}}) &= \left(\frac{\pi(\widetilde{\boldsymbol{\theta}'}) q_\gamma(\widetilde{\boldsymbol{\theta}} \mid \widetilde{\boldsymbol{\theta}'})}{\pi(\widetilde{\boldsymbol{\theta}}) q_\gamma(\widetilde{\boldsymbol{\theta}'} \mid \widetilde{\boldsymbol{\theta}})} \right) \\
&= \exp\left\{ U(\boldsymbol{\theta}') - U(\boldsymbol{\theta}) + \frac{1}{2\eta}(\|\boldsymbol{\theta} - \boldsymbol{\theta}_a\|^2 - \|\boldsymbol{\theta}' - \boldsymbol{\theta}'_a\|^2) \right\} \frac{\tilde{Z}}{\tilde{Z}} \cdot \\
&\exp\left\{ U(\boldsymbol{\theta}) - U(\boldsymbol{\theta}') - \frac{1}{2\eta}(\|\boldsymbol{\theta} - \boldsymbol{\theta}_a\|^2 - \|\boldsymbol{\theta}' - \boldsymbol{\theta}'_a\|^2) - \frac{\alpha_a}{8\eta^2}(\|\boldsymbol{\theta}' - \boldsymbol{\theta}'_a\|^2 - \|\boldsymbol{\theta} - \boldsymbol{\theta}_a\|^2) \right\} \frac{Z_\gamma(\widetilde{\boldsymbol{\theta}})}{Z_\gamma(\widetilde{\boldsymbol{\theta}'})} \\
&= \exp\left\{ -\frac{\alpha_a}{8\eta^2}(\|\boldsymbol{\theta}' - \boldsymbol{\theta}'_a\|^2 - \|\boldsymbol{\theta} - \boldsymbol{\theta}_a\|^2) \right\} \frac{Z_\gamma(\widetilde{\boldsymbol{\theta}})}{Z_\gamma(\widetilde{\boldsymbol{\theta}'})}
\end{aligned}
$$

where $\tilde{Z}$ is the normalizing constant for $\pi(\widetilde{\boldsymbol{\theta}})$.

with Acceptance Probability

$$
\mathcal{A}(\widetilde{\boldsymbol{\theta}'} \mid \widetilde{\boldsymbol{\theta}}) = \Big(\rho(\widetilde{\boldsymbol{\theta}'} \mid \widetilde{\boldsymbol{\theta}}) \wedge 1 \Big)
$$

and consider the transition kernel as

$$
p(\widetilde{\boldsymbol{\theta}'} \mid \widetilde{\boldsymbol{\theta}}) = \Big(\mathcal{A}(\widetilde{\boldsymbol{\theta}'} \mid \widetilde{\boldsymbol{\theta}}) \Big) q_\gamma(\widetilde{\boldsymbol{\theta}'} \mid \widetilde{\boldsymbol{\theta}}) + \Big(1 - L(\widetilde{\boldsymbol{\theta}}) \Big) \delta_{\widetilde{\boldsymbol{\theta}}}(\widetilde{\boldsymbol{\theta}'})
$$

where $\delta_{\widetilde{\boldsymbol{\theta}}}(\widetilde{\boldsymbol{\theta}'})$ is the Kronecker delta function and $L(\widetilde{\boldsymbol{\theta}})$ is the total acceptance probability from the point $\widetilde{\boldsymbol{\theta}}$ with

$$
L(\widetilde{\boldsymbol{\theta}}) = \int_{\boldsymbol{\theta}'_a \in \boldsymbol{\Theta}_a} \sum_{\boldsymbol{\theta}' \in \boldsymbol{\Theta}} \Big(\rho([\boldsymbol{\theta}'^T, \boldsymbol{\theta}'^T_a]^T \mid \widetilde{\boldsymbol{\theta}}) \wedge 1 \Big) q_\gamma([\boldsymbol{\theta}'^T, \boldsymbol{\theta}'^T_a]^T | \widetilde{\boldsymbol{\theta}}) \quad d\boldsymbol{\theta}'_a
$$

We note

$$
\begin{aligned}
p(\widetilde{\boldsymbol{\theta}}' \mid \widetilde{\boldsymbol{\theta}}) &= \Big(\mathcal{A}(\widetilde{\boldsymbol{\theta}}' \mid \widetilde{\boldsymbol{\theta}})\Big)\, q_\gamma(\widetilde{\boldsymbol{\theta}}' \mid \widetilde{\boldsymbol{\theta}}) + \Big(1 - L(\widetilde{\boldsymbol{\theta}})\Big)\, \delta_{\widetilde{\boldsymbol{\theta}}}(\widetilde{\boldsymbol{\theta}}') \\
&\geq \Big(\mathcal{A}(\widetilde{\boldsymbol{\theta}}' \mid \widetilde{\boldsymbol{\theta}})\Big)\, q_\gamma(\widetilde{\boldsymbol{\theta}}' \mid \widetilde{\boldsymbol{\theta}}) \\
&= \Big(\rho(\widetilde{\boldsymbol{\theta}}' \mid \widetilde{\boldsymbol{\theta}}) \wedge 1\Big)\, q_\gamma(\widetilde{\boldsymbol{\theta}}' \mid \widetilde{\boldsymbol{\theta}}) \\
&= \exp\left\{-\frac{\alpha_a}{8\eta^2}\left(\|\boldsymbol{\theta}' - \boldsymbol{\theta}'_a\|^2 - \|\boldsymbol{\theta} - \boldsymbol{\theta}_a\|^2\right)\right\} \frac{Z_\gamma(\widetilde{\boldsymbol{\theta}})}{Z_\gamma(\widetilde{\boldsymbol{\theta}}')} q_\gamma(\widetilde{\boldsymbol{\theta}}' \mid \widetilde{\boldsymbol{\theta}}) \\
&\geq \exp\left\{-\frac{\alpha_a}{8\eta^2}\|\boldsymbol{\theta}' - \boldsymbol{\theta}'_a\|^2\right\} \frac{Z_\gamma(\widetilde{\boldsymbol{\theta}})}{Z_\gamma(\widetilde{\boldsymbol{\theta}}')} q_\gamma(\widetilde{\boldsymbol{\theta}}' \mid \widetilde{\boldsymbol{\theta}}) \\
&\geq \exp\left\{-\frac{\alpha_a}{8\eta^2}\Delta(\boldsymbol{\Theta}, \boldsymbol{\Theta}_a)^2 + \frac{1}{2}(-U(\boldsymbol{\theta}) + U(\boldsymbol{\theta}'))\right\} \frac{\exp\left(-\frac{\alpha_a}{8\eta^2} - \frac{1}{2\eta})\Delta(\boldsymbol{\Theta}, \boldsymbol{\Theta}_a)^2 - \frac{(2-m\alpha)\mathrm{diam}(\boldsymbol{\Theta})^2}{4\alpha}\right)}{\exp\left(\frac{\Delta(\boldsymbol{\Theta},\boldsymbol{\Theta}_a)^2 - \vartheta(\boldsymbol{\Theta},\boldsymbol{\Theta}_a)}{2\eta}\right)} q_\gamma(\widetilde{\boldsymbol{\theta}}' \mid \widetilde{\boldsymbol{\theta}}) \\
&\geq \exp\left\{-\frac{\alpha_a}{8\eta^2}\Delta(\boldsymbol{\Theta}, \boldsymbol{\Theta}_a)^2 + \frac{1}{2}(-U(\boldsymbol{\theta}) + U(\boldsymbol{\theta}'))\right\} \frac{\exp\left(-\frac{\alpha_a}{8\eta^2} - \frac{1}{2\eta})\Delta(\boldsymbol{\Theta}, \boldsymbol{\Theta}_a)^2 - \frac{(2-m\alpha)\mathrm{diam}(\boldsymbol{\Theta})^2}{4\alpha}\right)}{\exp\left(\frac{\Delta(\boldsymbol{\Theta},\boldsymbol{\Theta}_a)^2 - \vartheta(\boldsymbol{\Theta},\boldsymbol{\Theta}_a)}{2\eta}\right)} \\
&\quad \cdot \frac{\exp\left\{-\frac{1}{2\alpha_a}\mathrm{diam}(\boldsymbol{\Theta}_a)^2\right\}}{\Phi_{\alpha_a}(\boldsymbol{\Theta}_a)} \frac{\exp\left\{(-\frac{M}{2} - \frac{1}{2\alpha})\mathrm{diam}(\boldsymbol{\Theta})^2 - \frac{1}{2}\|\nabla U(a)\|\mathrm{diam}(\boldsymbol{\Theta}) + \left(-\frac{1}{2\eta} - \frac{\alpha_a}{8\eta^2}\right)\Delta(\boldsymbol{\Theta}, \boldsymbol{\Theta}_a)^2\right\}}{\sum_{x\in\boldsymbol{\Theta}} \exp\left(\frac{U(x)}{2}\right) \exp\left(-\frac{U(\boldsymbol{\theta})}{2} + \frac{\Delta(\boldsymbol{\Theta},\boldsymbol{\Theta}_a)^2 - \vartheta(\boldsymbol{\Theta},\boldsymbol{\Theta}_a)}{2\eta}\right)} \\
&= \frac{\exp\left\{-\frac{1}{2\alpha_a}\mathrm{diam}(\boldsymbol{\Theta}_a)^2\right\}}{\Phi_{\alpha_a}(\boldsymbol{\Theta}_a)} \frac{\exp\left\{\frac{1}{2}U(\boldsymbol{\theta}')\right\}}{\sum_{x\in\boldsymbol{\Theta}} \exp\left(\frac{U(x)}{2}\right)} \exp\left\{(-\frac{3\alpha_a}{8\eta^2} - \frac{2}{\eta})\Delta(\boldsymbol{\Theta}, \boldsymbol{\Theta}_a)^2 + \frac{\vartheta(\boldsymbol{\Theta}, \boldsymbol{\Theta}_a)}{\eta}\right\} \\
&\quad \cdot \exp\left\{(-\frac{M}{2} - \frac{1}{\alpha} + \frac{m}{4})\mathrm{diam}(\boldsymbol{\Theta})^2 - \frac{1}{2}\|\nabla U(a)\|\mathrm{diam}(\boldsymbol{\Theta})\right\} \\
&= \epsilon_\gamma \frac{\exp\left\{\frac{1}{2}U(\boldsymbol{\theta}')\right\}}{\sum_{x\in\boldsymbol{\Theta}} \exp\left(\frac{U(x)}{2}\right)} \frac{\exp\left\{-\frac{1}{2\alpha_a}\mathrm{diam}(\boldsymbol{\Theta}_a)^2\right\}}{\Phi_{\alpha_a}(\boldsymbol{\Theta}_a)}
\end{aligned}
$$

Note: Proof of Theorem 5.6 follows from using Lemma $D.9$.

E Additional Experimental Results

E.1 4D Joint Bernoulli

To provide additional insights into the functionality of EDLP samplers, we explore their behavior on the 4D Joint Bernoulli Distribution, which serves as the simplest low-dimensional case among our experiments. This aids in visualizing and understanding the sampling process.

Target Distribution

The following represents the probability mass function (PMF) for the 4D Joint Bernoulli Distribution used in our test case. The distribution has 16 states with the corresponding probabilities:

Flatness Diagnostics

Under the experimental setup outlined in Section 6, we present the true Eigenspectrum of the Hessian, derived from the discrete samples collected for EDULA, EDMALA, DULA, and DMALA (Figure 10).We manually tune the stepsizes for EDULA and EDMALA to 0.1 and 0.4 respectively. This visualization is inspired by Section 6.3 of (Li & Zhang, 2024), where diagonal Fisher information matrix approximation was used to plot the Eigenvalues. The alignment of the Eigenvalues closer to 0 indicates that the sampled data corresponds to a flatter curvature of the energy function.

$$P_{\boldsymbol{\Theta}}(\boldsymbol{\theta}) = \begin{cases} 0.07688 & \text{if } \boldsymbol{\theta} = 0000, \\ 0.04725 & \text{if } \boldsymbol{\theta} = 0001, \\ 0.12500 & \text{if } \boldsymbol{\theta} = 0010, \\ 0.01667 & \text{if } \boldsymbol{\theta} = 0011, \\ 0.08688 & \text{if } \boldsymbol{\theta} = 0100, \\ 0.07688 & \text{if } \boldsymbol{\theta} = 0101, \\ 0.07688 & \text{if } \boldsymbol{\theta} = 0110, \\ 0.16756 & \text{if } \boldsymbol{\theta} = 0111, \\ 0.04725 & \text{if } \boldsymbol{\theta} = 1000, \\ 0.05825 & \text{if } \boldsymbol{\theta} = 1001, \\ 0.01667 & \text{if } \boldsymbol{\theta} = 1010, \\ 0.04725 & \text{if } \boldsymbol{\theta} = 1011, \\ 0.07688 & \text{if } \boldsymbol{\theta} = 1100, \\ 0.04725 & \text{if } \boldsymbol{\theta} = 1101, \\ 0.01900 & \text{if } \boldsymbol{\theta} = 1110, \\ 0.01335 & \text{if } \boldsymbol{\theta} = 1111. \end{cases}$$

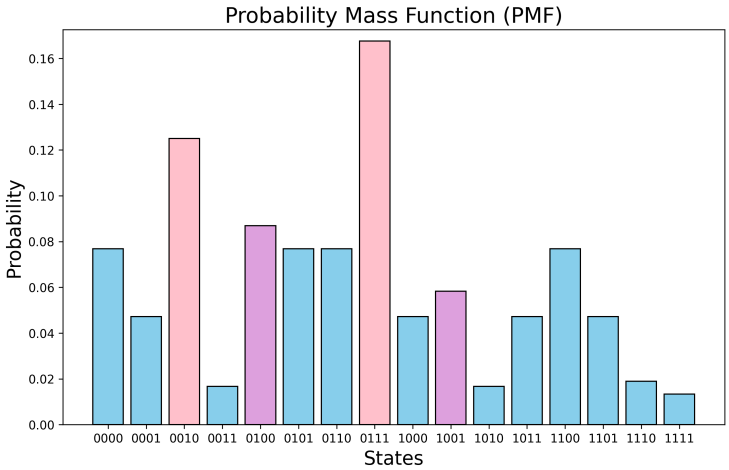

Figure 9: Target Distribution for 4D Joint Bernoulli

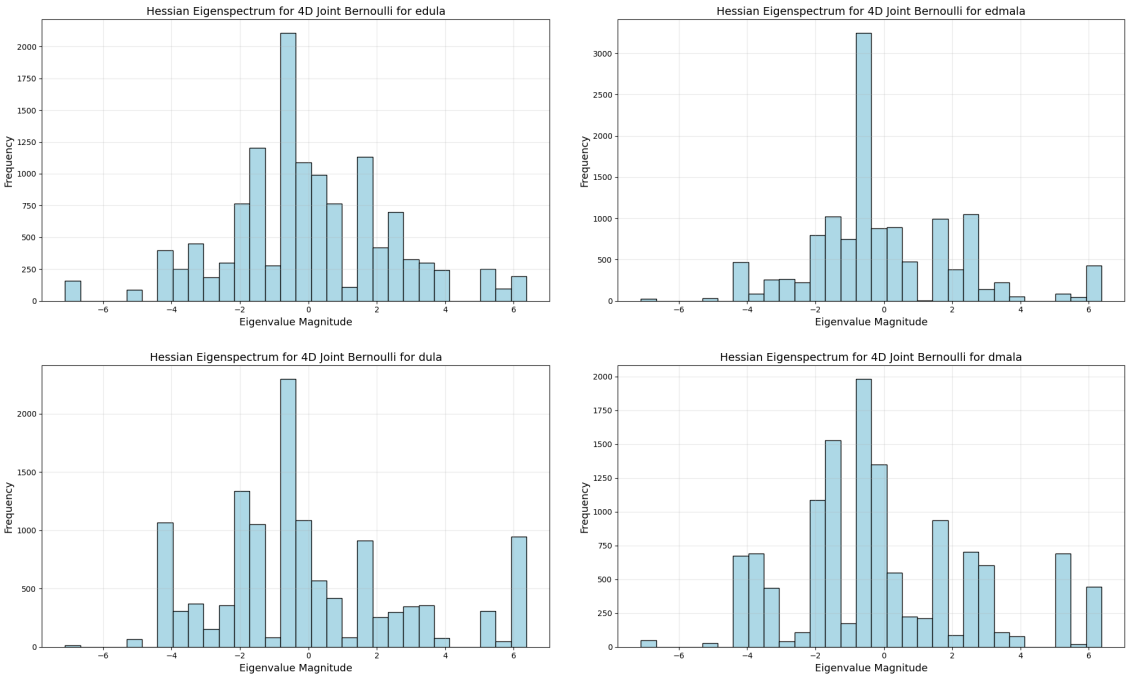

Figure 10: Eigenspectra of EDULA, EDMALA, DULA, and DMALA's performance on a Bernoulli distribution.

EDMALA and EDULA, specifically designed with entropy-aware flatness optimization, exhibit eigenvalue distributions that are notably tighter and more concentrated around zero compared to their non-entropic counterparts, DMALA and DULA.

Quantitatively, EDULA demonstrates a lower spectral dispersion, evidenced by a lower standard deviation (std = 2.401) and narrower interquartile range (IQR = 3.031), relative to DULA (std = 2.832, IQR = 3.466). Similarly, EDMALA outperforms DMALA in terms of spectral concentration, achieving a standard deviation of 2.197 and IQR of 2.747, compared to DMALA's standard deviation of 2.700 and IQR of 3.224. Furthermore, visual inspection corroborates these quantitative findings; EDMALA and EDULA feature fewer extreme eigenvalues and outliers, reflecting biasing into sampling from flatter regions. Collectively, these results affirm

that our entropy-guided methods (EDMALA, EDULA) effectively traverse flatter, aligning well with their intended design objectives.

Finite Time Behavior

In EDLP, the auxiliary variable $\boldsymbol{\theta}_a$ and its associated coupling parameter η serve as a bias mechanism toward flatter regions. Specifically, at moderate values, η provides a meaningful bias toward flat modes by guiding discrete samples to regions where multiple states with similar energies exist nearby. In these flat regions, gradient signals are weaker, and standard samplers (like DLP) typically have difficulty exploring efficiently. Thus, moderate η encourages sampling from flat regions at the cost of slightly slower finite-time convergence. As η grows large, the coupling weakens and the sampler's behavior naturally approaches that of standard DLP(Figure 3). This recovers unbiased sampling that targets high density regions as now the sampler solely utilizes $U(.)$'s gradient. Hence, large η values place minimal bias toward flatness but provide faster finite-time convergence to high-density regions.

Quantitatively, the balance can be seen explicitly in our non-asymptotic convergence guarantees (Theorems 5.5 and 5.6). Comparing our EDMALA bounds with standard DMALA bounds(Pynadath et al., 2024), one can observe that introducing any $\eta > 0$ does introduce an additional term in the bound, slightly impeding finite-time convergence. However, it is crucial to emphasize that this effect is explicitly finite-time. Given sufficient iterations, our method, like all valid MCMC algorithms, is guaranteed to converge exactly to the true target distribution $\pi(\boldsymbol{\theta})$, ensuring long-run correctness. Empirically, for 4D Joint Bernoulli Experiment, logMAE values for the marginal are as follows: DULA(-3.7217) vs EDULA(-3.743) and DMALA(-3.3949) vs EDMALA(-3.5503) . So, while there is preference towards flat modes(Figure 2), our samplers stay true to $\pi(\boldsymbol{\theta})$.

To highlight EDLP's mode scouting behavior as a function of time, we adopt a similar sampling analysis as EMCMC(Li & Zhang, 2024), Appendix E.1. We aim to show that, EDLP shows benefit when DLP does not

$$P_{\boldsymbol{\Theta}}(\boldsymbol{\theta}) = \begin{cases} 0.040 & \text{if } \boldsymbol{\theta} = 0000, \\ 0.100 & \text{if } \boldsymbol{\theta} = 0001, \\ 0.050 & \text{if } \boldsymbol{\theta} = 0010, \\ 0.025 & \text{if } \boldsymbol{\theta} = 0011, \\ 0.045 & \text{if } \boldsymbol{\theta} = 0100, \\ 0.025 & \text{if } \boldsymbol{\theta} = 0101, \\ 0.030 & \text{if } \boldsymbol{\theta} = 0110, \\ 0.110 & \text{if } \boldsymbol{\theta} = 0111, \\ 0.100 & \text{if } \boldsymbol{\theta} = 1000, \\ 0.110 & \text{if } \boldsymbol{\theta} = 1001, \\ 0.040 & \text{if } \boldsymbol{\theta} = 1010, \\ 0.100 & \text{if } \boldsymbol{\theta} = 1011, \\ 0.050 & \text{if } \boldsymbol{\theta} = 1100, \\ 0.100 & \text{if } \boldsymbol{\theta} = 1101, \\ 0.050 & \text{if } \boldsymbol{\theta} = 1110, \\ 0.025 & \text{if } \boldsymbol{\theta} = 1111. \end{cases}$$

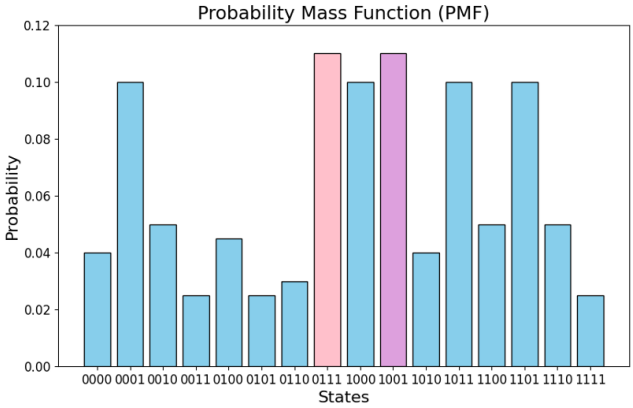

Figure 11: Target Distribution for 4D Joint Bernoulli

equilibriate. Specifically we extend our 4D Bernoulli Example(Section 6) to include a sharp mode(0111) and a flat mode(1001)(See Figure 11). Also, to ensure that *fight is fair*, we assign both our sharp mode and flat mode the same probability mass.

For each sampler, we track what state each chain visits using transition heatmaps, with no thinning, no burnin for a total of 100 iterations to model finite-time behavior. We run this simulation under sharp mode and flat mode initialization.

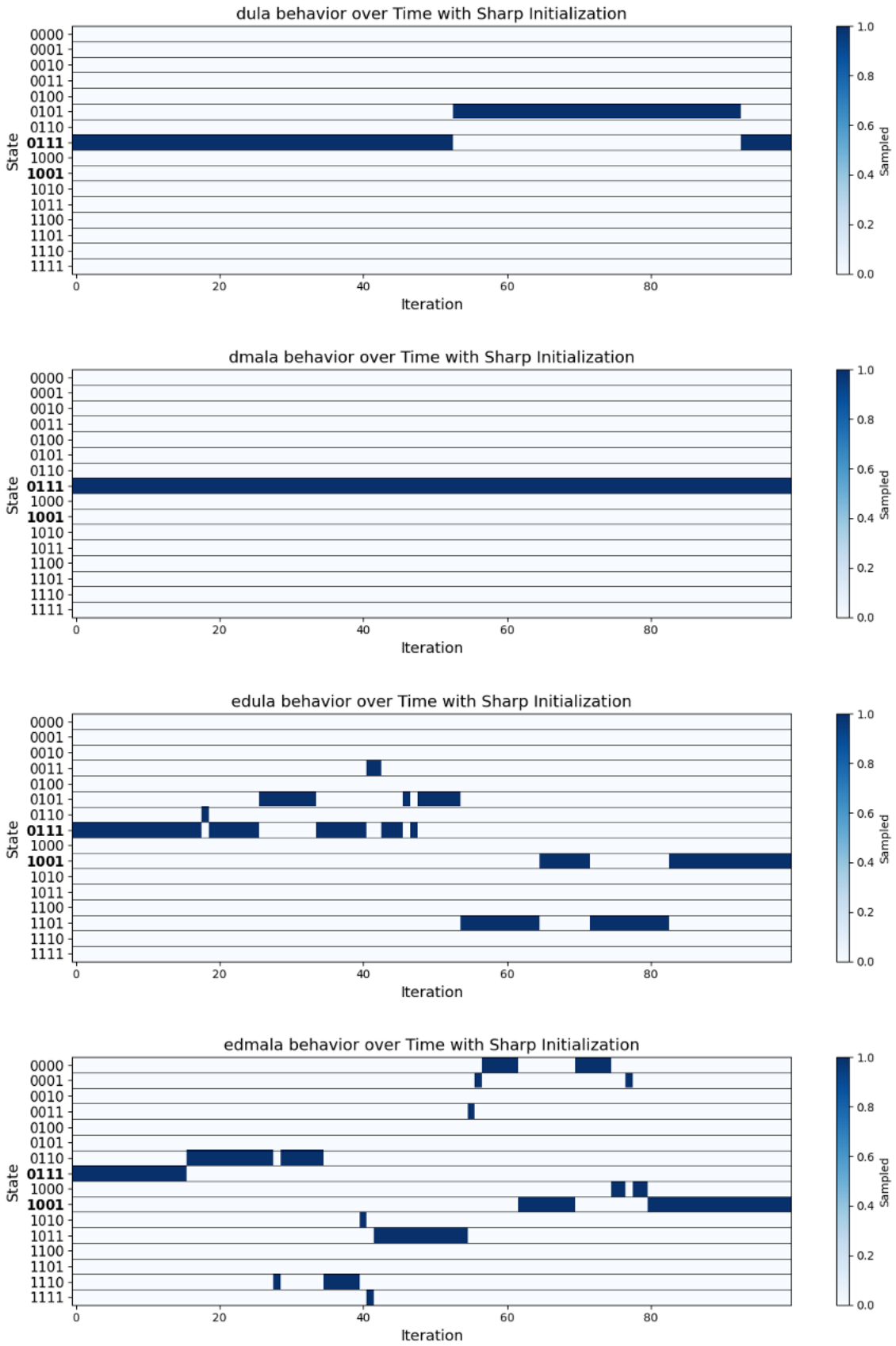

Figure 12: Finite-time behavior under sharp initialization.

Figure 12 illustrates that DLP samplers, when initialized in the sharp mode, exhibit minimal to no movement. In contrast, EDLP samplers swiftly transition to the flat mode and achieve stabilization.

Similarly, from Figure 13 DLP samplers, quickly escape the flat mode and find sharp modes. EDLP samplers, on the other hand, choose to remain at the flat mode.

The results clearly demonstrates that EDLP is successfully able to find flat modes under a computing budget irrespective of initialization.

E.2 TSP

Why DLP is inadept for structural and cost similarity?

In principle, standard gradient-based samplers are topology-agnostic. One could theoretically impose structural and cost similarity directly by augmenting the energy function with an explicit regularizer, that penalizes local sensitivity, such as:

$$U_{\text{new}}(\boldsymbol{\theta}) = U_{\text{original}}(\boldsymbol{\theta}) + \lambda \sum_{\boldsymbol{\theta}' \in \mathcal{N}(\boldsymbol{\theta})} \left(U(\boldsymbol{\theta}') - U(\boldsymbol{\theta})\right)^2$$

, where $\mathcal{N}(\boldsymbol{\theta})$ denotes the set of immediate neighbors (e.g., all states reachable by a single edge-swap). However, this approach is computationally intractable for large n as calculating the sensitivity term requires evaluating the energy function for every possible neighbor for every sample.

EDLP introduces a topological bias via the local entropy coupling. The coupling effectively smooths the landscape, allowing the sampler to *see* the volume of the solution basin. Thus, we circumvent the need for expensive, explicit summation over the neighborhood, allowing us access to robust solutions.

The Cost of Robustness.

Table 4: Solution quality characteristics across samplers.

Sampler	Average Cost	Unique Solutions
DULA	881.17 ± 76.11	108
DMALA	727.13 ± 67.81	21
EDULA	890.88 ± 53.07	44
EDMALA	855.33 ± 20.85	13

Recall, in the context of Constrained Combinatorial Optimization (CCO), our primary objective is not raw minimization of the energy function, but rather the identification of high-quality, structurally stable solution basins. We present the average cost and number of unique solutions found by each sampler under settings of Section 6 as illustrated in Table 4.

Theoretically, the introduction of the auxiliary variable $\boldsymbol{\theta}_a$ fundamentally alters the effective target distribution. By coupling the discrete variable to a continuous proxy via Langevin dynamics, we are no longer optimizing the original sharp energy $U(\boldsymbol{\theta})$. Instead, we are sampling from a smoothed joint distribution that penalizes isolated, brittle minima(see Lemma 4.1 in Section 4.1). Consequently, one should not expect entropic samplers to strictly outperform pure gradient-based methods in finding the absolute lowest theoretical cost. If the global minimum lies in a region of high curvature (a sharp peak), EDLP is explicitly designed to ignore it in favor of flatter, slightly higher-energy regions that offer robustness.

Notably, EDLP produces significantly fewer unique solutions compared to DLP. This reduction is not a failure of exploration, but a success of focus. The entropic coupling offers a leashing effect, preventing the sampler from wandering freely into high-energy or structurally dissimilar regions. It confines the search to the effective volume of the flat mode, ensuring that every sampled solution is a viable, robust candidate for the practitioner.

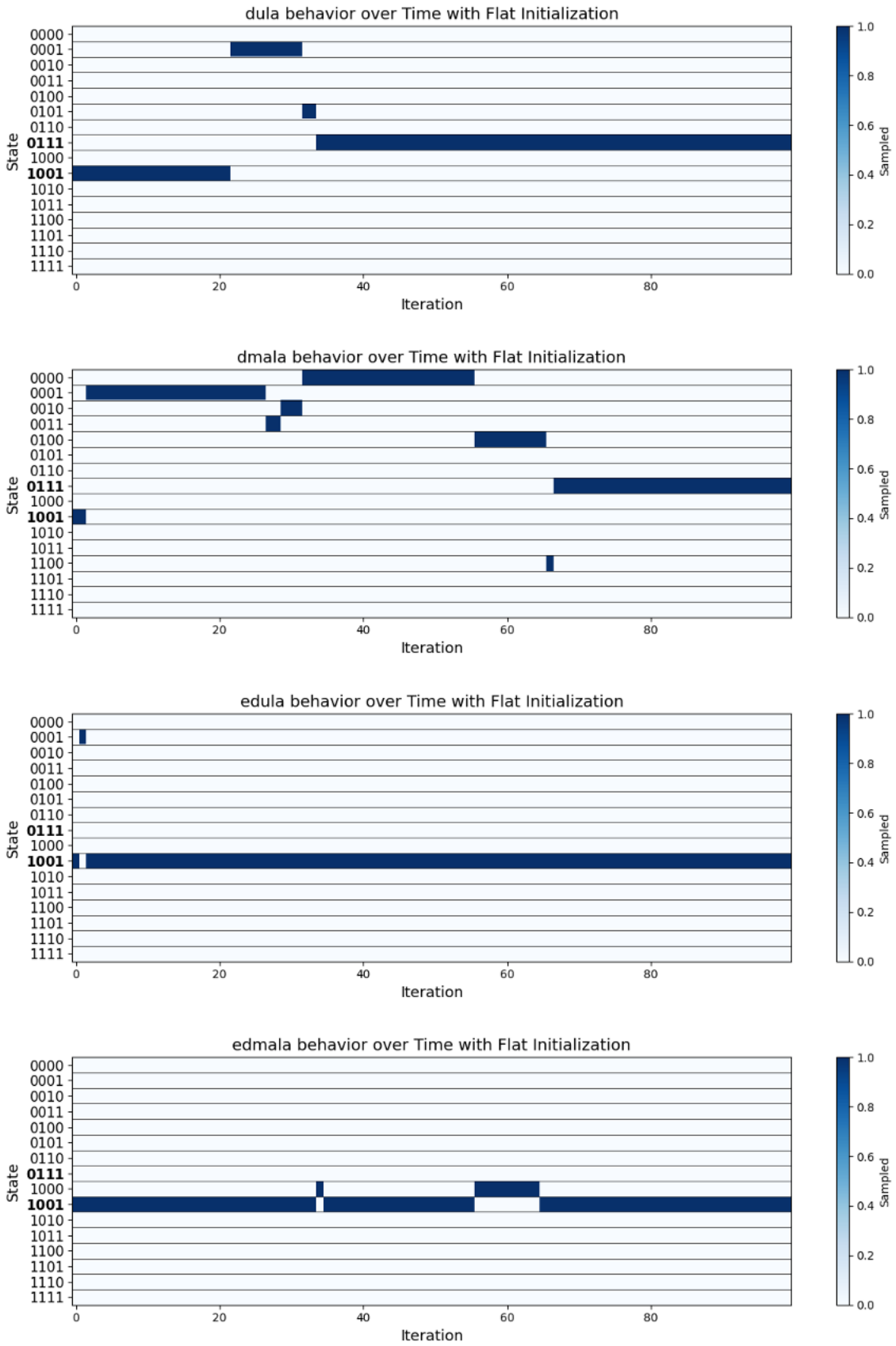

Figure 13: Finite-time behavior under flat initialization.

E.3 RBM

Perceptual Quality Analysis

Table 5: Reconstruction metrics (MSE, PSNR, SSIM) of different samplers on MNIST under clean, noisy, and occluded conditions.

Sampler	Setting	MSE (↓)	PSNR (↑)	SSIM (↑)
HB-10-1	Clean	0.0253 ± 0.0005	16.3555 ± 0.0858	0.5303 ± 0.0014
	Noisy	0.0267 ± 0.0004	15.9763 ± 0.0697	**0.3941** ± 0.0035
	Occluded	0.0256 ± 0.0004	16.2720 ± 0.0749	0.4963 ± 0.0017
BG-1	Clean	0.0257 ± 0.0007	16.2492 ± 0.1125	0.5294 ± 0.0025
	Noisy	0.0270 ± 0.0006	15.9086 ± 0.0885	0.3938 ± 0.0038
	Occluded	0.0260 ± 0.0006	16.1613 ± 0.0992	0.4947 ± 0.0024
DULA	Clean	0.0268 ± 0.0006	16.1160 ± 0.1022	0.5114 ± 0.0030
	Noisy	0.0280 ± 0.0005	15.7851 ± 0.0815	0.3907 ± 0.0041
	Occluded	0.0272 ± 0.0006	16.0187 ± 0.0922	0.4766 ± 0.0028
DMALA	Clean	0.0256 ± 0.0004	16.3305 ± 0.0709	0.5291 ± 0.0035
	Noisy	0.0270 ± 0.0004	15.9547 ± 0.0623	0.3939 ± 0.0032
	Occluded	0.0259 ± 0.0004	16.2372 ± 0.0632	0.4950 ± 0.0035
EDULA	Clean	0.0258 ± 0.0005	16.2979 ± 0.0891	0.5296 ± 0.0028
	Noisy	0.0272 ± 0.0005	15.9145 ± 0.0729	0.3881 ± 0.0038
	Occluded	0.0261 ± 0.0005	16.2153 ± 0.0796	0.4949 ± 0.0027
EDMALA	Clean	**0.0247** ± 0.0005	**16.4678** ± 0.0920	**0.5388** ± 0.0031
	Noisy	**0.0263** ± 0.0005	**16.0490** ± 0.0750	0.3931 ± 0.0037
	Occluded	**0.0250** ± 0.0005	**16.3792** ± 0.0819	**0.5043** ± 0.0033

To augment our analysis on perceptual quality, we report several widely accepted metrics: Mean Reconstruction Squared Error (MSE) to measure pixel-level differences between original and reconstructed images, Peak Signal Noise Ratio (PSNR) to measure the fidelity of the reconstructed images, and the Structural Similarity Index (SSIM) to assess the structural integrity of the reconstructions (Wang et al., 2004). EDMALA attains lowest MSE, highest PSNR, and highest SSIM (except for Noisy) among the samplers tested.

Mode Analysis

We performed mode analysis to validate the diversity and quality of MNIST digit samples generated by various samplers. Mode analysis assesses whether each sampler can capture the full range of MNIST digit classes (0-9) without falling into *mode collapse*, a phenomenon where a generative model fails to represent certain data modes, thus limiting diversity. We leveraged a *LeNet-5 convolutional neural network* (LeCun et al., 1998) trained on MNIST to classify each generated sample and produce a class distribution for each sampler. The choice of LeNet-5, a reliable architecture for digit recognition, ensures accurate class predictions, thus providing a robust method to assess the representativeness of the samples. We train the model for 10 epochs, and achieve a 98.85% accuracy on test data.

The results(Figure 14) from our analysis indicated that all samplers produced samples across all digit classes, showing no evidence of mode collapse. Although certain samplers exhibited a preference for specific classes these biases did not reach the level of complete mode omission. Each class was represented in the generated samples, confirming that the samplers achieved an acceptable level of *mode diversity*. By confirming that all classes are covered, we demonstrate that each sampler can adequately approximate the diversity of the MNIST dataset, assuring the samples' representativeness (Salimans et al., 2016; Goodfellow et al., 2014).

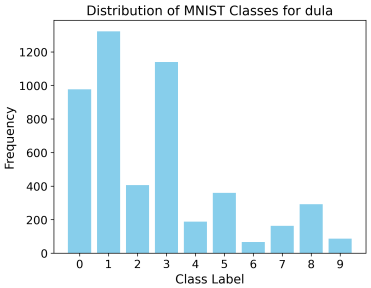

(a) DULA

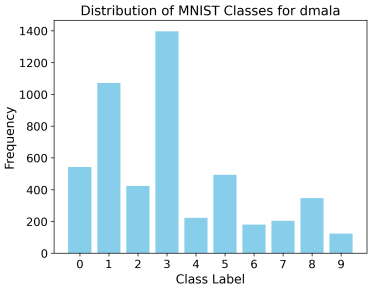

(b) DMALA

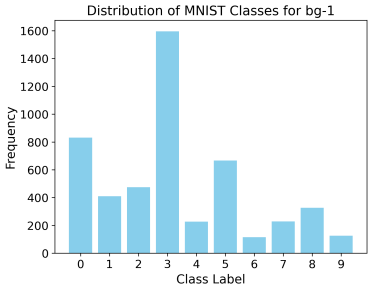

(c) BG-1

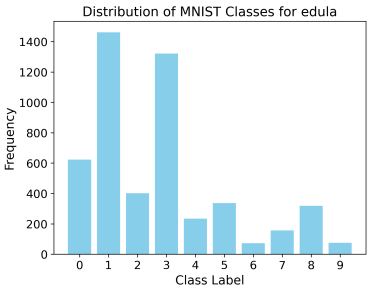

(d) EDULA

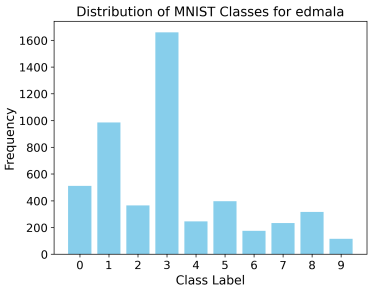

(e) EDMALA

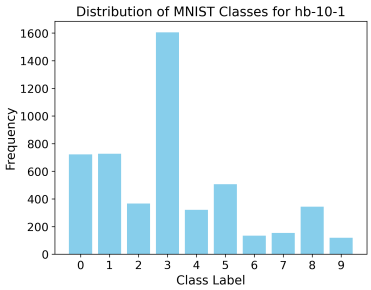

(f) HB-10-1

Figure 14: Mode Analysis

E.4 BBNN

We train 50 Binary Bayesian Neural Networks in parallel as in Section 6 and report the Average Training Log-Likelihood for our experiments in Table 6. Importantly, when EDLP does not yield a substantial improvement, it still manages to avoid significantly impacting the training log-likelihood negatively. The sampling vector's dimensions are as follows: COMPAS(7,501), News(30,001), Adult(45,001), and Blog(27,801).

Table 6: Average Training Log-Likelihood

Dataset	**Gibbs**	**GWG**	**DULA**	**DMALA**	**EDULA**	**EDMALA**
COMPAS	-0.4392 ± 0.0182	-0.4091 ±0.0291	-0.3611 ± 0.0134	**-0.3443** ±0.0168	-0.4147 ±0.0054	-0.4203 ±0.0007
News	-0.2372 ±0.0001	-0.2375 ±0.0002	-0.2348 ±0.0009	-0.2345 ±0.0008	**-0.2341** ±0.0007	-0.2342 ±0.0008
Adult	-0.4707 ±0.0043	-0.4623 ±0.0070	-0.3414 ± 0.0047	-0.3228 ±0.0171	-0.3246 ±0.0037	**-0.3186** 0.0030
Blog	-0.3920 ±0.0064	-0.3682 ±0.0170	-0.2708 ±0.011	-0.2686 ±0.0114	-0.2673 ±0.0032	**-0.2654** ±0.0027

The computational burden associated with sampling can be a major bottleneck in scenarios requiring fast training and prediction, such as online systems or real-time applications. Such requirements are seen in financial modeling and stock market prediction, where models must adapt to real-time data to ensure accuracy (Tsantekidis et al., 2017).

In Figure 15, we present the measured elapsed time per sample for the adult dataset to demonstrate these computational efficiencies, under the same settings as in Section 6, extending to include the GLU versions of the EDLP framework(Section B), alongside the results for the standard DLP and EDLP methods.

As illustrated, the EDLP versions exhibit an increase in runtime compared to DLP, due to the modifications discussed in Section 4.1. While the runtime difference between the DULA and EDULA algorithms (without MH correction) is negligible, the time difference between DMALA and EDMALA is more pronounced. This can be attributed to the more complex joint acceptance probability calculation required by EDMALA. Despite these variations, the overall runtime overhead for EDLP samplers is not substantial and remains practical.

For the EDLP-GLU variants, we maintained the same η and α values as their corresponding vanilla DLP samplers. The EDLP-GLU variants naturally achieve an approximate 50% reduction in runtime compared to EDLP. This efficiency stems from the alternating updates between sampling from a modified isotropic Gaussian and conditional DLP, designed to match the conditional distributions more effectively. However, this approach also introduces a higher standard deviation in runtime. The variability is primarily attributed to the contrasting computational costs between the two update types: sampling from the modified Gaussian is relatively lightweight, whereas the conditional DLP update is computationally intensive. As a result, the EDLP-GLU variants exhibit greater fluctuations in runtime compared to other samplers. Furthermore, the negative lower bounds are not physically meaningful and stem from the high variability in runtime measurements.

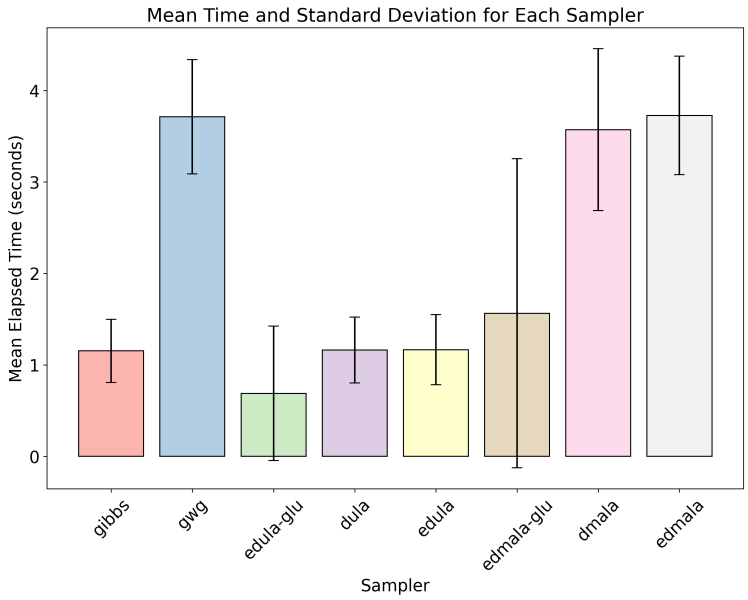

Figure 15: Runtime Analysis on Adult Dataset

For details of datasets used, refer to the Appendix of (Zhang et al., 2022).

We use α to 0.3 for the COMPAS dataset and $\alpha = 0.1$ for all other datasets. For more details on hyperparameters see Table 7.

Table 7: Hyper-parameter Settings

Hyperparameters for EDLP				
Dataset	**EDULA**		**EDMALA**	
	α_a	η	α_a	η
COMPAS	0.0100	4.00	0.0010	1.25
News	0.0040	2.00	0.0001	0.85
Adult	0.0001	2.00	0.0001	5.00
Blog	0.0100	1.00	0.0001	1.25